

Artificial Circular RNA Sponges as a Novel Tool in Molecular Biology and Medicine

Kumulative Inauguraldissertation

vorgelegt von

Janina Breuer

(Master of Science Biologie)

zur Erlangung des akademischen Grades:

Doctor rerum naturalium

(*Dr. rer. nat.*)

Eingereicht am Fachbereich 08 – Biologie und Chemie
der Justus-Liebig-Universität Gießen

Gießen, Juni 2022

Die vorliegende Arbeit wurde am Institut für Biochemie des Fachbereiches 08 der Justus-Liebig-Universität Gießen in der Zeit von August 2018 bis Juni 2022 unter der Leitung von Dr. Oliver Rossbach angefertigt.

Dekan	Prof. Dr. Thomas Wilke Institut für Tierökologie und Spezielle Zoologie Fachbereich für Biologie und Chemie Justus-Liebig-Universität Gießen
1. Gutachter	Dr. Oliver Rossbach Institut für Biochemie Fachbereich für Biologie und Chemie Justus-Liebig-Universität Gießen
2. Gutachter	Prof. Dr. Elena Evguenieva-Hackenberg Institut für Mikrobiologie und Molekularbiologie Fachbereich für Biologie und Chemie Justus-Liebig-Universität Gießen

Eidesstattliche Erklärung

Ich erkläre: Ich habe die vorgelegte Dissertation selbstständig und ohne unerlaubte fremde Hilfe und nur mit den Hilfen angefertigt, die ich in der Dissertation angegeben habe. Alle Textstellen, die wörtlich oder sinngemäß aus veröffentlichten Schriften entnommen sind, und alle Angaben, die auf mündlichen Auskünften beruhen, sind als solche kenntlich gemacht. Ich stimme einer evtl. Überprüfung meiner Dissertation durch eine Antiplagiat-Software zu. Bei den von mir durchgeführten und in der Dissertation erwähnten Untersuchungen habe ich die Grundsätze guter wissenschaftlicher Praxis, wie sie in der „Satzung der Justus-Liebig-Universität Gießen zur Sicherung guter wissenschaftlicher Praxis“ niedergelegt sind, eingehalten.

Gießen, 01.06.2022

Janina Breuer

Table of Contents

A.	Abstract	IX
B.	Zusammenfassung	XI
Introduction		1
C.	Naturally occurring circular RNAs	1
D.	Artificial circular RNAs	11
E.	Research objectives	23
F.	References	25
Published Articles		37
G.	Production and Purification of Artificial Circular RNA Sponges for Application in Molecular Biology and Medicine (Breuer et al. 2020)	37
H.	Synthetic circular miR-21 RNA decoys enhance tumor suppressor expression and impair tumor growth in mice (Müller et al. 2020)	57
	Supplementary Data	87
I.	What goes around comes around: Artificial circular RNAs bypass cellular antiviral responses (Breuer et al. 2022)	95
	Supplementary Data	121
Appendix		127
J.	Scientific Achievements	127
K.	Acknowledgements	129

Abstract

Within the recent years, *circular RNAs* (circRNAs) have aroused the interest of molecular biology, medicine and pharmaceutical science, due to their covalently closed structure and thus an elevated stability against exonucleolytic degradation compared to linear RNA molecules. Inspired by naturally occurring circRNAs functioning as sponges for cytoplasmic *microRNAs* (miRNAs), artificial circRNAs have been designed to not only specifically sequester but also functionally inhibit mature miRNAs related to human diseases like viral infections or cancer. The production of artificial *circular RNA sponges* (ciRS) displays a major limitation. To overcome this limitation, we promulgated a strategy for the efficient production and stringent purification of synthetic ciRS in a cell-free system, technically relying on enzyme-based *in vitro* transcription and RNA ligation. A former proof-of-principle study demonstrated the successful sequestration of the hepatocyte-specific miR-122 by engineered ciRS to impact the *Hepatitis C virus* (HCV) propagation. As part of this thesis, the oncogenic miR-21 was employed as a target for ciRS-based sequestration. Being the most abundant miRNA in human cancers, specific binding and functional inactivation of miR-21 by artificial ciRS not only impaired cancer cell proliferation and invasion in 3D tumor spheroids, but also inhibited tumor growth within a murine xenograft model system by de-repressing natural anti-proliferative miR-21 mRNA targets. Importantly,

circularization of ciRS substantially increased the intracellular stability and therefore the availability of functional miR-21 binding sites as the half-lives of artificial ciRS significantly exceeded those of their linear counterparts.

Concerning the rapidly gained importance of RNA pharmaceuticals worldwide as well as the potential application of synthetic ciRS as powerful therapeutic strategy, one question remains to be answered: Would the therapeutic application of artificial ciRS trigger the cellular innate immune system? On that account, as part of this thesis, *in vitro* produced artificial ciRS previously used to inhibit miRNA functions and administered by lipofection were found to bypass cellular antiviral defense mechanisms. Contrarily, a circular construct encompassing extensive double-stranded sequence elements was found to potently induce intracellular signalling as chemokine-, interferon- and other innate immunity associated mRNA levels were up-regulated in a time- and dose-dependent manner comparable to commercially available immune-stimulants. Immunoblotting revealed this highly double-stranded ciRS to trigger the activation of *Protein Kinase R* (PKR), an important RNA sensor in cellular immunity.

In sum, ciRS produced with the presented methodology display a promising antisense tool to sequester disease-relevant miRNAs with cellular innate immune signalling pathways being bypassed depending on their sequence composition and secondary structure.

A. Abstract

Zusammenfassung

Zirkuläre RNAs (circRNAs) haben in den vergangenen Jahren das Interesse der Molekularbiologie, Medizin sowie pharmazeutischen Wissenschaft geweckt, auch aufgrund ihrer kovalent geschlossenen Struktur und der damit einhergehenden erhöhten Stabilität gegenüber exonukleolytischem Abbau verglichen mit linearen RNA-Molekülen. Inspiriert durch natürlich vorkommende circRNAs, welchen unter anderem eine Funktion als Schwämme zytoplasmatischer *mikro-RNAs* (miRNAs) zugeschrieben werden konnte, wurden artifizielle circRNAs entwickelt. Letztere dienen nicht nur der spezifischen Sequestrierung, sondern auch der funktionellen Inhibition reifer miRNAs, die im Zusammenhang mit menschlichen Krankheitsbildern, wie viralen Infektionen oder Krebs, stehen. Vor diesem Hintergrund stellt die Produktion artifizieller, *zirkulärer RNA-Schwämme* (ciRS) eine wesentliche Limitierung dar. Aus diesem Grund haben wir eine Strategie für die effiziente Produktion und stringente Aufreinigung von synthetischen ciRS im Zell-freien System veröffentlicht, die technisch auf einer enzymbasierten *in vitro* Transkription und RNA-Ligation beruht. Eine vorangegangene *Proof-of-Principle* Studie konnte zeigen, dass die Sequestrierung der Hepatozyten-spezifischen miR-122 mit artifiziellen ciRS die Vermehrung des *Hepatitis-C-Virus* (HCV) hemmt. Im Rahmen der vorliegenden Arbeit wurde die onkogene miR-21 als Ziel für die ciRS-basierte Sequestrierung eingesetzt. Da

es sich um die am häufigsten vorkommende miRNA in menschlichen Krebserkrankungen handelt, beeinträchtigte die spezifische Bindung und funktionelle Inaktivierung von miR-21 nicht nur die Proliferation und Invasion von Krebszellen in 3D-Tumor-Sphäroiden, sondern hemmte auch das Tumorwachstum in einem murinen Xenograft Modell, indem natürliche anti-proliferative miR-21 Ziel-mRNAs de-reprimiert wurden. Dabei hat die Zirkularisierung die intrazelluläre Stabilität von ciRS und damit die Verfügbarkeit funktioneller miR-21-Bindungsstellen erheblich erhöht, da die Halbwertszeit künstlicher ciRS jene linearer RNA Schwämme deutlich übertraf.

In Anbetracht der rapide gestiegenen Bedeutung von RNA-basierten Arzneimitteln weltweit sowie der potenziellen Anwendung von synthetischen ciRS als therapeutische Strategie bleibt eine Frage unbeantwortet: Lösen therapeutische ciRS die Aktivierung des zellulären angeborenen Immunsystems aus? In diesem Zusammenhang wurde festgestellt, dass *in vitro* hergestellte künstliche ciRS, die zuvor zur Inhibition der Funktion von miRNAs verwendet und durch Lipofektion verabreicht wurden, zelluläre antivirale Abwehrmechanismen umgehen. Im Gegensatz dazu hat ein zirkuläres Konstrukt, welches lange doppelsträngige Sequenzelemente umfasst, die intrazelluläre Signalübertragung effizient induziert, da Chemokin-, Interferon- und andere mit der angeborenen Immunität

B. Zusammenfassung

zusammenhängenden mRNA-Level in einer zeit- und dosisabhängigen Weise hochreguliert wurden. Dabei waren die Effekte vergleichbar mit kommerziell erhältlichen Immunstimulanzien. Darüber hinaus zeigten Immunoblotting-Analysen, dass diese stark doppelsträngige ciRS die Aktivierung von *Protein Kinase R* (PKR), einem für die zelluläre Immunität wichtigen RNA-Sensor, auslöst.

Zusammenfassend stellen die mit der vorgestellten Methodik hergestellten ciRS ein vielversprechendes Instrument zur Regulierung krankheitsrelevanter miRNAs dar, wobei die zelluläre angeborene Immunantwort abhängig von ihrer Sequenzzusammensetzung und Sekundärstruktur umgangen werden kann.

Introduction

Naturally occurring circular RNAs

Scientific history: From discovery to initial characterization of circRNAs

The initial evidence of the existence of *circular RNAs* (circRNAs) was reported in 1976 by *Sänger et al.*, demonstrating the genomes of the *plant potato spindle tuber viroid* (PSTVd) pathogen to be composed of single-stranded covalently closed RNA molecules [1]. Three years later, in 1979, a second group found circular forms of RNA within electron micrographs of cytoplasmic extracts of several eukaryotic cells even under highly denaturing conditions [2]. After their discovery, the potential impact of circRNAs was underestimated for decades. Sporadic studies identified only few candidates of naturally occurring circRNAs. The *hepatitis delta (δ) virus* (HDV) genome was shown to be composed of single-stranded and covalently closed RNA, encoding proteins involved in viral replication [3,4]. Additionally, circRNAs were observed to be created as by-products of *ribosomal RNA* (rRNA) processing in archaea and in the context of self-splicing rRNA introns in eukaryotes [5,6].

However, circRNAs were still reported as events of aberrant splicing with negligible biological relevance. In 1991, *Nigro et al.* discovered abnormally spliced transcript isoforms from the tumor suppressor gene *deleted in colorectal cancer* (DCC) in rodent and human cells with low abundance

compared to normal transcripts. Being neatly joined at consensus splice sites, but in an order differing from primary transcripts, the authors refer to the DCC exons of these non-polyadenylated transcripts as “scrambled exons” – the first reported exon derived circRNAs [7]. As the exact mechanism of circularization remained elusive, hypotheses on the formation of scrambled exons ranged from splicing errors, to intermolecular splicing between two different DCC transcripts or intramolecular splicing processes [7]. Similar findings were published in 1992 by *Cocquerelle et al.*, reporting of a novel transcript variant of human proto-oncogene *ETS proto-oncogene 1* (*ETS-1*) containing pairs of scrambled exons [8]. The authors ruled out the possibility of PCR-artefacts via RNase protection assays and firstly associated the generation of these non-polyadenylated transcript isoforms to the presence of large flanking introns [8,9]. One year later, in 1993, the structure of this type of non-polyadenylated, “mis-spliced” RNA isoforms with scrambled exons was found to correspond to circular RNA molecules that might be functional [9–11]. Furthermore, initial stability analyses of cytoplasmic *ETS-1* “mis-spliced” transcripts demonstrated the circRNAs to be stable after a 48 h treatment of cells with actinomycin D [10]. Moreover, the circular transcript of the mouse testis-determining gene *sex determining region of Y* (*Sry*) was found to be the most abundant transcript in the cytoplasm of adult mouse testis tissue and to exhibit a higher expression level than its linear counterpart [11].

In the following years, a few studies were published that mainly focused on both the mechanism by which these molecules could be generated and potential functions of circRNAs. In 1995, *Dubin* and colleagues hypothesized that inverted repeats are necessary for *Sry* transcript circularization [12]. In the same year, *Chen and Sarnow* designed and produced the first synthetic *internal ribosome entry site* (IRES)-containing circRNA constructs via a T4 RNA ligase-based circularization of *in vitro* synthesized linear RNA demonstrating that circRNAs can be used as templates for translation *in vitro* [13]. In 1996, the incubation of linear pre-mRNAs with eukaryotic nuclear extracts was used to demonstrate that circRNAs can be produced *in vitro* [14,15]. Moreover, circRNA formation in transcripts of the cytochrome P-450 gene was shown to be correlated with exon skipping [16,17].

These early studies (i) unambiguously demonstrated the existence of circular RNA molecules, (ii) allowed initial insights into circRNA biogenesis and (iii) indicated potential functions. However, advances in RNA sequencing (RNA-seq) methods, together with the development of specialized bioinformatic pipelines, have allowed novel insights into the circRNA world by identifying thousands of human exonic circRNAs [9,18–20]. In 2013, circRNAs were estimated to account for about 1% as many molecules as poly(A) containing RNAs in humans [20,21]. Naturally occurring circRNAs appear to constitute the major RNA splicing isoforms of hundreds of genes, to be found in

diverse species throughout the eukaryotic tree of life and to be strictly regulated [18–20,22–24]. Cell-type- and tissue-specific as well as developmental stage-regulated dynamic expression of circular RNA isoforms of individual genes was confirmed in the recent years [9,20,21,25–28]. Altogether, circRNAs form a novel class of mainly non-coding RNAs and are part of a research area that is becoming increasingly important for molecular biology, medicine and pharmaceutical science.

Biogenesis of linear versus circular RNA molecules

Discovered in 1977 by *Phillip Sharp* and *Richard Roberts*, splicing defines the process of converting eukaryotic *messenger RNA precursors* (pre-mRNAs) into mature, functional and protein-coding *messenger RNAs* (mRNAs) [29–31]. This essential procedure in eukaryotic gene expression is catalyzed by a dynamic macromolecular ribonucleoprotein complex – the spliceosome [32,33]. During constitutive splicing, non-coding introns are removed and protein-coding exon segments are accurately joined together co-transcriptionally relying on spliceosomes [34,35]. The recognition and identification of three short, conserved sequence elements is indispensable, encompassing the 5'- and 3'-splice sites (5'-ss, 3'-ss) defining the intron/exon boundaries, as well as the branch point adenosine and its surrounding sequence motif crucial for the first catalytic step [36]. Splicing is a complex process involving five uridine-rich *small nuclear RNAs* (U snRNAs) and

about 300 proteins in mammalian cells acting together sequentially. Biochemically, the main splicing process can be reduced to a two-step transesterification (Figure 1). In the first step – a nucleophilic attack named branching – the 2'-hydroxyl group of the branch point adenosine nucleotide attacks the phosphate group of the guanosine at the 5'-ss, thereby releasing the 5'-exon and creating a lariat structure of the intron with a 2'-5' linkage [31,33]. In the second step – the ligation – the 3'-hydroxyl group of the 3' end nucleotide of the released upstream exon nucleophilically attacks the phosphate of the 5' end nucleotide of the downstream exon, thereby ligating both exons to form the mature mRNA, and releasing the intron lariat (Figure 1)[31,33]. Upon completion of the splicing reaction, the mature mRNA is released from the spliceosome and the intron lariats are linearized and degraded [37].

Alternative splicing mechanisms enormously expand the proteome deriving from a limited number of genes and dramatically increase the complexity of higher organisms [31,38,39]. Approximately 95% of human genes undergo one or more forms of alternative splicing, such as skipping or inclusion of individual cassette exons, intron retention, switching between alternative 5'- or 3'-ss as well as mutually exclusive exons [31,40]. *Zheng et al.* report that shorter exon length, weaker splicing signals at alternative splice sites or higher sequence conservation surrounding orthologous alternative exons promote

the exons that are included in the mature mRNA molecule [31,41].

In addition to canonical and alternative linear splicing, naturally occurring circRNAs arise by a special alternative splicing mechanism termed “backsplicing” [18] or “head-to-tail-splicing” [23]. As reported by *Ashwal-Fluss* and colleagues, this process directly requires the canonical spliceosome machinery, occurs co-transcriptionally and – although being less favorable [42] – competes with splicing of linear transcripts [43]. Mutational analyses addressing the sequence requirements for circRNA processing revealed both canonical splice sites to be required for circularization, although featuring a high level of tolerance to sequence mutations [44]. Generally, backsplicing is characterized by joining a downstream 5'-ss to an upstream instead of a downstream 3'-ss relying on canonical splicing signal (Figure 1)[45]. In detail, the 2'-hydroxyl group of the branchpoint adenosine, upstream of the circularized exon, attacks the phosphate group of the guanosine at the downstream 5'-ss within the first transesterification-reaction. The resulting free 3'-hydroxyl group of the 5'-ss subsequently nucleophilically attacks the 3'-ss. Consequently, a pre-mRNA intermediate as well as a circularized exon is released (Figure 1). Apart from the particular reaction of direct backsplicing, mechanistically exon skipping and intron lariats resistant to debranching procedures can also result in circular RNA molecules (Figure 2)[45–48]. Therefore,

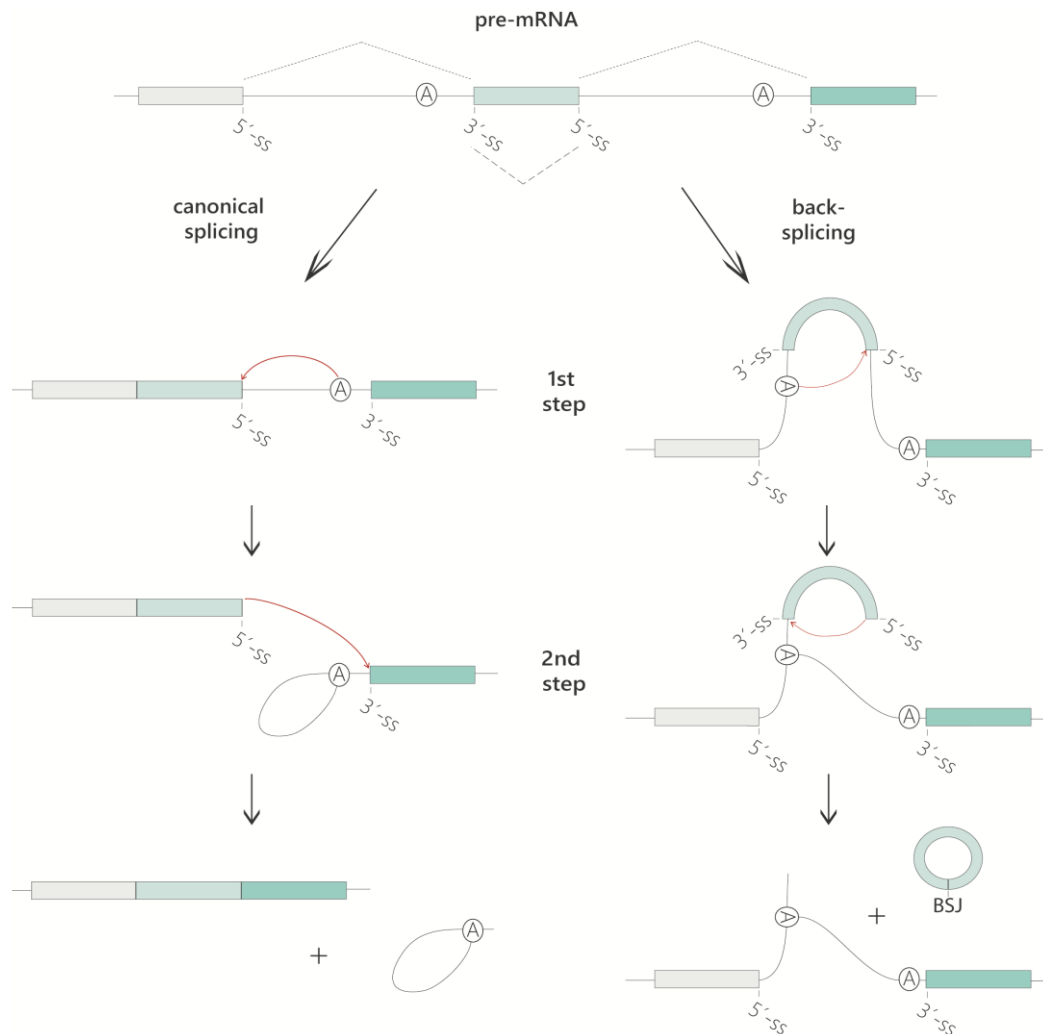


Figure 1: Biochemical steps of splicing: linear canonical splicing versus circular backsplicing. Biochemically, both canonical splicing, and backsplicing of *precursor messenger RNAs* (pre-mRNAs) rely on two sequential steps of transesterification. During canonical splicing, the 2'-hydroxyl of the branchpoint adenosine (within this figure referred to as A) nucleophilically attacks an upstream 5'-splice site (5'-ss), thereby leading to the first transesterification reaction, with a 2'-5' linked intron lariat being formed. In a second transesterification, the free 3'-hydroxyl of the respective 5'-ss attacks the downstream 3'-splice site (3'-ss). Canonical splicing results in linear exon ligation (3'-5' linkage) and linear RNA molecules, and the 2'-5' linked intron is released. In contrast, the transesterification reactions within backsplicing are characterized by, first, the nucleophilic attack of a downstream 5'-ss by the branchpoint adenosine and, second, the attack of the upstream 3'-ss by the respective 5'-ss. Therefore, *circular RNA* (circRNA) molecules (3'-5' linkage) are created. The linear pre-mRNA intermediate (2'-5' linkage) includes intron sequences and can be subjected to further linear splicing reactions.

circRNAs containing introns (circular intronic RNAs; ciRNAs), exons (circular exonic RNAs; EciRNAs) or exons with retained introns (exon-intron circRNAs; EiciRNAs) are distinguished (Figure 2)[45,46,48,49]. Common, naturally

occurring circRNAs were observed to often include two to three exons without internal intronic sequence(s) [45]. The major requirement for circRNAs to arise naturally by backsplicing reaction, is the physical proximity of splice sites,

allowed by two described elements: intronic *cis*-acting sequences or *trans*-acting protein factors (Figure 2B, 2C)[48]. As already discussed very early in 1993 for *Sry* circRNA [11], base pairing between intronic *cis*-acting inverted elements, including reverse complementary Alu repeats and non-repetitive sequences, were found to facilitate the generation of many circRNAs [18,45,48]. CRISPR/Cas9 technology-based mutational analyses revealed that disrupting base-pairing between such repeats eliminated circRNA generation, while compensatory mutations were sufficient to restore backsplicing [42,50]. Additionally, a variety of *trans*-acting protein factors accomplishes the fine-tuning of backsplicing efficiency, thereby allowing a combinatorial control and tissue- as well as cell-state-specific circRNA expression patterns [45,48].

Functions of endogenous circRNAs

The properties of endogenous circRNAs have aroused the interest of many scientists worldwide. As covalently closed structures with neither 5'- nor 3'-termini, circRNAs were shown to be resistant to exonucleolytic degradation resulting in elevated stabilities compared to linear RNAs [18,48,51]. Concerning these elevated stabilities of circRNAs compared to linear counterparts to be associated with prolonged regulatory effects, one intriguing question arises: What are the functions of these particularly stable molecules?

Even though a variety of circRNAs has been identified to date, the functions of endogenous circRNAs are still largely unknown. Nevertheless, there are several lines of evidence showing circRNAs to have diverse, important regulatory and developmental roles [20,23,52–54]. As described by *Holdt et al.*, conceptually there are two principle ways for circRNAs to reveal their functions. First – as backsplicing might decrease linear splice products – the process of circRNA generation itself and second, once formed, the function as a *trans*-acting molecular unit (Figure 3) [43,55]. Recent studies demonstrate naturally occurring circRNAs to have at least three main functions in eukaryotic cells: (i) circRNAs function as *microRNA* (miRNA) sponges, (ii) interact with *RNA binding proteins* (RBPs) and (iii) act as nuclear transcriptional regulators – illustrating the impact of circular RNAs on the regulatory networks governing gene expression (Figure 3) [43,46,54].

The majority of circRNAs was shown to be localized in the cytoplasm [18,19]. However, for some circRNAs, nuclear-localization could be observed. ElicRNAs, like circEIF3J and circPAIP2, were found to directly interact with the U1 snRNA *in cis*. The resulting RNA-RNA complex associates with the *RNA polymerase II* (RNAPII) at promoter regions, by this means facilitating the gene expression of their parental genes at the transcriptional level [56]. The intronic circRNA ci-ankrd52 was observed to accumulate at the site of transcription and to associate with the RNAPII machinery during elongation,

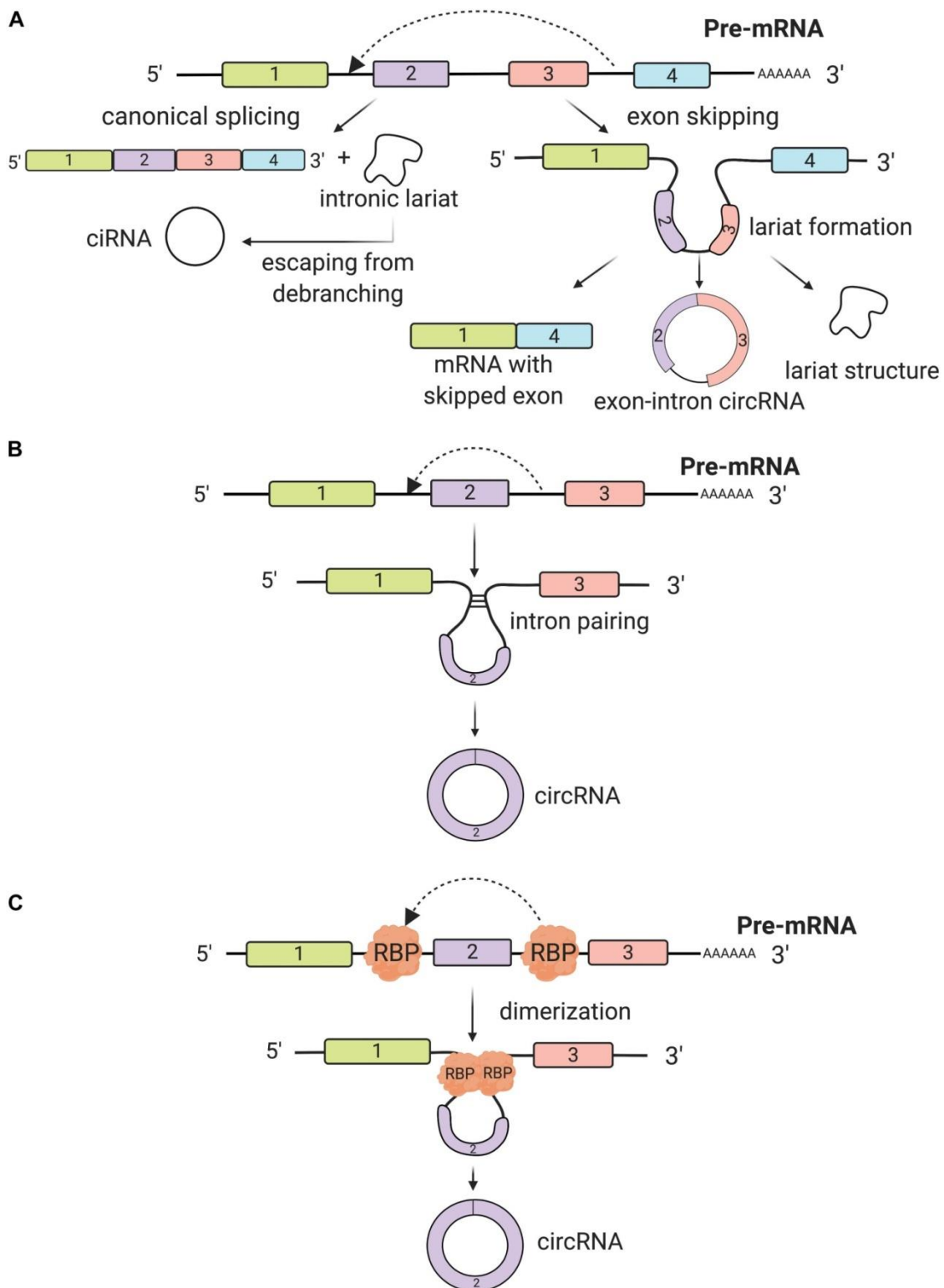
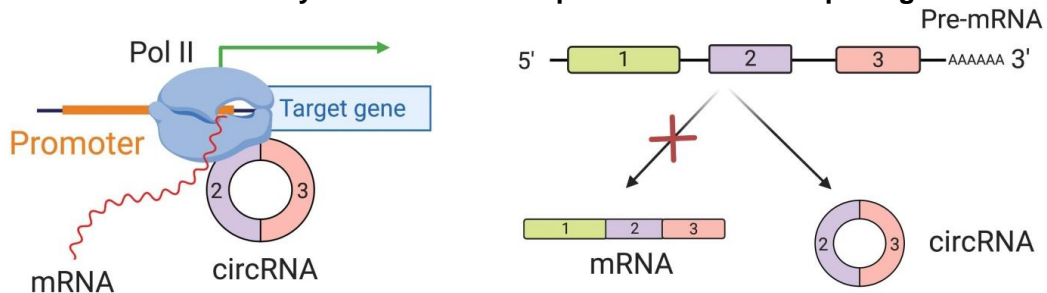


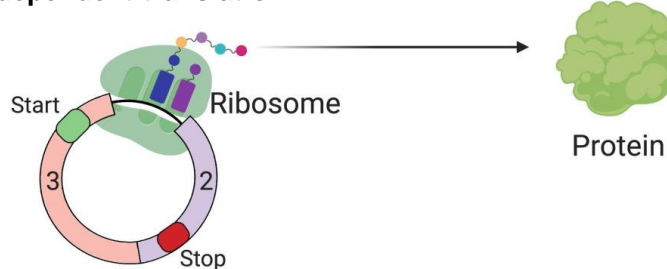
Figure 2: Endogenous mechanisms of circRNA biogenesis. Canonical splicing results in linear mRNAs, whereas backsplicing of the same linear pre-mRNA produces circular RNA isoforms. CircRNAs can be composed of introns, one or several exons (*exonic circRNAs* (EciRNA)), as well as both intronic and exonic regions (*exon-intron circRNAs* (EiRNAs)). Different mechanisms were characterized to promote circRNA formation. (A) Exon skipping mechanism can not only result in the generation of an alternatively spliced linear mRNA with skipped exons and a lariat structure, but can also lead to the formation of circRNAs. Furthermore, *circular intronic RNAs* (ciRNAs) were described to arise from intronic lariat structures escaping the debranching

procedure. Commonly backsplicing of an exon is facilitated by either (B) intron pairing of long flanking introns or (C) dimerization of RNA binding proteins associating with the neighboring introns of the circularized exon. (Modified from Tran et al. 2020)

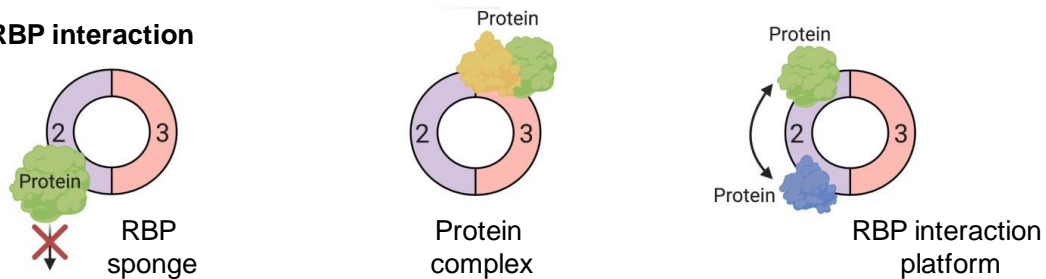
A Stimulation of RNA Polymerase II and competition with linear splicing



B 5'-Cap-independent translation



C RBP interaction



D miRNA sponge

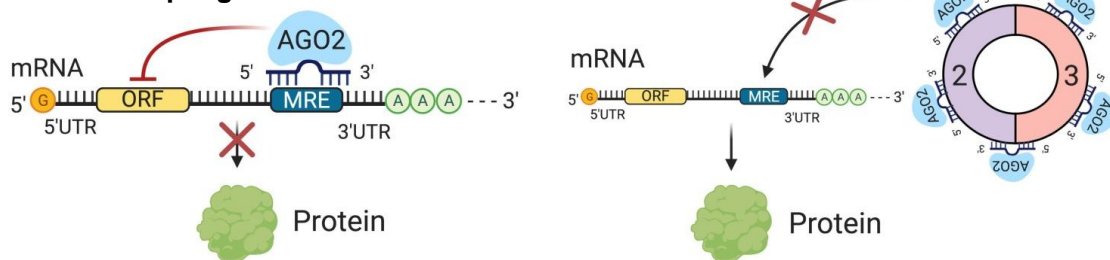


Figure 3: CircRNA functions. Until now, functions of endogenous circRNAs are largely unknown. However, circRNAs were found to exhibit diverse important and regulatory roles. (A) CircRNAs interact with promoter regions and/or the *RNA polymerase II* (Pol II) machinery, thereby facilitating gene expression of their target genes. Furthermore, also the competition of linear versus backsplicing can affect the biogenesis of functional mRNAs. (B) Several studies report circRNAs to function as templates for 5'-cap-independent translation. (C) Moreover, circRNAs were found to interact with *RNA binding proteins* (RBPs), altering their availability and impacting the regulation of natural RBP-targets. Endogenous circRNAs functioning as RBP interaction platform, acting as transport vehicle for RBPs or assembly of circRNA-protein complexes would be conceivable. However, details on functional protein interaction remain elusive. (D) The most common function of circRNAs is the sequestration of miRNAs associated

with *Argonaute-2* (Ago2) as circular miRNA sponges. CircRNA-mediated sequestration of miRNAs prevents their binding to *miRNA-regulatory elements* (MRE) on target mRNAs. The downregulation of target mRNAs is prohibited and expression is increased. *Open reading frame* (ORF). (Modified from Tran et al. 2020)

hence acting as positive transcriptional regulator of its parental genes [46]. These results indicate circRNAs to contribute to the regulatory mechanisms facilitating gene expression (Figure 3A) [56].

Although generally considered as “non-coding” thus far, whether naturally occurring circRNAs inhabit the ability to act as templates for translation is heavily studied and highly discussed within literature over the past decade (Figure 3B). Published concurrently in 2017, three groups presented the candidates *circRNA Zinc Finger Protein 609* (circ-ZNF609) and *circRNA muscleblind 3* (circMbl3) to be translated in a cap-independent manner utilizing *N6-Methyladenosine* (m⁶A) modification as driver for circRNA translation [57–59]. Controversially, the majority of circRNAs addressed so far provide no evidence for translation [18,28,53,60–62]. As highlighted by *Schneider and Bindereif* in 2017, despite the initially described studies, many unanswered questions need to be elucidated to appraise the functional significance of the translation of naturally occurring circRNAs [63].

The most prominent mechanism of function of circRNAs was found to be the interaction with RBPs and miRNAs (Figure 3C, 3D). CircRNAs like circMbl, circ-Foxo3, and circPABPN1 were shown to bind RBPs (Figure 3C) [43,64,65]. By virtue of these binding

events the availability of RBPs is affected, *vice versa* having an impact on the regulation of natural RBP targets. The splicing factor *muscleblind* (MBL) was found to specifically bind to circMbl, a circRNA deriving of exon 2 of the MBL pre-mRNA. It contains numerous binding sites for the MBL protein, thereby participating in an autoregulatory feedback loop in *Drosophila melanogaster* and humans [43]. Furthermore, circFoxo3 not only interacts with *mouse double-minute 2* (MDM2) protein – a known negative regulator of the tumor suppressor p53 – but also with p53 itself [64]. Consequently, this leads to the induction of apoptosis through ubiquitination and subsequent degradation of p53, as well as stimulation of Foxo3 activity [64]. Translation was demonstrated to be modulated via the competition between a circRNA and its cognate mRNA for an RBP that influences gene expression programs. CircPABN1, a circRNA arising from the pre-mRNA of the *nuclear poly(A)-binding protein 1* (PABPN1) pre-mRNA, negatively modulates PABPN1 and *autophagy-related gene 16 like 1* (ATG16L1) translation, by preventing the post-transcriptional regulator HuR from binding its target mRNAs [65]. Interestingly, in 2019 *Liu* and colleagues showed endogenous circRNAs with an imperfect double-stranded region of 16-26 *basepairs* (bp) to inhibit the intracellular *protein kinase R* (PKR).

Upon viral infection, circRNAs were globally degraded by the endonuclease RNase L and circRNA-associated PKR was released, thereby allowing its activation followed by recognition of exogenous dsRNAs longer than 33 bp [66].

The groups of Jørgen Kjems and Nikolaus Rajewsky simultaneously found the endogenous circRNA *cerebellar degeneration-related protein 1 antisense / circular RNA sponge for miR-7* (CDR1as/ciRS-7) to harbor more than 70 conserved binding sites for miR-7, therewith introducing circRNAs as miRNA sponges (Figure 3D) [23,24]. This designation of circRNAs as “sponges” has its origin in artificially expressed linear transcripts containing concatenated miRNA binding sites, which sequester and block the activity of a specific miRNA [67,68]. CDR1as/ciRS-7 was identified as a highly expressed circRNA in human and mouse brain [23,24,69]. In neocortical and hippocampal neurons, the observed co-expression of CDR1as/ciRS-7 with miR-7 leads to a suppression of miR-7 functions, thereby de-repressing natural miR-7 targets [24]. Furthermore, the overexpression of CDR1as/ciRS-7 from a minigene phenotypically copied miR-7 loss of function *in situ* [18]. Displaying a misregulation of other miRNAs, dysfunctional synaptic transmission and sensorimotor gating, also associated with human neurological disorders, like schizophrenia or Alzheimer's disease, CDR1as/ciRS-7 knockout mice indicate the importance of CDR1as/miR-7-interactions for normal brain function

[70]. MiR-7 binding site analyses revealed these CDR1as/miR-7 interaction to be characterized by a non-basepaired “bulged” region at the central part of the duplex [24]. In contrast, miR-671 was found to bind CDR1as/ciRS-7 via one almost perfect complementary binding site [69,70]. These data have shaped the hypothesis of CDR1as densely binding and storing or transporting miR-7, until *Argonaut 2* (Ago2) protein leads to an endonucleolytic slicing in a miR-671-mediated manner [23,24,70]. The downregulation of the circRNA causes the release of the miR-7 cargo, thus allowing the regulation of its targets [24,45,70]. The endogenous circRNA *Sry* was proposed to function as a circRNA sponge as it contains 16 binding sites for miR-138 [24]. These exemplary results not only confirm endogenous circRNAs to function as molecular sponges modulating the availability and function of miRNAs (Figure 3D), but also indicate their importance for normal cell functions and emphasize the capabilities of circRNAs for molecular biology, medicine, and pharmaceutical science.

Artificial circular RNAs

Therapeutic applications of artificial circRNAs

Naturally occurring circRNAs are described as particularly stable molecules with a wide range of characterized functions [18,43,48,51,54]. Artificial circRNAs have only recently been considered as a new therapeutic strategy to combat human diseases, like viral infections or cancer [71,72]. To date, potential applications of artificial circRNAs enclose (i) templates for exogenous protein generation [73,74], (ii) aptamers or protein sponges [75,76] and (iii) sponges sequestering miRNAs [71,72,77].

Initial analyses revealed the translation of engineered artificial circRNAs for exogenous protein generation within rabbit reticulocyte lysates to be feasible, but less efficient compared to linear control RNAs [13]. Hitherto, circRNAs were shown to allow robust protein synthesis in eukaryotic systems, thereby extending the duration of protein expression compared to full-length mRNA counterparts [73,78]. Engineering of translatable circRNAs thereby critically relies on the inclusion of an IRES element to initiate cap-independent translation and protein synthesis, both *in vitro* and *in vivo* [13,74]. Different types of IRES elements (e.g. deriving from different viruses) were shown to determine circRNA translation efficiency, as well as cell/tissue-specificity [74]. The IRES element derived from the *encephalomyocarditis virus* (EMCV) was found to be most efficient [74]. Artificial circRNAs are

believed to be effective templates for the expression of therapeutic proteins [73,74].

Resembling endogenous circRNAs that act as molecular sponges, artificial circRNAs perturbing protein functions were designed. As demonstrated by Litke and Jaffrey in 2019, short circularized RNA aptamers inhibit *Nuclear Factor kappa B* (NF- κ B) signalling in *Interleukin-1 β* (IL-1 β) treated *human embryonic kidney cells* (HEK293). Circularization enhanced the stability and improved the effectiveness of the NF- κ B-pathway-inhibiting aptamers compared to their linear counterparts [75]. The *heterogeneous nuclear ribonucleoprotein L* (hnRNP L), a classic RBP involved in the regulation of alternative splicing, was recently targeted using artificial circRNAs [76]. Relying on the hnRNP L binding motif, Schreiner *et al.* evaluated numerous types of artificial circRNAs, containing CA-repeat or CA-rich sequence clusters, varying in length and production-strategy. These were shown to specifically bind to hnRNP L, thereby efficiently inactivating the RBP and modulating the alternative splicing pattern of target transcripts comparable to a siRNA-mediated hnRNP L knockdown [76]. These results highlight the use of artificial circRNAs, designed for the sequestration of proteins mis-regulated in regards to pathogenic mechanisms, as potential therapeutic strategy in molecular biology and medicine.

This thesis focuses on the usage of artificial *circular RNA sponges* (ciRS) sequestering and functionally inhibiting

mature miRNAs related to human disease. The joined work of the research groups of *Oliver Rossbach* and *Michael Niepmann* first utilized the *Hepatitis C virus* (HCV) replication as model system in a proof-of-principle study [79]. The hepatocyte specific miRNA miR-122 binds to two distinct binding sites at the 5'-end of the positive-sense single-stranded RNA virus genome [80,81]. Thereby, the viral RNA is protected from exonucleolytic degradation, and viral translation as well as replication is enhanced, consequently facilitating HCV propagation [81–84]. Miravirsin (SPC3649; Roche, Switzerland), the first *locked nucleic acid* (LNA)-containing antisense miRNA drug, has been shown to functionally sequester miR-122 and inhibit viral propagation in patients by decreasing virus titers to non-detectable levels within phase II clinical trials [85,86]. Artificial *circular RNA sponges* (ciRS) containing eight miRNA binding sites were demonstrated to be a novel and cost-effective complementary approach to efficiently bind and sequester cellular miR-122 in *in vitro* and *in vivo* studies, thereby reducing viral intracellular protein levels similar to Miravirsin [79]. The artificial circRNAs used can be turned over within standard cellular RNA decay mechanism as they do not contain any synthetic nucleotides [79]. The potential risk of hepatotoxic side effects, as reported for unmetabolized nucleotides of LNA contained in anti-miRNA drugs like Miravirsin [87], is diminished [79]. Upon transfection into *human hepatocellular carcinoma* (HuH-7.5) cells, these circRNAs were detectable within both the nucleus and the cytoplasm, and

particularly more stable than their linear counterparts [79]. The combination of Northern blot and stemloop-primer-mediated RT and qPCR analyses revealed the steady-state miR-122 levels to be unaltered after treatment with artificial circRNAs and demonstrated the circRNAs applied to efficiently sequester miR-122 by significantly reducing accessible miR-122 molecules within HuH-7.5 cells [79]. As part of the present work, our group designed, produced and analysed artificial circular RNA sponges targeting miR-21 within an interdisciplinary collaboration project with the groups of *Stefan Hüttelmaier* (Institute of Molecular Medicine, Martin Luther University Halle-Wittenberg) and *Achim Aigner* (Department of Clinical Pharmacology, Leipzig University). MiR-21 was one of the earliest identified oncogenic miRNAs, as it was shown to be upregulated in numerous pathological conditions, including cancer, and was found to be the most abundant miRNA across cancer transcriptomes [71,88,89]. The oncogenic characteristics of miR-21 are widely attributed to repressing a plethora of tumour suppressor-encoding mRNAs, resulting in proliferation, apoptosis and invasion, in this way pathophysiologically fostering carcinogenesis [88,90,91]. Within a xenograft mouse model, the specific knockout of MIR21 enforced the expression of tumor suppressive miR-21 targets and resulted in reduced tumour growth [71]. Artificial ciRS containing four perfectly complementary or bulged binding sites for miR-21 (ciRS-21-bu or ciRS-21-comp) were produced and characterized within the work presented

here to impair miR-21 functions [71]. Cellular decay analyses revealed the circularization to substantially increase the intracellular stability of ciRS as the half-lives of artificial ciRS significantly exceeded those of their linear counterparts [71]. We demonstrated the sequestration of miR-21 by ciRS-21-bu and ciRS-21-comp to be specific compared to non-miRNA binding random controls (ciRS-21-rnd) based on *in vivo* miR-21/ciRS-21 interaction assays relying on RNA affinity purifications [71]. Sequestration of miR-21 by ciRS-21-bu and ciRS-21-comp led to an upregulation of known miR-21 targets, thereby causing a significant reduction in cell proliferation as well as invasion of 3D spheroid model systems (robotics microscopy platform, Stefan Hüttelmaier, University Halle) and resulting in the significant inhibition of tumor growth in a lung adenocarcinoma xenograft mouse model (animal facility, Achim Aigner, University Leipzig) [71]. In a related study, *Liu* and colleagues sequestered miR-21 in gastric cancer cell lines using circRNAs which led to elevated apoptosis levels and induced expression of miR-21 repressed proteins [72]. As critically discussed by *Oliver Rossbach* in 2019, within that study the authors did not provide essential controls, e.g. interaction assays providing that the observed effects are caused by the specific interaction of miR-21 and the engineered circRNA [92]. Within a recent study, *Lavenniah et al.* engineered ciRS to target the cardiac pro-hypertrophic miRNAs, miR-132 and miR-212 [93,94]. The artificial ciRS competitively inhibited the miRNAs of interest, thereby attenuating

hypertrophic disease characteristics and preserving cardiac function in mice [93]. The *in vitro* efficacy of synthetic ciRS inhibiting miRNA function was higher compared to standard antagomiRs [93]. As circular miRNA sponges provide the possibility to target any miRNA of interest, the use of artificial ciRS represents a widespread and powerful therapeutic technology that is broadly applicable.

Production and purification of artificial circRNAs

Both, the further analysis and ultimately the clinical use of artificial circRNAs targeting human disease critically require the production of circRNAs in large amounts. In general, within the past few years, a broad range of circRNA expression systems were established – both in cell culture (hereafter termed "*in vivo*") and in cell free systems (hereafter termed "*in vitro*"): The latter range from chemical and enzymatical circularization of linear RNA templates *in vitro* to producing circRNAs with specifically engineered overexpression vectors *in vivo*. However, state-of-the-art technologies for circRNA preparation include (i) engineered ribozymes [75], (ii) constructed autocatalytic group I introns [73,95–97] or (iii) enzymatic intramolecular transcript ligation using recombinant RNA ligases (Figures 4 and 5) [77,97].

In 2019, *Litke* and *Jaffrey* established the *Twister-optimized RNA for durable overexpression* (tornado) system for ribozyme-based production of circRNAs *in vivo* which is inspired by tRNA

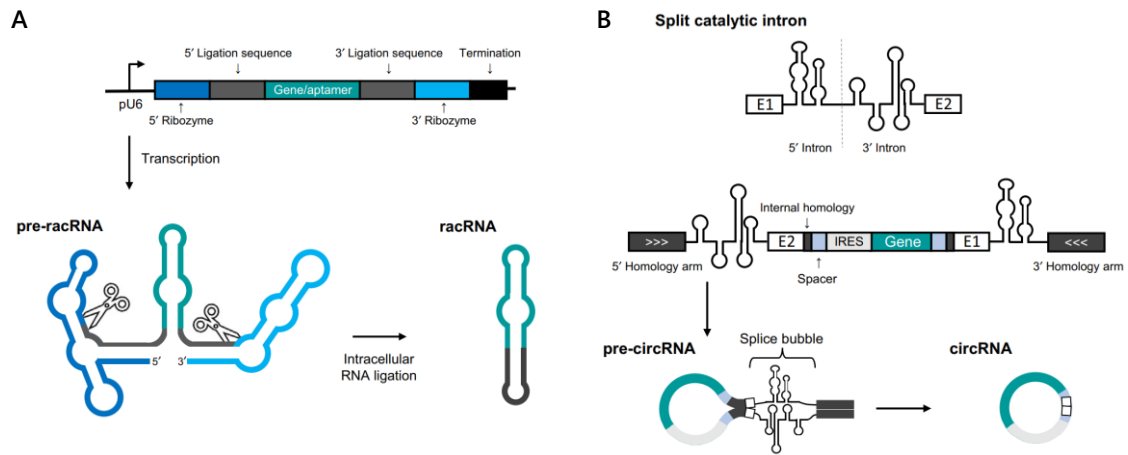


Figure 4: Tornado- and PIE-based strategies for generation of artificial circRNA. (A) Within *Twister-optimized RNA for durable overexpression* (Tornado) expression constructs, the sequence of interest (gene/aptamer) is flanked by both 5'- and 3' Ligation sequences as well as Twister ribozymes. Twister-mediated autocatalytic cleavage of *pre-ribozyme-assisted circular RNA* (pre-racRNA) provides a substrate for the intracellular RNA ligase RtcB, which mediates RNA circularization. Short racRNA aptamers are created. (B) Within the *permuted intron-exon* (PIE) splicing strategy, fused partial exons flanked by half-intron sequences of naturally occurring group I catalytic introns exhibit RNA circularization. Internal and terminal homology regions flanking the split autocatalytic introns, as well as permissive spacer elements, in sum, facilitate the circular splicing reaction of long transcripts. Introduction of an *internal ribosome entry site* (IRES) allows circRNA translation. (Adapted from Costello et al. 2019)

processing (Figure 4A) [75]. Naturally occurring tRNA splicing involves the cleavage of introns, resulting in 5' hydroxyl and 2',3'-cyclic phosphate ends that are subsequently recognized and ligated relying on the ubiquitous endogenous RNA ligase, RtcB [98–100]. Within the U6 promoter-driven tornado expression cassette, the sequence to be circularized is flanked by self-cleaving Twister ribozymes [75]. Twister ribozymes autocatalytically cleave the RNA, resulting in the same 5' hydroxyl and 2',3'-cyclic phosphate ends as found in tRNA processing [101]. Ligation of the RNA construct in an RtcB-dependent manner is facilitated, leading to *ribozyme-assisted circular RNA* (racRNA) (Figure 4A) [75]. In previous reports, hammerhead ribozyme-mediated RNA circularization

in vivo was decelerated by slow cleavage rates under physiological conditions. Twister ribozymes undergo autocatalysis several hundred-fold faster, thereby allowing high expression levels of racRNA [75,102–104]. Tornado-mediated racRNA expression was observed to be comparable with the expression levels of the 5.8S and 5S small RNAs in HEK293 cells, far exceeding naturally occurring amounts of circRNAs [75]. The authors report that the tornado expression system is feasible for any RNA of interest although initially introduced for the rapid circularization of small RNA aptamers. Introduction of RNA-based metabolite biosensors, e.g. fluorogenic RNA aptamers like Spinach or Broccoli, can be used to detect metabolite fluctuations in mammalian cells [75].

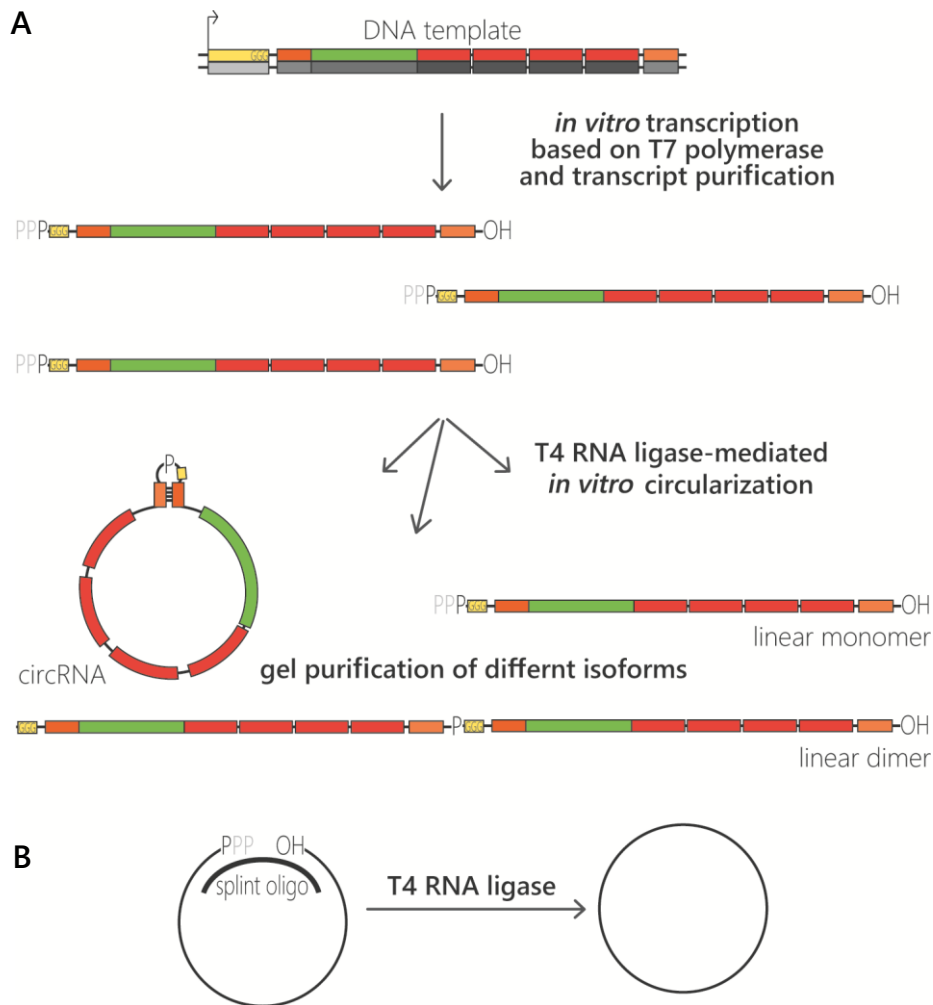


Figure 5: Enzyme-based *in vitro* production of artificial circRNAs. (A) T7 Polymerase-mediated transcription and subsequent ligation of purified transcripts based on the T4 RNA ligase is feasible for the production of circRNAs *in vitro*. Artificial circular miRNA sponges may contain multiple miRNA binding sites for the sequestration of a miRNA of interest (red), as well as a sequence tag (constant region; green), universal for all circRNAs analysed. As the enzymatic ligation reaction results in mixture of intramolecularly-ligated circRNAs, intermolecularly-ligated linear transcript dimers or non-ligated linear monomers, circularization efficiency is increased by the introduction of a short double-stranded stem-loop sequences (11 nt; orange). Subsequently, the circRNA is separated from the linear products and purified by polyacrylamide-urea gel electrophoresis. (B) Alternatively, also the use of splint oligonucleotides may favor intramolecular transcript ligation. (Modified from Breuer et al. 2020)

Wesselhoeft and colleagues recently optimized the *permuted intron-exon* (PIE) self-splicing strategy – first described in 1992 [95] – for *in vitro* circularization, utilizing run-off transcription, autocatalytic group I intron-mediated circularization and circRNA purification [73]. The engineered group I catalytic

introns consist of fused partial exons flanked by half-intron sequences, and undergo two transesterification reactions, therewith excising the fused exons as covalently linked (5'-3' linkage) circRNAs (Figure 4B) [73,95,97]. Despite the initially used permuted group I catalytic intron of the *thymidylate*

synthase (Td) gene of the T4 phage, as described elsewhere [96,105], an alternative group I catalytic intron from the *Anabaena* pre-tRNA was reported to be superior [73,95]. When including 5' and 3' homology arms flanking the split autocatalytic introns, as well as short internal homology domains, and permissive spacer elements within the sequence to be circularized, circularization of long transcripts (up to 5 kb in length) can be achieved (Figure 4B) [73]. Comparison of five different RNA sequences revealed that long RNAs were less efficiently circularized and more prone to nicking in the presence of magnesium ions, compared to shorter RNAs. Exogenous circRNAs harbouring a full length EMCV-IRES were generated based on the PIE strategy and showed efficient translation in mammalian HEK293 cells, leading to a robust protein production comparable to linear mRNAs [73].

CircRNAs can also be generated by enzymatic RNA ligation [97]. Exemplifying the production of artificial circRNA sponges for miRNA sequestration, as part of this work, our group promulgated a technique for the efficient production and purification of circRNAs relying on enzymatic activity *in vitro* (Figure 5A) [77]. Linearized DNA templates, including T7 promoter sequences, were transcribed relying on the recombinant T7 RNA polymerase [77]. The transcription reaction is performed in presence of a 10-fold excess of *guanosine 5'-monophosphate* (GMP) to obtain mainly GMP-primed transcripts [77], therewith circumventing two additional enzymatic

steps of transcript de- and rephosphorylation, as described in other protocols [97,106,107]. Subsequently, transcripts were purified via RQ1 DNase digestion and gel filtration and subjected to enzymatic RNA ligation using the T4 RNA ligase (Figure 5A). Increased reaction volumes with small concentrations of the nucleic acids circularized and the inclusion of complementary terminal double-stranded stem-loop sequences enhanced circularization efficiencies [77,97]. Complementary base-pairing in a short stem-loop structure provides proximity of the 5'-phosphate and 3'-hydroxyl ends, thereby facilitating the catalysation of the intramolecular phosphodiester bond formation during enzymatic RNA ligation (Figure 5A) [77,97]. Instead of utilizing such terminal stem-loop sequences, comparable efficiencies can be reached by DNA splint oligonucleotides annealing at both ends of the linear RNA (Figure 5B) [97]. The circRNA production is easily adaptable to any sequence of interest by altering the composition of the DNA template used. The incorporation of miRNA binding sites into the DNA template ultimately allows the circRNAs to sequester miRNAs of interest as previously described for circRNA sponges (Figure 5A) [71,77,79]. A sequence tag, universal for all circRNAs analysed, may be used to monitor the produced circRNAs via various detection methods, including e.g. northern blotting or RT-PCR (Figure 5A) [77]. Our described technique typically yields approximately 80% circularization efficiency at RNA lengths of 200 nucleotides [77].

In contrast to *in vivo* techniques, circRNA production *in vitro* necessitates stringent purification of circular products. The purity of artificial circRNAs is crucial in order to avoid unspecific side effects [92]. Hence, by-products deriving from circRNA productions must be removed. PIE-derived circRNAs need to be purified from remaining introns and precursors, splicing intermediates, as well as linear RNA molecules [73,97,108]. In enzymatic ligations, non-ligated linear monomers or intermolecular-ligated linear di- or multimers need to be removed [77]. The denaturing polyacrylamide-urea gel system assess circularization efficiencies compared to the presence of linear by-products as well as circRNA quality and additionally allows circRNA purification via gel extraction as part of the method presented here [77,92]. Circular RNA isoforms were reported to migrate more slowly within increasing polyacrylamide concentrations, thereby permitting the discrimination of different RNA species [109]. The analysis of circularization reactions within polyacrylamide-urea gels of differing polyacrylamide concentrations allows the separation and distinction of linear and circular RNA isoforms [71,79]. Thus, circRNA extraction from polyacrylamide gels can be achieved [77]. Besides, preparative exoribonucleolytic *Ribonuclease R* (RNase R) treatment and *high-performance liquid chromatography* (HPLC) based size exclusion chromatography are feasible for the elimination of non-circular components

[73,108,110]. Several protocols suggest the removal of 5' phosphates from remaining free ends by using the alkaline phosphatase prior to utilization [108,110]. In accordance with the production and stringent purification, the circularity of the purified RNA needs to be verified. For this purpose, apart from analytic RNase R treatment and polyacrylamide-urea gels differing in polyacrylamide contents, RT-PCR or DNA-oligo-mediated RNase H-cleavage analyses are feasible [111]. In summary, the efficient purification of artificial circRNAs and the validation of their circularity are crucial prerequisites for the quality of subsequent experiments.

CircRNAs and Cellular Innate Immunity

There are two fundamental parameters crucially important for the fate of any pharmaceutical of interest: (i) the efficacy and (ii) the toxicity. As already described above, research within the past years has highlighted circRNAs as a novel, powerful and promising application for the treatment of human diseases. Besides circRNA translation [73] or protein sponging [76], artificial circRNAs were suggested as antisense approach to efficiently inhibit miRNA functions [71,79], therefore raising the interest of pharmaceutical science and medicine. Beyond these proposed implementations of synthetic circRNAs, one important question remains: Do artificial circRNAs provoke cellular antiviral innate immune response mechanisms?

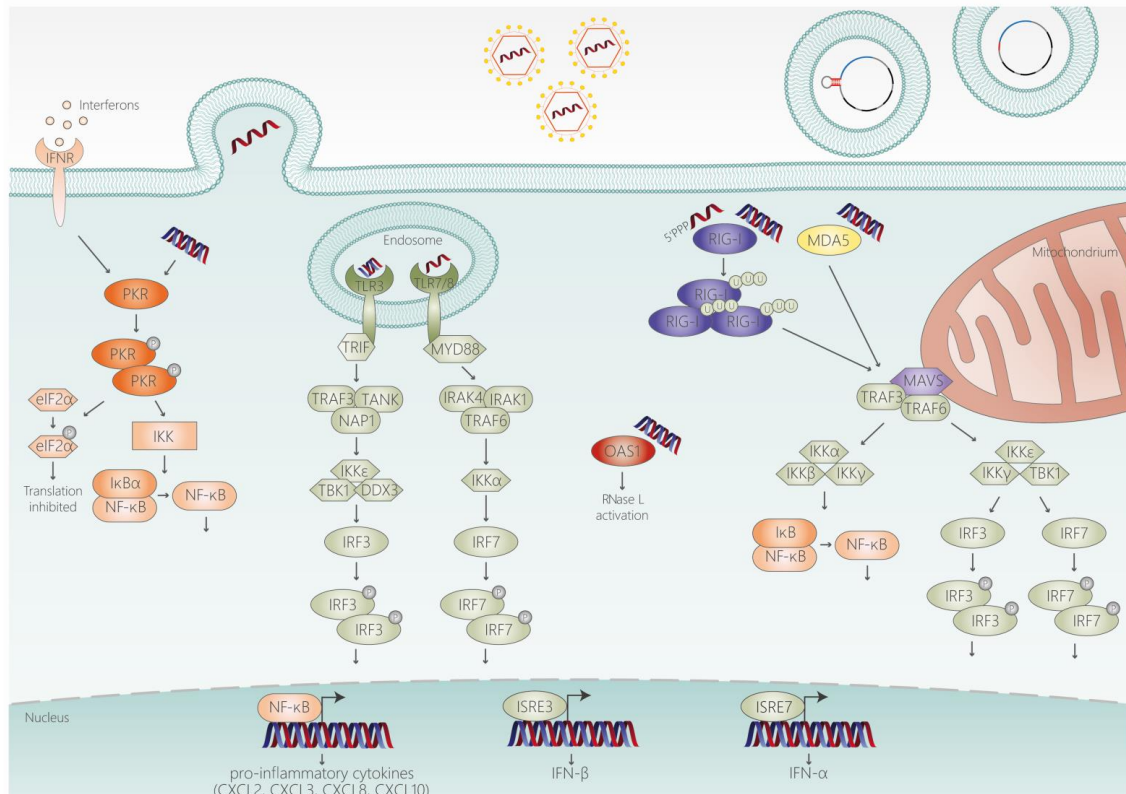


Figure 6: Foreign RNAs entering the cell - cellular innate immune response mechanisms. The cellular innate immune system of eukaryotic cells is able to detect invading pathogens as a first-line of defense. *Pathogen-associated molecular patterns* (PAMPs), like viral single- or double-stranded RNA within the endosome or cytoplasm, are recognized by cellular *pattern recognition receptors* (PRRs), including PKR, RIG-I, TLR3/7/8, OAS1 or MDA5. The stimulation of these RNA sensors leads to the activation of signalling pathways, ultimately leading to the induction of chemokines, cytokines and interferons. The cellular mechanisms detecting artificial circRNA molecules are a subject of current research and controversial discussion. (Breuer et al. 2022)

This question has recently been the subject of intense discussion [105,108,110]. In general, the human innate immune system is able to identify foreign RNAs – e.g. introduced by viral infections – via intracellular nucleic acid sensor molecules like *retinoic acid inducible gene 1* (RIG-I), PKR, *toll-like receptor 3/7/8* (TLR3/7/8), *melanoma differentiation-associated protein 5* (MDA5) or *2'-5'-oligoadenylate synthetase 1* (OAS1) [112,113]. The activation of signalling pathways ultimately leads to the induction of chemokines, cytokines and interferons (Figure 6) [112,113]. Analyses of common human anti-viral

RNA recognition pathways upon introduction of artificial circular RNAs arose with divergent results. In 2017, the group of *Howard Y. Chang* found that exogenous circRNAs, produced using a cell-free PIE-strategy, potently induce cellular innate immunity genes of mammalian cells. The authors postulated RIG-I to be required to sense foreign circRNA, based on luciferase reporter assays as well as RIG-I knockout in *Henrietta Lacks cervical cancer* (HeLa) and *mouse embryonic fibroblast* (MEF) cells [105]. However, circRNAs neither contain 5' triphosphate ends nor long and blunt-

ended double-stranded RNA duplexes, which were previously described as RIG-I ligands [114]. Utilization of human Alu repeats containing ZKSCAN1 introns abrogated the observed immune response within qRT-PCR analyses [105]. Thus, the splicing-mechanism was reported to discriminate endogenous and exogenous circRNAs, as RNA binding proteins deposited on the circRNA reflect its origin and biogenesis [105]. In strong contrast to these results by *Grace Y. Chen, Alexander Wesselhoeft* and colleagues demonstrated exogenous, and PIE-derived circRNAs to bypass the anti-viral innate immune response in RIG-I and TLR reporter cells and mice. Further examination revealed that the immunogenicity was critically dependent on circRNA purity [110]. The authors demonstrated *adenocarcinomic human alveolar basal epithelial* (A549) cells to robustly express *Interleukin-6* (IL-6), *Regulated on Activation, Normal T cell Expressed and Secreted* (RANTES) and *Interferon-gamma induced Protein 10 kD* (IP-10; CXCL10) after transfection of unpurified PIE self-splicing reactions, or precursor RNAs, but not after transfection with purified circRNAs [110]. Induction of the RNA sensor RIG-I and *Interferon-beta-1* (IFN- β 1) within A549 cells treated with purified circRNAs was weaker compared to cells transfected with unpurified PIE-derived self-splicing reactions or precursor RNAs. Since even minor amounts of contaminants robustly triggered the cellular immune response, the authors suggested that the immunogenicity after circRNA transfections reported earlier possibly derive from

5'-triphosphorylated linear RNA impurities within circRNA preparations [110]. Considering the potential therapeutic purposes of circRNAs, these data demonstrate the importance of further analyses of cellular innate immune response mechanisms to circRNAs. As part of this work, the anti-viral immunogenicity of artificial ciRS, previously used to efficiently sequester the oncogenic miR-21 [71], was examined as a consequence of liposome-based transfection in highly immuneresponsive A549 cells [115]. Produced *in vitro*, and stringently purified by polyacrylamide-urea gel extraction, artificial ciRS containing either a randomized control sequence (ciRS-21-random) or four bulged miRNA binding sites (ciRS-21-bulge) bypassed the cellular anti-viral immune response as evident from the mRNA levels of its downstream components [115]. Surprisingly, a highly double-stranded construct containing a randomized self-complementary sequence of 50 bp, ciRS-21-ds stimulated anti-viral responses to a comparable extent as *polyinosinic:polycytidylic acid* (Poly(I:C)) in a dose-dependent manner and induced the activation of the *double-stranded RNA* (dsRNA) sensor protein PKR in A549 cells [115]. Supporting our data, recent findings by *Ling-Ling Chen's* group presented the cellular immunogenicity to treatment with *in vitro* produced circRNAs to be distinctively relying on the production strategy as well as the structural conformation. CircRNAs generated by the T4 RNA ligase displayed minimized immunogenicity [116]. Interestingly, directly ligated circRNAs containing

short dsRNA-regions of 16-33 bp were presented as effective PKR inhibitors, thereby exhibiting higher suppressive effects on PKR activation *in vitro* and *in vivo* compared to commonly utilized chemical PKR inhibitors [116]. Adding to the discussion about impurity-based immunogenicity of *in vitro* generated circRNA, enzymatically ligated RNA circles were compared to those circularized via PIE-strategies. Permuted self-splicing introns, either deriving from T4 bacteriophage *thymidylate synthase* (td) introns or from *Anabaena* pre-tRNA group I introns, were used [116]. Although stringently purified, circRNAs produced by group I introns had an immunogenic effect in the cells used here, as introduced extraneous fragments (~74 nt T4 bacteriophage td introns or ~186 nt *Anabaena* pre-tRNA group I introns) affected circRNA secondary structures and provoked cellular anti-viral innate immune responses [116]. Even though PIE-derived circRNAs were non-immunogenic [110], the latest findings are in line with previous experiments indicating that these circRNAs induce cellular innate immunity genes [105,116].

Additionally, in 2019, *Chen et al.* identified m⁶A RNA modification as a marker of endogenous circRNAs that abrogated circRNA immunity, whereas unmodified circRNAs activated RIG-I and innate immune signalling [108]. Other nucleoside modifications such as *pseudouridine* (ψ), *5-methylcytidine* (m5C) or *N1-methyl-pseudouridine* (m1 Ψ) decreased immune-stimulatory effects of *in vitro* transcribed linear mRNAs *in*

vitro and *in vivo* [117–119]. Compared to non-modified RNAs, the modifications mentioned above prevented linear mRNAs from stimulating cellular RNA sensors such as TLR3, TLR7 and/or TLR8 [117–119]. The replacement of uridine with m1 Ψ in the *in vitro* transcribed mRNA vaccines encoding the SARS-CoV-2 spike protein increased translation efficiency but also diminished the activity of innate immune sensors therewith critically attributing the vaccine efficacy [120]. *Wesselhoeft* and colleagues found capped and polyadenylated unmodified linear mRNAs to provoke a greater cytokine response compared to unmodified circRNAs, whereas m1 Ψ -modified mRNAs and m1 Ψ -modified circRNAs showed similar cytokine release profiles in A549 cells [110]. As part of this thesis, enzymatically produced and stringently purified ciRS (ciRS-21-bulge and ciRS-21-randome), of about 200 nucleotides in length without any RNA modifications, were shown to bypass cellular anti-viral response mechanisms [115]. However, depending on the length and secondary structure of a circRNA of interest, introduction of nucleoside modifications could be a useful tool to prevent unwanted immune reactions, as indicated for linear mRNAs.

These results once more illustrate the importance of attentive engineering, choice of production strategy and purification of artificial circRNAs. In summary, the entirety of all properties of artificial circRNAs may be crucial for the immunogenic potential and therapeutic application, including (i) the designated production strategy, (ii) the

purity of the circRNA product, (iii) the secondary structure as well as (iv) the introduction of RNA modifications and (v) the dose of the circRNA administered [115]. Considering the potential biomedical applications of artificial circRNAs, the features described above could be contemplated to either specifically trigger or bypass the cellular innate immune system depending on the application.

Research objectives

With the aim of targeting miRNAs misregulated in the context of human diseases like viral infections or cancer, the three publications presented here focused on (i) the generation and characterization of artificial circRNAs as well as (ii) the application of artificial circRNAs as potential therapeutic strategy targeting a miRNA misregulated in cancer cells and (iii) the analysis of the influence of artificial circRNA sponges on the cellular antiviral innate immune response.

As most abundant miRNA across cancer transcriptomes, artificial circRNA sponges targeting miR-21 were generated and characterized as part of an interdisciplinary collaboration project with the groups of *Stefan Hüttelmaier* (Institute of Molecular Medicine, Martin Luther University Halle-Wittenberg) and *Achim Aigner* (Department of Clinical Pharmacology, Leipzig University). In a first step, a production technique relying on *in vitro* transcription and enzymatic RNA ligation was utilized to efficiently produce and stringently purify ciRS. Moreover, ciRS *in vivo* stability was addressed relying on northern blotting upon transfection of ES-2 cells allowing the analysis and quantification of RNA half-lives of circular versus linear RNA species. The specific interaction between endogenous miR-21 and artificial ciRS was pursued via pulldown analyses and miR-21 affinity purification assays *in vitro* and *in vivo*. Finally, the ciRS were used to functionally characterize the effects of ciRS-based miR-21 inactivation

within A549, H1975 and ES-2 3D tumour spheroids and A549 Xenograft mice in a collaborative effort *in situ*.

Based on these experiments and the efficacy of ciRS as a potential therapeutic, this work also focuses on the impact of artificial ciRS on the cellular immunogenicity – the latter being controversially debated within the literature. RNA-sequencing was utilized for global transcriptome analysis, aiming to obtain more insights on pathways activated upon liposome-based ciRS transfection into A549 cells. Next, immunestimulants were used as positive controls to induce a profound activation of the cellular innate immune system. Apart from using commercially available immunestimulants like Poly(I:C), a circRNA containing extensive double-stranded sequence elements was generated within this work. Real-time qPCR analyses were conducted to evaluate the induction of selected downstream mRNA candidates in a time- and dose-dependent manner. Finally, the activation of the ds-RNA sensor PKR upon ciRS treatment of A549 cells was examined by immunoblotting.

In sum, we have not only produced and characterized artificial circRNAs designed to specifically sequester the oncomiR-21, but also argued for their potential as a novel antisense approach bypassing the cellular anti-viral innate immune signalling pathways depending on their sequence composition and secondary structure.

References

- [1] Sanger H.L., Klotz G., Riesner D., Gross H.J., Kleinschmidt A.K. (1976) Viroids are single-stranded covalently closed circular RNA molecules existing as highly base-paired rod-like structures. *Proceedings of the National Academy of Sciences of the United States of America*, 73:3852–3856. DOI:10.1073/pnas.73.11.3852.
- [2] Hsu M.T., Coca-Prados M. (1979) Electron microscopic evidence for the circular form of RNA in the cytoplasm of eukaryotic cells. *Nature*, 280:339–340. DOI:10.1038/280339a0.
- [3] Kos A., Dijkema R., Arnberg A.C., van der Meide P.H., Schellekens H. (1986) The hepatitis delta (delta) virus possesses a circular RNA. *Nature*, 323:558–560. DOI:10.1038/323558a0.
- [4] Weiner A.J., Choo Q.L., Wang K.S., Govindarajan S., Redeker A.G., Gerin J.L., Houghton M. (1988) A single antigenomic open reading frame of the hepatitis delta virus encodes the epitope(s) of both hepatitis delta antigen polypeptides p24 delta and p27 delta. *Journal of virology*, 62:594–599. DOI:10.1128/jvi.62.2.594-599.1988.
- [5] Kjems J., Garrett R.A. (1988) Novel splicing mechanism for the ribosomal RNA intron in the archaeobacterium *desulfurococcus mobilis*. *Cell*, 54:693–703. DOI:10.1016/s0092-8674(88)80014-x.
- [6] Grabowski P.J., Zaug A.J., Cech T.R. (1981) The intervening sequence of the ribosomal RNA precursor is converted to a circular RNA in isolated nuclei of tetrahymena. *Cell*, 23:467–476. DOI:10.1016/0092-8674(81)90142-2.
- [7] Nigro J.M., Cho K.R., Fearon E.R., Kern S.E., Ruppert J., Oliner J.D., Kinzler K.W., Vogelstein B. (1991) Scrambled exons. *Cell*, 64:607–613. DOI:10.1016/0092-8674(91)90244-S.
- [8] Cocquerelle C., Daubersies P., Majérus M.A., Kerckaert J.P., Bailleul B. (1992) Splicing with inverted order of exons occurs proximal to large introns. *The EMBO Journal*, 11:1095–1098.
- [9] Patop I.L., Wüst S., Kadener S. (2019) Past, present, and future of circRNAs. *The EMBO Journal*, 38:e100836. DOI:10.15252/emboj.2018100836.
- [10] Cocquerelle C., Mascrez B., Héтуin D., Bailleul B. (1993) Mis-splicing yields circular RNA molecules. *FASEB journal : official publication of the Federation of American Societies for Experimental Biology*, 7:155–160. DOI:10.1096/fasebj.7.1.7678559.
- [11] Capel B., Swain A., Nicolis S., Hacker A., Walter M., Koopman P., Goodfellow P., Lovell-Badge R. (1993) Circular transcripts of the testis-determining gene Sry in adult mouse testis. *Cell*, 73:1019–1030. DOI:10.1016/0092-8674(93)90279-Y.

- [12] Dubin R.A., Kazmi M.A., Ostrer H. (1995) Inverted repeats are necessary for circularization of the mouse testis Sry transcript. *Gene*, 167:245–248. DOI:10.1016/0378-1119(95)00639-7.
- [13] Chen C.Y., Sarnow P. (1995) Initiation of protein synthesis by the eukaryotic translational apparatus on circular RNAs. *Science (New York, N.Y.)*, 268:415–417. DOI:10.1126/science.7536344.
- [14] Pasman Z., Been M.D., Garcia-Blanco M.A. (1996) Exon circularization in mammalian nuclear extracts. *RNA (New York, N.Y.)*, 2:603–610.
- [15] Schindewolf C., Braun S., Domdey H. (1996) In vitro Generation of a Circular Exon from a Linear Pre-mRNA Transcript. *Nucleic Acids Research*, 24:1260–1266. DOI:10.1093/nar/24.7.1260.
- [16] Zaphiropoulos P.G. (1996) Circular RNAs from transcripts of the rat cytochrome P450 2C24 gene: correlation with exon skipping. *Proceedings of the National Academy of Sciences of the United States of America*, 93:6536–6541. DOI:10.1073/pnas.93.13.6536.
- [17] Zaphiropoulos P.G. (1997) Exon skipping and circular RNA formation in transcripts of the human cytochrome P-450 2C18 gene in epidermis and of the rat androgen binding protein gene in testis. *Molecular and cellular biology*, 17:2985–2993. DOI:10.1128/mcb.17.6.2985.
- [18] Jeck W.R., Sorrentino J.A., Wang K., Slevin M.K., Burd C.E., Liu J., Marzluff W.F., Sharpless N.E. (2013) Circular RNAs are abundant, conserved, and associated with ALU repeats. *RNA (New York, N.Y.)*, 19:141–157. DOI:10.1261/rna.035667.112.
- [19] Salzman J., Gawad C., Wang P.L., Lacayo N., Brown P.O. (2012) Circular RNAs are the predominant transcript isoform from hundreds of human genes in diverse cell types. *PLoS one*, 7:e30733. DOI:10.1371/journal.pone.0030733.
- [20] Salzman J., Chen R.E., Olsen M.N., Wang P.L., Brown P.O. (2013) Cell-type specific features of circular RNA expression. *PLoS genetics*, 9:e1003777. DOI:10.1371/journal.pgen.1003777.
- [21] Huang G., Li S., Yang N., Zou Y., Zheng D., Xiao T. (2017) Recent progress in circular RNAs in human cancers. *Cancer letters*, 404:8–18. DOI:10.1016/j.canlet.2017.07.002.
- [22] Wang P.L., Bao Y., Yee M.-C., Barrett S.P., Hogan G.J., Olsen M.N., Dinneny J.R., Brown P.O., Salzman J. (2014) Circular RNA is expressed across the eukaryotic tree of life. *PLoS one*, 9:e90859. DOI:10.1371/journal.pone.0090859.
- [23] Memczak S., Jens M., Elefsinioti A., Torti F., Krueger J., Rybak A., Maier L., Mackowiak S.D., Gregersen L.H.,

- Munschauer M., Loewer A., Ziebold U., Landthaler M., Kocks C., Le Noble F., Rajewsky N. (2013) Circular RNAs are a large class of animal RNAs with regulatory potency. *Nature*, 495:333–338. DOI:10.1038/nature11928.
- [24] Hansen T.B., Jensen T.I., Clausen B.H., Bramsen J.B., Finsen B., Damgaard C.K., Kjems J. (2013) Natural RNA circles function as efficient microRNA sponges. *Nature*:384–388. DOI:10.1038/nature11993.
- [25] Westholm J.O., Miura P., Olson S., Shenker S., Joseph B., Sanfilippo P., Celniker S.E., Graveley B.R., Lai E.C. (2014) Genome-wide analysis of drosophila circular RNAs reveals their structural and sequence properties and age-dependent neural accumulation. *Cell reports*, 9:1966–1980. DOI:10.1016/j.celrep.2014.10.062.
- [26] Rybak-Wolf A., Stottmeister C., Glažar P., Jens M., Pino N., Giusti S., Hanan M., Behm M., Bartok O., Ashwal-Fluss R., Herzog M., Schreyer L., Papavasileiou P., Ivanov A., Öhman M., Refojo D., Kadener S., Rajewsky N. (2015) Circular RNAs in the Mammalian Brain Are Highly Abundant, Conserved, and Dynamically Expressed. *Molecular cell*, 58:870–885. DOI:10.1016/j.molcel.2015.03.027.
- [27] Venø M.T., Hansen T.B., Venø S.T., Clausen B.H., Grebing M., Finsen B., Holm I.E., Kjems J. (2015) Spatio-temporal regulation of circular RNA expression during porcine embryonic brain development. *Genome biology*, 16:245. DOI:10.1186/s13059-015-0801-3.
- [28] You X., Vlatkovic I., Babic A., Will T., Epstein I., Tushev G., Akbalik G., Wang M., Glock C., Quedenau C., Wang X., Hou J., Liu H., Sun W., Sambandan S., Chen T., Schuman E.M., Chen W. (2015) Neural circular RNAs are derived from synaptic genes and regulated by development and plasticity. *Nature neuroscience*, 18:603–610. DOI:10.1038/nn.3975.
- [29] Berget S.M., Moore C., Sharp P.A. (1977) Spliced segments at the 5' terminus of adenovirus 2 late mRNA. *Proceedings of the National Academy of Sciences of the United States of America*, 74:3171–3175. DOI:10.1073/pnas.74.8.3171.
- [30] Chow L.T., Gelinas R.E., Broker T.R., Roberts R.J. (1977) An amazing sequence arrangement at the 5' ends of adenovirus 2 messenger RNA. *Cell*, 12:1–8. DOI:10.1016/0092-8674(77)90180-5.
- [31] Wilkinson M.E., Charenton C., Nagai K. (2020) RNA Splicing by the Spliceosome. *Annual review of biochemistry*, 89:359–388. DOI:10.1146/annurev-biochem-091719-064225.
- [32] Wahl M.C., Will C.L., Lührmann R. (2009) The spliceosome: design principles of a dynamic RNP

- machine. *Cell*, 136:701–718. DOI:10.1016/j.cell.2009.02.009.
- [33] Shi Y. (2017) Mechanistic insights into precursor messenger RNA splicing by the spliceosome. *Nature reviews. Molecular cell biology*, 18:655–670. DOI:10.1038/nrm.2017.86.
- [34] Hong X., Scofield D.G., Lynch M. (2006) Intron size, abundance, and distribution within untranslated regions of genes. *Molecular biology and evolution*, 23:2392–2404. DOI:10.1093/molbev/msl111.
- [35] Moore M.J., Sharp P.A. (1993) Evidence for two active sites in the spliceosome provided by stereochemistry of pre-mRNA splicing. *Nature*, 365:364–368. DOI:10.1038/365364a0.
- [36] Lim L.P., Burge C.B. (2001) A computational analysis of sequence features involved in recognition of short introns. *Proceedings of the National Academy of Sciences of the United States of America*, 98:11193–11198. DOI:10.1073/pnas.201407298.
- [37] Yoshimoto R., Kataoka N., Okawa K., Ohno M. (2009) Isolation and characterization of post-splicing lariat-intron complexes. *Nucleic Acids Research*, 37:891–902. DOI:10.1093/nar/gkn1002.
- [38] Pan Q., Shai O., Lee L.J., Frey B.J., Blencowe B.J. (2008) Deep surveying of alternative splicing complexity in the human transcriptome by high-throughput sequencing. *Nature genetics*, 40:1413–1415. DOI:10.1038/ng.259.
- [39] Wang E.T., Sandberg R., Luo S., Khrebtkova I., Zhang L., Mayr C., Kingsmore S.F., Schroth G.P., Burge C.B. (2008) Alternative isoform regulation in human tissue transcriptomes. *Nature*, 456:470–476. DOI:10.1038/nature07509.
- [40] Ule J., Blencowe B.J. (2019) Alternative Splicing Regulatory Networks: Functions, Mechanisms, and Evolution. *Molecular cell*, 76:329–345. DOI:10.1016/j.molcel.2019.09.017.
- [41] Zheng C.L., Fu X.-D., Gribskov M. (2005) Characteristics and regulatory elements defining constitutive splicing and different modes of alternative splicing in human and mouse. *RNA (New York, N.Y.)*, 11:1777–1787. DOI:10.1261/rna.2660805.
- [42] Zhang Y., Xue W., Li X., Zhang J., Chen S., Zhang J.-L., Yang L., Chen L.-L. (2016) The Biogenesis of Nascent Circular RNAs. *Cell reports*, 15:611–624. DOI:10.1016/j.celrep.2016.03.058.
- [43] Ashwal-Fluss R., Meyer M., Pamudurti N.R., Ivanov A., Bartok O., Hanan M., Evantal N., Memczak S., Rajewsky N., Kadener S. (2014) circRNA biogenesis competes with pre-mRNA splicing. *Molecular cell*, 56:55–66. DOI:10.1016/j.molcel.2014.08.019.

- [44] Starke S., Jost I., Rossbach O., Schneider T., Schreiner S., Hung L.-H., Bindereif A. (2015) Exon circularization requires canonical splice signals. *Cell reports*:103–111. DOI:10.1016/j.celrep.2014.12.002.
- [45] Wilusz J.E. (2018) A 360° view of circular RNAs: From biogenesis to functions. *Wiley interdisciplinary reviews. RNA*, 9:e1478. DOI:10.1002/wrna.1478.
- [46] Zhang Y., Zhang X.-O., Chen T., Xiang J.-F., Yin Q.-F., Xing Y.-H., Zhu S., Yang L., Chen L.-L. (2013) Circular intronic long noncoding RNAs. *Molecular cell*, 51:792–806. DOI:10.1016/j.molcel.2013.08.017.
- [47] Barrett S.P., Wang P.L., Salzman J. (2015) Circular RNA biogenesis can proceed through an exon-containing lariat precursor. *eLife*, 4:e07540. DOI:10.7554/eLife.07540.
- [48] D'Ambra E., Capauto D., Morlando M. (2019) Exploring the Regulatory Role of Circular RNAs in Neurodegenerative Disorders. *International journal of molecular sciences*, 20. DOI:10.3390/ijms20215477.
- [49] Tran A.M., Chalbatani G.M., Berland L., Cruz De Los Santos M., Raj P., Jalali S.A., Gharagouzloo E., Ivan C., Dragomir M.P., Calin G.A. (2020) A New World of Biomarkers and Therapeutics for Female Reproductive System and Breast Cancers: Circular RNAs. *Frontiers in cell and developmental biology*, 8:50. DOI:10.3389/fcell.2020.00050.
- [50] Zhang X.-O., Dong R., Zhang Y., Zhang J.-L., Luo Z., Zhang J., Chen L.-L., Yang L. (2016) Diverse alternative back-splicing and alternative splicing landscape of circular RNAs. *Genome research*, 26:1277–1287. DOI:10.1101/gr.202895.115.
- [51] Eger N., Schoppe L., Schuster S., Laufs U., Boeckel J.-N. (2018) Circular RNA Splicing. *Advances in experimental medicine and biology*, 1087:41–52. DOI:10.1007/978-981-13-1426-1_4.
- [52] Jeck W.R., Sharpless N.E. (2014) Detecting and characterizing circular RNAs. *Nature biotechnology*, 32:453–461. DOI:10.1038/nbt.2890.
- [53] Guo J.U., Agarwal V., Guo H., Bartel D.P. (2014) Expanded identification and characterization of mammalian circular RNAs. *Genome biology*, 15:409. DOI:10.1186/s13059-014-0409-z.
- [54] Ebbesen K.K., Kjems J., Hansen T.B. (2016) Circular RNAs: Identification, biogenesis and function. *Biochimica et biophysica acta*, 1859:163–168. DOI:10.1016/j.bbagr.2015.07.007.
- [55] Holdt L.M., Kohlmaier A., Teupser D. (2018) Molecular roles and function of circular RNAs in eukaryotic cells. *Cellular and molecular life sciences : CMLS*, 75:1071–1098. DOI:10.1007/s00018-017-2688-5.

- [56] Li Z., Huang C., Bao C., Chen L., Lin M., Wang X., Zhong G., Yu B., Hu W., Dai L., Zhu P., Chang Z., Wu Q., Zhao Y., Jia Y., Xu P., Liu H., Shan G. (2015) Exon-intron circular RNAs regulate transcription in the nucleus. *Nature structural & molecular biology*, 22:256–264. DOI:10.1038/nsmb.2959.
- [57] Legnini I., Di Timoteo G., Rossi F., Morlando M., Briganti F., Sthandier O., Fatica A., Santini T., Andronache A., Wade M., Laneve P., Rajewsky N., Bozzoni I. (2017) Circ-ZNF609 Is a Circular RNA that Can Be Translated and Functions in Myogenesis. *Molecular cell*, 66:22–37.e9. DOI:10.1016/j.molcel.2017.02.017.
- [58] Pamudurti N.R., Bartok O., Jens M., Ashwal-Fluss R., Stottmeister C., Ruhe L., Hanan M., Wyler E., Perez-Hernandez D., Ramberger E., Shenzis S., Samson M., Dittmar G., Landthaler M., Chekulaeva M., Rajewsky N., Kadener S. (2017) Translation of CircRNAs. *Molecular cell*, 66:9–21.e7. DOI:10.1016/j.molcel.2017.02.021.
- [59] Yang Y., Fan X., Mao M., Song X., Wu P., Zhang Y., Jin Y., Yang Y., Chen L.-L., Wang Y., Wong C.C., Xiao X., Wang Z. (2017) Extensive translation of circular RNAs driven by N6-methyladenosine. *Cell research*, 27:626–641. DOI:10.1038/cr.2017.31.
- [60] Schneider T., Hung L.-H., Schreiner S., Starke S., Eckhof H., Rossbach O., Reich S., Medenbach J., Bindereif A. (2016) CircRNA-protein complexes: IMP3 protein component defines subfamily of circRNPs. *Scientific reports*, 6:31313. DOI:10.1038/srep31313.
- [61] Stagsted L.V., Nielsen K.M., Dugaard I., Hansen T.B. (2019) Noncoding AUG circRNAs constitute an abundant and conserved subclass of circles. *Life science alliance*, 2. DOI:10.26508/lsa.201900398.
- [62] Ho-Xuan H., Glažar P., Latini C., Heizler K., Haase J., Hett R., Anders M., Weichmann F., Bruckmann A., van den Berg D., Hüttelmaier S., Rajewsky N., Hackl C., Meister G. (2020) Comprehensive analysis of translation from overexpressed circular RNAs reveals pervasive translation from linear transcripts. *Nucleic Acids Research*, 48:10368–10382. DOI:10.1093/nar/gkaa704.
- [63] Schneider T., Bindereif A. (2017) Circular RNAs: Coding or noncoding? *Cell research*, 27:724–725. DOI:10.1038/cr.2017.70.
- [64] Du W.W., Fang L., Yang W., Wu N., Awan F.M., Yang Z., Yang B.B. (2017) Induction of tumor apoptosis through a circular RNA enhancing Foxo3 activity. *Cell death and differentiation*, 24:357–370. DOI:10.1038/cdd.2016.133.
- [65] Abdelmohsen K., Panda A.C., Munk R., Grammatikakis I., Dudekula D.B., De S., Kim J., Noh J.H., Kim K.M., Martindale J.L., Gorospe M. (2017) Identification of

- HuR target circular RNAs uncovers suppression of PABPN1 translation by CircPABPN1. *RNA biology*, 14:361–369. DOI:10.1080/15476286.2017.1279788.
- [66] Liu C.-X., Li X., Nan F., Jiang S., Gao X., Guo S.-K., Xue W., Cui Y., Dong K., Ding H., Qu B., Zhou Z., Shen N., Yang L., Chen L.-L. (2019) Structure and Degradation of Circular RNAs Regulate PKR Activation in Innate Immunity. *Cell*, 177:865-880.e21. DOI:10.1016/j.cell.2019.03.046.
- [67] Ebert M.S., Sharp P.A. (2010) Emerging roles for natural microRNA sponges. *Current biology* : CB, 20:R858-61. DOI:10.1016/j.cub.2010.08.052.
- [68] Hentze M.W., Preiss T. (2013) Circular RNAs: splicing's enigma variations. *The EMBO Journal*, 32:923–925. DOI:10.1038/emboj.2013.53.
- [69] Hansen T.B., Wiklund E.D., Bramsen J.B., Villadsen S.B., Statham A.L., Clark S.J., Kjems J. (2011) miRNA-dependent gene silencing involving Ago2-mediated cleavage of a circular antisense RNA. *The EMBO Journal*, 30:4414–4422. DOI:10.1038/emboj.2011.359.
- [70] Piwecka M., Glažar P., Hernandez-Miranda L.R., Memczak S., Wolf S.A., Rybak-Wolf A., Filipchyk A., Klironomos F., Cerda Jara C.A., Fenske P., Trimbuch T., Zywitza V., Plass M., Schreyer L., Ayoub S., Kocks C., Kühn R., Rosenmund C., Birchmeier C., Rajewsky N. (2017) Loss of a mammalian circular RNA locus causes miRNA deregulation and affects brain function. *Science (New York, N.Y.)*, 357. DOI:10.1126/science.aam8526.
- [71] Müller S., Wedler A., Breuer J., Glaß M., Bley N., Lederer M., Haase J., Misiak C., Fuchs T., Ottmann A., Schmachtel T., Shalamova L., Ewe A., Aigner A., Rossbach O., Hüttelmaier S. (2020) Synthetic circular miR-21 RNA decoys enhance tumor suppressor expression and impair tumor growth in mice. *NAR Cancer*, 2. DOI:10.1093/narcan/zcaa014.
- [72] Liu X., Abraham J.M., Cheng Y., Wang Z., Wang Z., Zhang G., Ashktorab H., Smoot D.T., Cole R.N., Boronina T.N., DeVine L.R., Talbot C.C., Liu Z., Meltzer S.J. (2018) Synthetic Circular RNA Functions as a miR-21 Sponge to Suppress Gastric Carcinoma Cell Proliferation. *Molecular therapy. Nucleic acids*, 13:312–321. DOI:10.1016/j.omtn.2018.09.010.
- [73] Wesselhoeft R.A., Kowalski P.S., Anderson D.G. (2018) Engineering circular RNA for potent and stable translation in eukaryotic cells. *Nature communications*:2629. DOI:10.1038/s41467-018-05096-6.
- [74] Meganck R.M., Liu J., Hale A.E., Simon K.E., Fanous M.M., Vincent H.A., Wilusz J.E., Moorman N.J., Marzluff W.F., Asokan A. (2021) Engineering highly efficient backsplicing and translation of

- synthetic circRNAs. *Molecular therapy. Nucleic acids*, 23:821–834. DOI:10.1016/j.omtn.2021.01.003.
- [75] Litke J.L., Jaffrey S.R. (2019) Highly efficient expression of circular RNA aptamers in cells using autocatalytic transcripts. *Nature biotechnology*:667–675. DOI:10.1038/s41587-019-0090-6.
- [76] Schreiner S., Didio A., Hung L.-H., Bindereif A. (2020) Design and application of circular RNAs with protein-sponge function. *Nucleic Acids Research*, 48:12326–12335. DOI:10.1093/nar/gkaa1085.
- [77] Breuer J., Rossbach O. (2020) Production and Purification of Artificial Circular RNA Sponges for Application in Molecular Biology and Medicine. *Methods and protocols*, 3. DOI:10.3390/mps3020042.
- [78] Wang Y., Wang Z. (2015) Efficient backsplicing produces translatable circular mRNAs. *RNA (New York, N.Y.)*, 21:172–179. DOI:10.1261/rna.048272.114.
- [79] Jost I., Shalamova L.A., Gerresheim G.K., Niepmann M., Bindereif A., Rossbach O. (2018) Functional sequestration of microRNA-122 from Hepatitis C Virus by circular RNA sponges. *RNA biology*, 15:1032–1039. DOI:10.1080/15476286.2018.1435248.
- [80] Sarnow P., Sagan S.M. (2016) Unraveling the Mysterious Interactions Between Hepatitis C Virus RNA and Liver-Specific MicroRNA-122. *Annual review of virology*, 3:309–332. DOI:10.1146/annurevvirology-110615-042409.
- [81] Nieder-Röhrmann A., Dünnes N., Gerresheim G.K., Shalamova L.A., Herchenröther A., Niepmann M. (2017) Cooperative enhancement of translation by two adjacent microRNA-122/Argonaute 2 complexes binding to the 5' untranslated region of hepatitis C virus RNA. *The Journal of general virology*, 98:212–224. DOI:10.1099/jgv.0.000697.
- [82] Li Y., Masaki T., Yamane D., McGivern D.R., Lemon S.M. (2013) Competing and noncompeting activities of miR-122 and the 5' exonuclease Xrn1 in regulation of hepatitis C virus replication. *Proceedings of the National Academy of Sciences of the United States of America*, 110:1881–1886. DOI:10.1073/pnas.1213515110.
- [83] Henke J.I., Goergen D., Zheng J., Song Y., Schüttler C.G., Fehr C., Jünemann C., Niepmann M. (2008) microRNA-122 stimulates translation of hepatitis C virus RNA. *The EMBO Journal*, 27:3300–3310. DOI:10.1038/emboj.2008.244.
- [84] Machlin E.S., Sarnow P., Sagan S.M. (2011) Masking the 5' terminal nucleotides of the hepatitis C virus genome by an unconventional microRNA-target RNA complex. *Proceedings of the National Academy of Sciences of the United States of*

- America*, 108:3193–3198.
DOI:10.1073/pnas.1012464108.
- [85] Hildebrandt-Eriksen E.S., Aarup V., Persson R., Hansen H.F., Munk M.E., Ørum H. (2012) A locked nucleic acid oligonucleotide targeting microRNA 122 is well-tolerated in cynomolgus monkeys. *Nucleic acid therapeutics*, 22:152–161. DOI:10.1089/nat.2011.0332.
- [86] Janssen H.L.A., Reesink H.W., Lawitz E.J., Zeuzem S., Rodriguez-Torres M., Patel K., van der Meer A.J., Patick A.K., Chen A., Zhou Y., Persson R., King B.D., Kauppinen S., Levin A.A., Hodges M.R. (2013) Treatment of HCV infection by targeting microRNA. *The New England journal of medicine*, 368:1685–1694. DOI:10.1056/NEJMoa1209026.
- [87] Swayze E.E., Siwkowski A.M., Wancewicz E.V., Migawa M.T., Wyrzykiewicz T.K., Hung G., Monia B.P., Bennett C.F. (2007) Antisense oligonucleotides containing locked nucleic acid improve potency but cause significant hepatotoxicity in animals. *Nucleic Acids Research*, 35:687–700. DOI:10.1093/nar/gkl1071.
- [88] Feng Y.-H., Tsao C.-J. (2016) Emerging role of microRNA-21 in cancer. *Biomedical reports*, 5:395–402. DOI:10.3892/br.2016.747.
- [89] Kumarswamy R., Volkmann I., Thum T. (2011) Regulation and function of miRNA-21 in health and disease. *RNA biology*, 8:706–713. DOI:10.4161/rna.8.5.16154.
- [90] Feng Y.-H., Wu C.-L., Tsao C.-J., Chang J.-G., Lu P.-J., Yeh K.-T., Uen Y.-H., Lee J.-C., Shiau A.-L. (2011) Deregulated expression of sprouty2 and microRNA-21 in human colon cancer: Correlation with the clinical stage of the disease. *Cancer biology & therapy*, 11:111–121. DOI:10.4161/cbt.11.1.13965.
- [91] Fulci V., Chiaretti S., Goldoni M., Azzalin G., Carucci N., Tavolaro S., Castellano L., Magrelli A., Citarella F., Messina M., Maggio R., Peragine N., Santangelo S., Mauro F.R., Landgraf P., Tuschl T., Weir D.B., Chien M., Russo J.J., Ju J., Sheridan R., Sander C., Zavolan M., Guarini A., Foà R., Macino G. (2007) Quantitative technologies establish a novel microRNA profile of chronic lymphocytic leukemia. *Blood*, 109:4944–4951. DOI:10.1182/blood-2006-12-062398.
- [92] Rossbach O. (2019) Artificial Circular RNA Sponges Targeting MicroRNAs as a Novel Tool in Molecular Biology. *Molecular therapy. Nucleic acids*, 17:452–454. DOI:10.1016/j.omtn.2019.06.021.
- [93] Lavenniah A., Luu T.D.A., Li Y.P., Lim T.B., Jiang J., Ackers-Johnson M., Foo R.S.-Y. (2020) Engineered Circular RNA Sponges Act as miRNA Inhibitors to Attenuate Pressure Overload-Induced Cardiac Hypertrophy. *Molecular therapy : the journal of the American Society of Gene*

- Therapy*, 28:1506–1517.
DOI:10.1016/j.ymthe.2020.04.006.
- [94] Ucar A., Gupta S.K., Fiedler J., Erikci E., Kardasinski M., Batkai S., Dangwal S., Kumarswamy R., Bang C., Holzmann A., Remke J., Caprio M., Jentzsch C., Engelhardt S., Geisendorf S., Glas C., Hofmann T.G., Nessling M., Richter K., Schiffer M., Carrier L., Napp L.C., Bauersachs J., Chowdhury K., Thum T. (2012) The miRNA-212/132 family regulates both cardiac hypertrophy and cardiomyocyte autophagy. *Nature communications*, 3:1078. DOI:10.1038/ncomms2090.
- [95] Puttaraju M., Been M.D. (1992) Group I permuted intron-exon (PIE) sequences self-splice to produce circular exons. *Nucleic Acids Research*, 20:5357–5364. DOI:10.1093/nar/20.20.5357.
- [96] Ford E., Ares M. (1994) Synthesis of circular RNA in bacteria and yeast using RNA cyclase ribozymes derived from a group I intron of phage T4. *Proceedings of the National Academy of Sciences of the United States of America*, 91:3117–3121. DOI:10.1073/pnas.91.8.3117.
- [97] Petkovic S., Müller S. (2015) RNA circularization strategies in vivo and in vitro. *Nucleic Acids Research*, 43:2454–2465. DOI:10.1093/nar/gkv045.
- [98] Laski F.A., Fire A.Z., RajBhandary U.L., Sharp P.A. (1983) Characterization of tRNA precursor splicing in mammalian extracts. *J. biol. chem.*, 258:11974–11980.
- [99] Filipowicz W., Shatkin A.J. (1983) Origin of splice junction phosphate in tRNAs processed by HeLa cell extract. *Cell*, 32:547–557. DOI:10.1016/0092-8674(83)90474-9.
- [100] Tanaka N., Chakravarty A.K., Maughan B., Shuman S. (2011) Novel mechanism of RNA repair by RtcB via sequential 2',3'-cyclic phosphodiesterase and 3'-Phosphate/5'-hydroxyl ligation reactions. *J. biol. chem.*, 286:43134–43143. DOI:10.1074/jbc.M111.302133.
- [101] Roth A., Weinberg Z., Chen A.G.Y., Kim P.B., Ames T.D., Breaker R.R. (2014) A widespread self-cleaving ribozyme class is revealed by bioinformatics. *Nature chemical biology*, 10:56–60. DOI:10.1038/nchembio.1386.
- [102] Khvorova A., Lescoute A., Westhof E., Jayasena S.D. (2003) Sequence elements outside the hammerhead ribozyme catalytic core enable intracellular activity. *Nature structural biology*, 10:708–712. DOI:10.1038/nsb959.
- [103] La Peña M. de, Gago S., Flores R. (2003) Peripheral regions of natural hammerhead ribozymes greatly increase their self-cleavage activity. *The EMBO Journal*, 22:5561–5570. DOI:10.1093/emboj/cdg530.
- [104] Canny M.D., Jucker F.M., Kellogg E., Khvorova A., Jayasena

- S.D., Pardi A. (2004) Fast cleavage kinetics of a natural hammerhead ribozyme. *Journal of the American Chemical Society*, 126:10848–10849. DOI:10.1021/ja046848v.
- [105] Chen Y.G., Kim M.V., Chen X., Batista P.J., Aoyama S., Wilusz J.E., Iwasaki A., Chang H.Y. (2017) Sensing Self and Foreign Circular RNAs by Intron Identity. *Molecular cell*, 67:228-238.e5. DOI:10.1016/j.molcel.2017.05.022.
- [106] Harris M.E., Christian E.L. (1999) Use of circular permutation and end modification to position photoaffinity probes for analysis of RNA structure. *Methods (San Diego, Calif.)*, 18:51–59. DOI:10.1006/meth.1999.0756.
- [107] Petkovic S., Müller S. (2013) RNA self-processing: formation of cyclic species and concatemers from a small engineered RNA. *FEBS letters*, 587:2435–2440. DOI:10.1016/j.febslet.2013.06.013.
- [108] Chen Y.G., Chen R., Ahmad S., Verma R., Kasturi S.P., Amaya L., Broughton J.P., Kim J., Cadena C., Pulendran B., Hur S., Chang H.Y. (2019) N6-Methyladenosine Modification Controls Circular RNA Immunity. *Molecular cell*, 76:96-109.e9. DOI:10.1016/j.molcel.2019.07.016.
- [109] Tabak H.F., van der Horst G., Smit J., Winter A.J., Mul Y., Groot Koerkamp M.J. (1988) Discrimination between RNA circles, interlocked RNA circles and lariats using two-dimensional polyacrylamide gel electrophoresis. *Nucleic Acids Research*, 16:6597–6605. DOI:10.1093/nar/16.14.6597.
- [110] Wesselhoeft R.A., Kowalski P.S., Parker-Hale F.C., Huang Y., Bisaria N., Anderson D.G. (2019) RNA Circularization Diminishes Immunogenicity and Can Extend Translation Duration In Vivo. *Molecular cell*, 74:508-520.e4. DOI:10.1016/j.molcel.2019.02.015.
- [111] Costello A., Lao N.T., Barron N., Clynes M. (2020) Reinventing the Wheel: Synthetic Circular RNAs for Mammalian Cell Engineering. *Trends in biotechnology*, 38:217–230. DOI:10.1016/j.tibtech.2019.07.008.
- [112] Schlee M., Hartmann G. (2016) Discriminating self from non-self in nucleic acid sensing. *Nature reviews. Immunology*, 16:566–580. DOI:10.1038/nri.2016.78.
- [113] Pindel A., Sadler A. (2011) The role of protein kinase R in the interferon response. *Journal of interferon & cytokine research : the official journal of the International Society for Interferon and Cytokine Research*, 31:59–70. DOI:10.1089/jir.2010.0099.
- [114] Lu C., Xu H., Ranjith-Kumar C.T., Brooks M.T., Hou T.Y., Hu F., Herr A.B., Strong R.K., Kao C.C., Li P. (2010) The structural basis of 5' triphosphate double-stranded RNA recognition by RIG-I C-terminal domain. *Structure*, 18:1032–1043. DOI:10.1016/j.str.2010.05.007.

- [115] Breuer J., Barth P., Noe Y., Shalamova L., Goesmann A., Weber F., Rossbach O. (2022) What goes around comes around: artificial circular RNAs bypass cellular antiviral responses. *Molecular therapy. Nucleic acids*. DOI:10.1016/j.omtn.2022.04.017.
- [116] Liu C.-X., Guo S.-K., Nan F., Xu Y.-F., Yang L., Chen L.-L. (2021) RNA circles with minimized immunogenicity as potent PKR inhibitors. *Molecular cell*. DOI:10.1016/j.molcel.2021.11.019.
- [117] Karikó K., Buckstein M., Ni H., Weissman D. (2005) Suppression of RNA recognition by Toll-like receptors: the impact of nucleoside modification and the evolutionary origin of RNA. *Immunity*, 23:165–175. DOI:10.1016/j.immuni.2005.06.008.
- [118] Karikó K., Weissman D. (2007) Naturally occurring nucleoside modifications suppress the immunostimulatory activity of RNA: implication for therapeutic RNA development. *Current opinion in drug discovery & development*, 10:523–532.
- [119] Durbin A.F., Wang C., Marcotrigiano J., Gehrke L. (2016) RNAs Containing Modified Nucleotides Fail To Trigger RIG-I Conformational Changes for Innate Immune Signaling. *mBio*, 7. DOI:10.1128/mBio.00833-16.
- [120] Morais P., Adachi H., Yu Y.-T. (2021) The Critical Contribution of Pseudouridine to mRNA COVID-19 Vaccines. *Frontiers in cell and developmental biology*, 9:789427. DOI:10.3389/fcell.2021.789427.

Published Articles

Production and Purification of Artificial Circular RNA Sponges for Application in Molecular Biology and Medicine

Janina Breuer and Oliver Rossbach*

Institute of Biochemistry, Faculty of Biology and Chemistry, University of Giessen, Heinrich-Buff-Ring 17, D-35392 Giessen, Germany

*To whom correspondence should be addressed: oliver.rossbach@bc.jlug.de; Tel.: +49-641-99-35-422

Abstract: Characterized by their covalently closed structure and thus an elevated stability compared to linear RNA molecules, circular RNAs (circRNAs) form a novel class of mainly non-coding RNAs. Although the biological functions of naturally occurring circRNAs are largely unknown, they were reported to act as molecular sponges, sequestering microRNAs (miRNAs), resulting in a de-repression of target mRNAs. Taking these characteristics of naturally occurring circRNAs into account, artificial circRNAs could be a potential tool in molecular biology and medicine. Using the Hepatitis C virus (HCV) as a model system, this application of artificial circular RNAs was demonstrated. The virus requires cellular miRNA miR-122 for its life cycle, and circRNAs specifically engineered to efficiently sequester this miRNA impacted viral propagation. Since in this context the production of engineered circRNA remains the limiting factor, we present a method to produce and efficiently purify artificial circRNA sponges (ciRS) *in vitro*. In this protocol we provide insights into a small-scale and large-scale production technique of artificial circular RNA sponges relying on *in vitro* transcription and RNA ligation.

This publication represents a component of my doctoral (Dr. rer. nat.) thesis in the Faculty of Biology and Chemistry at the Justus Liebig-University Giessen, Germany. Published in: *Methods and Protocols*, doi:10.3390/mps3020042 (2020). Received: 27 April 2020; Accepted: 22 May 2020.

1. Introduction

Circular RNAs (circRNAs) form a novel class of mainly non-coding RNAs. Naturally occurring circRNAs arise by an alternative splicing mechanism termed “backsplicing” [1] or “head-to-tail-splicing” [2]. A splice donor is covalently joined to an upstream instead of a downstream splice acceptor site relying on canonical splicing signals [1–5]. Therefore, a circularized RNA molecule is created,

which has neither a 5' cap nor a 3' poly(A) tail, but forms a covalently closed structure. This conformation appears to make circRNAs resistant to exonucleolytic degradation, resulting in an elevated stability compared to linear RNAs [1,6]. The first evidence of the existence of circRNAs was reported in 1976, demonstrating plant viroid genomes are composed of single-stranded covalently closed RNA molecules [7]. After their discovery,

circRNAs were underestimated as events of aberrant splicing with neglectable biological relevance, and only few candidates of naturally occurring circular RNA, such as SRY, ETS-1, and DCC, were found [6,8–10]. Since 2012, advances in RNA sequencing (RNA-seq) methodologies and bioinformatics have gained novel insights into the circRNA world by identifying thousands of human exonic circRNAs [1,11,12]. To not only identify, but rather increase the functional understanding of circRNAs, a broad range of circRNA expression systems was established. Relying on specifically designed overexpression vectors, desired circRNAs can be produced in cell culture (hereafter termed “*in vivo*”) by both a spliceosome-dependent exon circularization strategy [2,13,14] and a spliceosome-independent strategy based on engineered ribozymes derived from the tRNA splicing machinery (e.g., the “tornado” system) [15]. Additionally, strategies relying on circRNA production via cell-free systems (hereafter termed “*in vitro*”) using recombinant phage RNA polymerase-mediated transcription and circularization by either employing genetically engineered autocatalytic group I introns (e.g., the permuted exon-intron (PEI) system) [14,16–18] or enzymatic intramolecular transcript ligation using recombinant RNA ligases [14,19] gained importance to further characterize circRNA utilities.

Although the biological functions of endogenous circRNAs are still largely unknown, there are several lines of evidence showing that circRNAs have

diverse important regulatory and developmental roles [2,12,20–22]. In this context, the cellular circRNA CDR1as/ciRS-7 was identified as a molecular sponge or decoy sequestering the cytoplasmic miRNA miR-7 via 70 highly conserved binding sites [2,13]. The observed co-expression of CDR1as/ciRS-7 with miR-7 in neocortical and hippocampal neurons leads to a suppression of miR-7 functions, thereby de-repressing natural miR-7 targets. CDR1as/ciRS-7 knockout mice display misregulation of other miRNAs, dysfunctional synaptic transmission, and sensorimotor gating, which has also been associated with human neuropsychiatric disorders. These results indicate the importance of CDR1as/miR-7-interactions for normal brain functions [23]. Furthermore, circRNAs have been shown to act as sponges for RNA-binding proteins (RBPs), as well as nuclear transcriptional regulators—illustrating their relevance in the context of the regulatory networks governing gene expression [22,24,25].

Considering these functions and characteristics of naturally occurring circRNAs, artificial circRNAs could be a potential tool for molecular biology and medicine applied for the development of new strategies to combat human diseases such as viral infections or cancer. In this context, our laboratory utilized the Hepatitis C virus (HCV) as a model system in a proof of principle study. The single-stranded RNA genome of the hepatocyte-specific virus is bound by miR-122 at two distinct binding sites at its 5'-end (besides others), thereby protecting the viral

RNA from exonucleolytic degradation and enhancing viral translation. Sequestration of miR-122 had already been shown to inhibit viral propagation in patients using the first locked nucleic acid (LNA)-containing antisense miRNA drug (Miravirsen). As a novel complementary approach, artificial circular RNA sponges (ciRS) produced as described in this protocol, were shown to efficiently bind and sequester the cellular miR-122 *in vitro* and *in vivo*. When transfected into cells, these circRNAs are both present in the nucleus and the cytoplasm, and are more stable than their linear counterparts [19].

With the aim of targeting miRNAs misregulated within human diseases, artificial circular RNA sponges represent an efficiently functioning and inexpensive alternative to commercially available LNA-containing anti-miRNA drugs. Furthermore, circular RNA sponges facilitate functional analyses of cellular miRNAs by sequestration comparable to siRNA-based approaches to decrease the target mRNA level. However, since the production of engineered circRNA remains the limiting factor, this protocol provides insights into an efficient production technique of artificial circular RNA sponges relying on *in vitro* transcription and RNA ligation suitable for small and middle-sized RNAs. In this article, a small-scale as well as a large-scale production procedure will be described, typically yielding up to 20 µg and 350 µg of artificial circular RNA sponges, respectively.

2. Experimental Design

2.1. Materials

2.1.1. Kits and Enzymes

- HiScribe T7 High Yield RNA Synthesis Kit (New England Biolabs; Ipswich, MA, USA; Cat. no.: E2040S)
- Ribonuclease R (Lucigen Corporation, Middleton, WI, USA; Cat. no.: RNR07250)
- RNaseOUT Recombinant Ribonuclease Inhibitor (Thermo Fisher Scientific, Waltham, MA, USA; Cat. no.: 10777019)
- RQ1 RNase-free DNase (Promega Corporation; Madison, WI, USA; Cat. no.: M6101)
- T4 RNA Ligase (Thermo Fisher Scientific, Waltham, MA, USA; Cat. no.: EL0021)

2.1.2. Reagents

- Adenosine triphosphate (ATP; Roche Diagnostics GmbH, Basel, Switzerland; Cat. no. 11140965001)
- Dithiothreitol (DTT; 100 mM; Thermo Fisher Scientific, Waltham, MA, USA; Cat. no.: R0862)
- Ethidium bromide solution 1% (Carl Roth GmbH + Co. KG, Karlsruhe, Germany; Cat. no.: 2218.1)
- Guanosine 5'-monophosphate disodium salt hydrate (GMP; Merck

KGaA; Darmstadt, Germany; Cat. no.: G8377)

- Lipofectamine 2000 Transfection Reagent (Thermo Fisher Scientific, Waltham, MA, USA; Cat. no.: 11668027)
- Polyethylenimine (Merck KGaA; Darmstadt, Germany; Cat. no.: 764604-1G)
- SYBR Gold Nucleic Acid Gel Stain (Thermo Fisher Scientific, Waltham, MA, USA; Cat. no.: S11494)

2.1.3. Buffers

- Urea solution (50% urea (w/v) in 1 × Tris-Borate-EDTA (TBE))
- 20% denaturing polyacrylamide solution (20% polyacrylamide (19:1 acrylamide/bisacrylamide) in 1× TBE containing 50% urea (w/v))
- 10 × circRNA annealing buffer (100 mM Tris pH 7.5, 500 mM NaCl)
- Formamide loading buffer (1 × TBE, 90% formamide, 0.05% bromphenol blue (w/v), 0.05% xylene cyanol (w/v))
- PK buffer (100 mM Tris/HCl pH 7.5, 150 mM NaCl, 12.5 mM EDTA, 1% SDS)

▲ Ensure used materials are RNase-free prior to use.

2.2. Equipment

- Bunsen burner

- Corning Costar Spin-X Plastic Centrifuge Tube Filters (Merck KGaA; Darmstadt, Germany Cat. no.: CLS8160)
- Eppendorf Tubes 5.0 mL Snap cap (Eppendorf AG, Hamburg, Germany; Cat. no.: 0030119401)
- mini Quick Spin RNA Columns (Merck KGaA; Darmstadt, Germany Cat. no.: 11814427001)
- Phase Lock Gel Heavy 2 mL Tubes (QuantaBio; Beverly, MA, USA; Cat. no.: 2302830)
- Pre-coated TLC plates CEL 400-10 UV254 (Macherey Nagel GmbH & Co. KG; Düren, Deutschland; Cat. no.: 808083)
- Sterican Gr. 18, G 26 × 1"/ø 0,45 × 25 mm (B. Braun Melsungen AG, Melsungen, Germany; Cat. no.: 4657683)

3. Procedure

3.1. Engineering of Templates for Artificial Circular RNA Sponges

1. Design of microRNA binding sites.

The initial design of the miRNA binding sites present in the circular RNA sponges, or the corresponding control sequences, is crucial to the procedure. Therefore, several features and limitations have to be considered. The goal is to design an array of miRNA binding sites that is specific for binding to the miRNA of interest, has sufficient thermodynamic stability to be able to compete with the endogenous miRNA targets, and is able to harbour the

maximum number of binding sites without impairing *in vitro* circularization.

- *Number of miRNA binding sites:* The natural prototype of a circular miRNA sponge, ciRS-7/CDR1as, has ~70 miR-7 binding sites [2,13]. This large number cannot be recapitulated in artificial circRNAs. The main reasons are on one hand, the transcript size impairing the circularisation efficiency and on the other hand, the repetitive nature of these arrays interfering with most procedures in molecular biology, such as cloning, PCR or Sanger sequencing. Therefore, we found that an array of 4 to 8 miRNA binding sites is optimal for the production of artificial circular RNA sponges. Furthermore, as eight binding sites impaired efficient circularization, four binding sites were used in this protocol. Despite sharing the same basic structure as used by Jost et al. 2018, this protocol is based on the production of two exemplary ciRS (construct A and construct B) containing four binding sites for an miRNA of interest and differing in the presence of a double-stranded stem-loop sequence (see Section 3.1., paragraph 2.) [19]. Another benefit is that a sequence stretch containing four typical miRNA binding sites (including spacing and flanking restriction sites) can be easily ordered via DNA oligonucleotide synthesis. These 4-binding site arrays can subsequently be multimerized by cloning or *in vitro* ligation. Generally, shorter transcripts tend to circularize

more efficiently compared to longer RNAs.

- *Binding site spacing:* Besides the sequence composition and thus degree of complementarity to the target miRNA, the optimal spacing of miRNA binding sites is considered here. Based on analyses of natural miRNA:mRNA interactions (16–20 nt between seed sequences; [26]), a spacing of 4 nt between binding sites was chosen, resulting in a distance of 19 nt between the adjacent miRNA seed sequences (Figure 1A).
- *Binding site types and specificity:* The configuration of the miRNA binding site itself is also an important feature (Figure 1B). In sequestration of miR-122 from HCV, a bulged binding site lacking complementarity at nucleotides 10–12 was most effective [19]. Although a perfectly complementary site might appear thermodynamically superior, the occurrence of miRNAs in a complex with Ago2 in the cytoplasm renders bulged binding sites most effective [19,27]. In addition, a perfectly complementary binding site is assumed to be cleaved by the miRNA-RISC complex [27,28], although we did not observe cleavage of the perfectly complementary binding sites in any circular RNA sponges in cells [19]. Another feature to consider is the complementarity at the miRNA 5' and 3' ends (Figure 1B, compare “bulged 1” and “bulged 2”). Base-paired ends of binding sites were reported to cause tailing or

trimming of the targeted miRNA, which can lead to miRNA degradation [29,30]. In the context of the miRNA sponges tested, we never observed tailing, trimming or degradation of miR-122 [19]. To test the specificity of the chosen miRNA binding sites and to prevent off-target effects, a

miRNA binding site can also be designed and/or tested using a publicly available bioinformatics tool tailored to generate and test artificial miRNA binding sites. The “miRNAsong” tool (MicroRNA SpONge Generator and tester) is a valuable resource in this regard [31].

ciRS array used in Jost et al.:

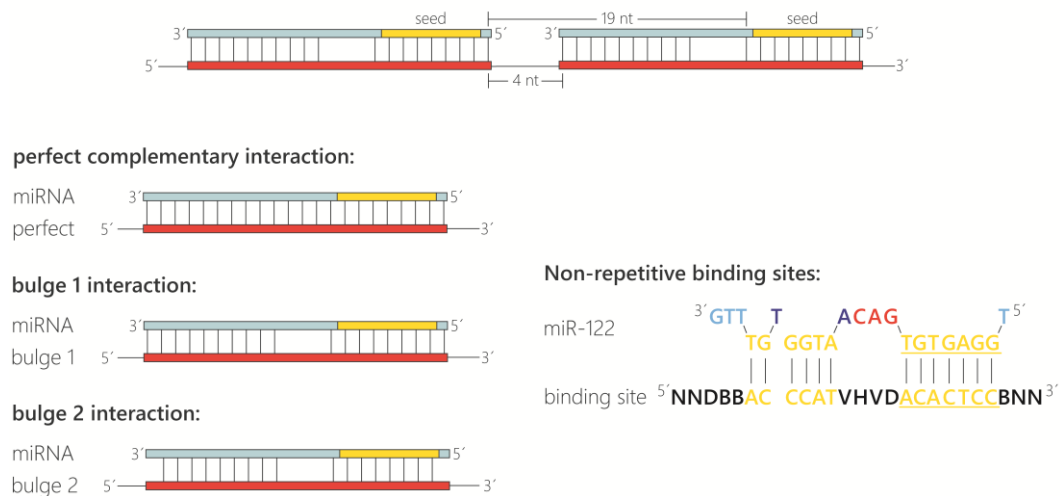


Figure 1. Design of miRNA binding sites contained in circular RNA sponges. (A) Representation of the ciRS array used by Jost et al. (2018) for sequestration of miR-122 (light blue). The array is characterized by miRNA binding sites (red) containing a bulge between nucleotides (nt) 10–12 and a spacing of 4 nt between binding sites resulting in a distance of 19 nt between the adjacent miRNA seed sequences (yellow). (B) Schematic representation of different potential miRNA binding sites with distinct complementarity to the target miRNA. (C) Non-repetitive miR-122 binding site for more efficient circularization.

- *Binding site repetitiveness for longer miRNA binding site arrays (OPTIONAL STEP):* In case longer stretches of miRNA binding site arrays are desired, the perfectly repetitive units of the binding sites and spacer sequences (described above; Figure 1A,B) are not feasible. A very effective approach to prevent repetitiveness and to allow gene synthesis of longer fragments is randomization of bases in the binding site that are not essential for

the interaction with the miRNA. Based on biophysical data obtained from the analysis of cellular miRNA:mRNA interactions [32], we determined the bases within miR-122 that are supposedly not essential for an efficient interaction and randomized them across an array of up to 20 binding sites. Including G:U wobble base-pairs in the non-seed interaction region may help to achieve a degree of sequence diversity for gene synthesis

approaches. Circularization efficiency was much higher with these randomized arrays compared to a similar number of repetitive binding site arrays. This approach might be useful for miRNA binding site arrays that compete with weaker endogenous sites, e.g., on cellular mRNAs, or when aiming to shift binding equilibria in the cell.

- *Negative controls:* The last important consideration, when designing circRNA sponges to sequester miRNAs, is the appropriate negative controls. Besides efforts to keep the length and overall base composition of the control sponges as similar as possible compared to the actual miRNA sponge, there are different concepts of control design. In Jost et al 2018, we used the actual binding site array and randomized the complete sequence stretch using publicly available sequence randomizers. To ensure no miR-122 binding sites were randomly generated, a sequence alignment of the miRNA on the randomized sequences was performed. Another approach that generates control binding sites with drastically reduced miRNA affinity is targeted mutation of the complete seed sequence (nt 2–8 of the miRNA). Note that seed mutant binding sites retain a certain non-canonical miRNA-binding activity [19]. Optimally, several different negative controls should be tested in an experimental set, since

unwanted secondary RNA structures generated by chance may impair the *in vitro* circularization efficiency.

2. *Template generation as starting point for ciRS production in vitro.* Conventionally, templates contain the following elements: a T7 promoter sequence for *in vitro* transcription, several binding sites complementary to the miRNA of interest, and optionally a double-stranded stem-loop sequence at the respective 5'- and 3'-termini to enhance circularization efficiency (Figure 2). The latter is characterized by a double-stranded stem of 11 nt with a non-basepaired overhang of 5 nt on both ends forming the open loop of 10 nt in total (contained in construct B, Figure 3). Despite using a double-stranded stem-loop, other circularization strategies (e.g., using splint oligonucleotides that anneal at both ends) can be used. Note that depending on, e.g., the length and sequence of individual templates, circularisation can also be observed for transcripts lacking the double-stranded stem-loop and without using a splint oligonucleotide (see Figure 3, construct A). Despite the mentioned features, we also typically include a region that is universal for all miRNA-sponge constructs and negative controls of a certain set ("constant region"), which serves as a binding site for PCR primers, antisense probes in northern blotting or *in situ* hybridization procedures. This region spans 63 nt in the templates used here. Moreover, it enables a reliable comparative

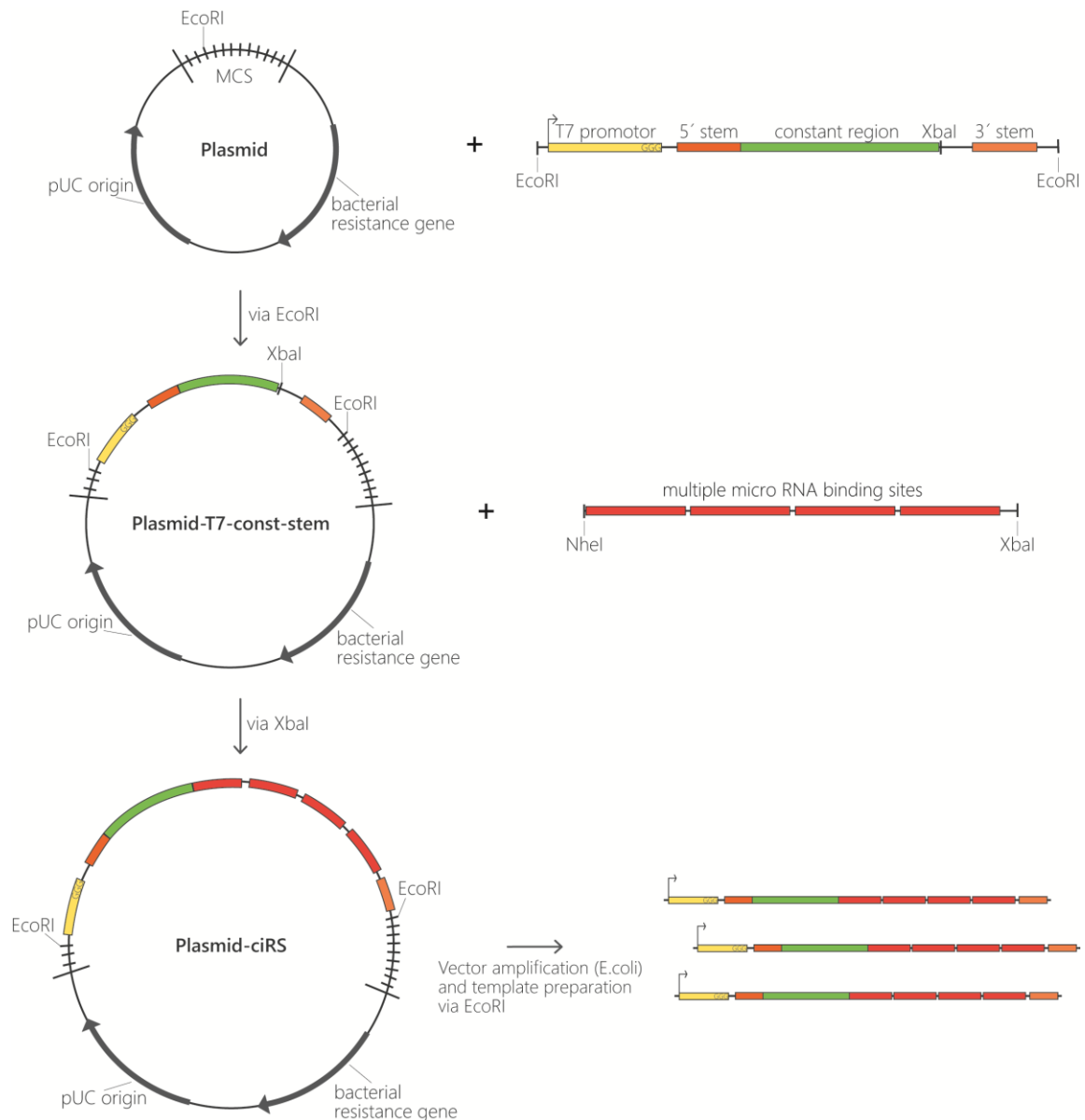


Figure 2. Template generation for ciRS production. Overview of cloning procedure for ciRS construction starting with insertion of the T7 promoter (yellow), a double-stranded stem-loop region (5' stem and 3' stem; orange), and a constant region (green) via EcoRI into a multipurpose vector backbone. Afterwards XbaI is used to insert the designed ciRS array consisting of multiple miRNA binding sites for the miRNA of interest. The final ciRS-vector is amplified, and templates are prepared.

quantification of different constructs. Adding flanking restriction sites enables cloning into a plasmid of choice. The upon request. Plasmids can be purified at a **large scale**, and the *in vitro* transcription template can be excised and gel-purified via agarose gel

electrophoresis (Figure 2). Afterwards, templates are subjected to *in vitro* transcription reaction.

▲ CRITICAL STEP: Unless described otherwise, all of the following procedures should be performed on ice!

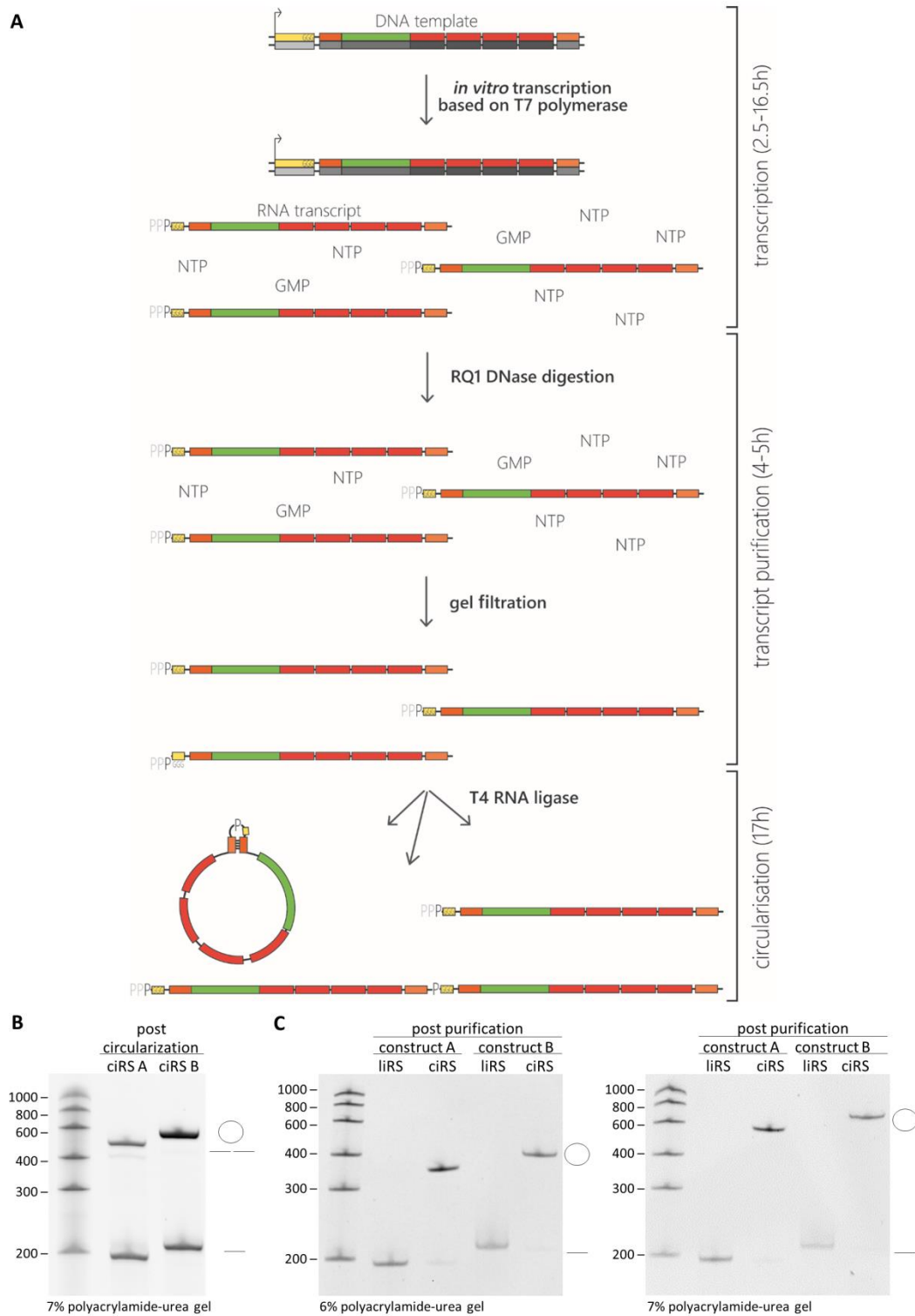


Figure 3. *In vitro* preparation of circular RNA sponges. (A) Schematic overview of the ciRS production procedure—starting with *in vitro* transcription with 10-fold excess of GMP, followed by DNase digestion to remove template DNA, gel filtration to clear away excess nucleotides (NTP, GMP) derived from the transcription reaction, and ligation of the purified transcript. Considering the activity of the T4 RNA ligase, transcript ligation can result in both linear monomers and dimers of the transcript and circularized transcripts (indicated by the dash/double dash or the circle in (B) and (C)). (B) *In vitro* circularisation reaction of two exemplary constructs was analysed by 7% polyacrylamide-urea gel electrophoresis, followed by

ethidium bromide staining showing linear and circular transcripts with a circularisation efficiency of ~ 40%–60% and only small amounts of linear dimers detectable. As described in Section 3.1, the transcripts are characterized by a constant region and four miRNA binding sites but differ in the presence of a double-stranded stem-loop region increasing the circularisation efficiency (construct A: 197 nt, lacking the 11 nt 3' stem-loop-sequence; construct B: 208 nt, with stem-loop). (C) Circular and linear isoforms of the RNA sponges (ciRS and liRS) were purified, and quality was verified on analytic 6% and 7% polyacrylamide-urea gels by ethidium bromide staining. While the mobility of linear RNAs remains unchanged compared to the RNA ladder, the mobility of circular RNA appears lower in higher percentage polyacrylamide-urea gels, resulting in a shift of the circular RNA when comparing the polyacrylamide-urea gels with different concentrations.

3.2. *In Vitro* Transcription. Time for Completion: 2.5–16.5 h

In vitro transcription is performed using the HiScribe T7 High Yield RNA Synthesis Kit and 10-fold excess of guanosine 5'-monophosphate (GMP). The GMP-initiated *in vitro* transcription aims to obtain mainly 5'-monophosphorylated linear RNA transcripts which can be directly used for RNA circularization. Since all T7 polymerase-created *in vitro* transcripts start with three guanosines, a stochastic subset of RNAs will be initiated with GMP instead of guanosintriphosphate (GTP) (Figure 3A). Thereby, the two enzymatic steps of de- and rephosphorylation used in other protocols are circumvented [14,33,34]. Assuming the active centre of the RNA-polymerase accepts GMP and GTP with the same affinity, transcription with 10-fold excess of GMP results in a mixture of total transcripts consisting of 90% monophosphate 5'ends. The latter can be subjected to circularization reaction using the T4 RNA ligase. Note that GMP cannot be used for the polymerization itself. The transcription reaction contains the following components: 1/10 vol. 10 × T7 Reaction Buffer, 10 mM final concentration of

ATP, GTP, CTP, and UTP (100 mM), 100 mM final concentration of GMP (400 mM), final concentration of 130 nM (**small scale**: 200 ng; **large scale**: 1 µg) of DNA template, and 1/10 vol. of T7 RNA Polymerase Mix (10×). Adjust to final volume with RNase-free water:

- **small scale**: prepare 20 µL total volume of the transcription reaction
 - **large scale**: prepare 100 µL total volume of the transcription reaction
- Incubate 2 h up to overnight at 37°C.

3.3. Transcript Purification. Time for Completion: Small Scale 4 h; Large Scale 5 h

1. DNase digestion to remove the template DNA (Figure 3A).

- **small scale**: Continue with RQ1 DNase digestion by adding 10 mM Dithiothreitol, 20 U RNaseOUT, 5 U RQ1 DNase, 10 × RQ1 DNase buffer to a final concentration of 1×, supplement to 100 µL with RNase-free water, and incubate 30 min at 37°C.
- **large scale**: Continue with RQ1 DNase digestion by adding 10 mM Dithiothreitol, 100 U RNaseOUT, 25 U RQ1 DNase, 10 × RQ1 DNase

buffer to a final concentration of 1×, supplement to 500 µL with RNase-free water, and incubate 1 h at 37°C.

2. *Phenol/Chloroform/Isoamylalcohol extraction to remove the enzymes.*

- **small scale:** For extraction, use RNase-free water to increase the reaction volume to 400–800 µL. Mix the sample with 1 volume Phenol/Chloroform/Isoamylalcohol (25:24:1), vortex, transfer into a Phase Lock Gel tube, and centrifuge 5 min, 20,000× g at room temperature. Transfer the aqueous upper phase into a new tube.
- **large scale:** Distribute RQ1-digested transcripts to two 2 mL tubes. For extraction, use RNase-free water to increase the reaction volume to 800 µL each. Mix each sample with 1 volume Phenol/Chloroform/Isoamylalcohol, vortex, transfer into Phase Lock Gel tubes, and centrifuge 5 min, 20,000× g at room temperature. Transfer each of the aqueous upper phases into a new tube.

3. *Ethanol or isopropanol precipitation to remove residual chloroform and salts.*

Ⓜ **PAUSE STEP:** Precipitate samples with 0.1 volumes 3 M NaAc (pH 6.5) and 2.5 volumes 100% ethanol or 0.7 volumes isopropanol at –20°C for at least 30 min to overnight. Centrifuge at 4°C for at least 20 min at 20,000× g. Wash the pellet with 70% ethanol and centrifuge again for 5 min, 20,000× g. Discard the supernatant completely, air dry the pellet briefly, and dissolve in 40 µL RNase-free water (**large scale:** 2 × 50 µL). **OPTIONAL STEP:** Mix 1% of the transcript with formamide

gel-loading buffer and verify RNA integrity on denaturing polyacrylamide gel.

4. *Size exclusion chromatography to remove excess nucleoside triphosphates* (Figure 3A). Apply sample onto mini Quick Spin RNA Columns following the manufacturer's instructions for gel filtration of the transcripts (**large scale:** use 2 columns per transcript); the sample volume increases to ~80 µL per column. Finally, measure the transcript concentration.

3.4. *In Vitro Circularization to Generate Circular RNA Sponges. Time for Completion: 17 h*

1. *Annealing of transcript ends.* Within the annealing reaction, the double-stranded stem-loop (if included) is formed (or a splint oligonucleotide complementary to both ends of the transcript is annealed), thereby bringing 5'- and 3'-ends into close proximity, promoting an efficient circularization. This, together with an increased ligation reaction volume used in the next step, additionally favours intramolecular over intermolecular ligation reactions. **OPTIONAL STEP:** In this step, addition of equimolar amounts of a splint oligonucleotide can be useful if no stem-loop structure was included in the construct.

Add 10× annealing buffer to a final concentration of 1× to purified transcripts and allow the annealing of the double-stranded stem-loop regions (or splint oligonucleotide) by incubating the samples for 2 min at 95°C and decreasing the temperature by

1°C/10 sec to 25°C within a thermocycler.

2. *In vitro* circularization: ligation of 5' and 3'-ends, thereby creating a covalently closed transcript.

- **small scale:** Add 0.99 volume RNase-free water, 0.28 volume 10× reaction buffer for T4 RNA ligase (25 µL, 1× in final volume), and 40 U RNaseOUT (2 µL, 6.25 U/µL in final volume) to annealed transcripts. The volume should be 202.5 µL. Incubate for 10 min at 37°C. Then, add 0.02 volume 10 mM ATP (5 µL, 0.2 mM in final volume), 0.15 volume DMSO (37.5 µL, 15% in final volume), and 50 U T4 RNA ligase (5 µL, 0.2 U/µL in final volume) for a total volume of 250 µL.
- **large scale:** Scale up the above reaction two-fold to a total volume of 500 µL.

Incubate at 16°C overnight. Considering the activity of the T4 RNA ligase, there are three possible scenarios: (i) the transcript is not ligated and remains a linear monomer, (ii) the transcripts are ligated in an intermolecular way, resulting in the formation of dimerized (or multimerized) linear transcripts or (iii) the transcript is ligated in an intramolecular way, forming a covalently closed circular RNA molecule (Figure 3A,B). Increased reaction volumes with small concentrations of nucleic acids to be circularized [14] — amongst other techniques given in this protocol — contribute to preferentially intramolecular ligation events. In this fashion, circularization efficiencies reach between 40% and 60%.

3.5. Purification of Circular RNA Sponges. Time for Completion: 12 h

1. **OPTIONAL STEP:** In small scale circRNA production procedures, the following gel purification may be omitted and a preparative RNase R exonuclease treatment may be performed to digest remaining linear molecules and obtain exclusively circular RNA (directly to step 3.4.6). Note that rare larger multimeric circular RNA ligation products and RNase R-resistant linear RNA molecules remain if gel purification is omitted.

2. *Phenol/Chloroform/Isoamylalcohol extraction and ethanol or isopropanol precipitation are performed to ensure the purity of the reaction as previously described in Section 3.2 point 2 and 3.* The RNA pellet is dissolved in 50 µL formamide gel-loading buffer (**large scale:** RNA pellet is dissolved in 2 × 100 µL formamide gel-loading buffer).

3. *Polyacrylamide-urea gel electrophoresis for quality control and circRNA purification.* While the mobility of linear RNAs within polyacrylamide-urea gels is proportional to an RNA standard, circular RNAs show an aberrant mobility. Due to their circular conformation, the migration of the latter within polyacrylamide-urea gels is much slower compared to their linear counterparts. This aberrant migration can be compared between polyacrylamide gels of different acrylamide content and allows distinguishing linear di- or multimers from circular RNA—detectable as a size shift. Generally, the polyacrylamide content of the gels is dependent on the

circRNA size. Referring to a circRNA size of ~200 nt, we recommend using 6% (300 V, 150 mA, 42 min) and 7% (300 V, 150 mA, 49 min) denaturing polyacrylamide gels, whereas circRNAs with a size of ~350 nt can be identified within 5% (300 V, 150 mA, 35 min) and 6% denaturing polyacrylamide gels. The optimal acrylamide concentrations should be determined experimentally for different RNA lengths. In order to analyse the circularization efficiency, 1% of the RNA transcript is loaded onto analytic denaturing polyacrylamide urea gels, followed by ethidium bromide (Figure 3B) or SYBR gold staining. The remaining 99% of the RNA mixture is loaded onto preparative denaturing polyacrylamide containing gel.

4. *RNA gel purification.* Visualization of RNA on a preparative gel is achieved by UV-shadowing upon transferring the gel onto a plastic-foil-wrapped thin-layer chromatography (TLC) plate coated with cellulose using a 254 nm fluorescent indicator. Irradiation with UV light at 254 nm excites the plate coating and results in a green fluorescence. The RNA on the contrary absorbs the UV light at this wavelength, casting a shadow against the fluorescent background. Note that the lower detection limit of this method is around 500 ng. Cut the circular RNA band (identified by the differential migration of circular RNA products in analytic gels of different acrylamide concentration) from the gel using a clean razor blade. ▲ **CRITICAL STEP**—In order to increase the RNA purification efficiency, the excised

polyacrylamide-urea gel fragments are to be crushed, as described in the following:

- **Small scale:** Take a 500 μ L safe-lock microcentrifuge tube. The latter is pierced in the centre of the bottom. A thin (e.g., 26 G) syringe needle is heated on a Bunsen burner flame to penetrate the plastic easily. In order to avoid injuries, we recommend extreme caution and suggest externally fixing the microcentrifuge tube in a tube stand within the course of piercing the tube, so no hands can be injured in the piercing process. Transfer the excised polyacrylamide-urea gel fragment into the pierced 500 μ L safe-lock microcentrifuge tube and insert the latter into a fresh 1.5 mL Eppendorf tube. Centrifuge for 1 min at 20,000 \times g to crush the gel. ① **PAUSE STEP:** Gel fragments can be stored at -80°C overnight. Add 400–800 μ L 1 \times PK-buffer to the crushed gel and incubate on a rotating wheel either overnight at room temperature or at 50°C for 1 h. Freezing (e.g., using dry ice or liquid nitrogen) and thawing may increase yields. Use Costar Spin-X centrifuge tube filters to remove gel pieces by centrifuging for 1 min at 20,000 \times g.
- **large scale:** Take a 15 mL Falcon tube, which is cleaved at the 3 mL sign using either strong scissors or a heated blade. In order to avoid injuries, we again recommend extreme caution and suggest externally fixing the tube within the course of cutting the tube, so no hands can be injured in the slicing process. The upper part of the tube is

discarded, whereas the bottom is subjected to the piercing procedure as described above for the 500 μ L tube. Transfer the excised polyacrylamide-urea gel fragment into the pierced lower 15 mL Falcon tube part and insert the latter into a fresh 5 mL Eppendorf tube. Centrifuge for 1 min at 20,000 \times g to crush the polyacrylamide-urea gel. **II PAUSE STEP:** Gel fragments can be stored at -80°C overnight. Add 8 mL 1 \times PK-buffer to crushed gel, transfer this to the 15 mL Falcon tube, and rotate on a wheel either overnight at room temperature or at 50°C for 1.5 h. Freezing with dry ice or liquid nitrogen and thawing in between may increase yields. Spin for 10 min at 20,000 \times g. Transfer the liquid into a fresh 15 mL tube, thereby preventing gel particle transfer.

5. *Phenol/Chloroform/Isoamylalcohol extraction and ethanol or isopropanol precipitation to purify and concentrate the produced circular RNAs.*

- **small scale:** Follow the protocol described in Section 3.2 point 2 and 3. Circular RNA pellet—regularly yielding up to 20 μ g of *in vitro*-produced artificial circular RNA—is dissolved in an appropriate amount of RNase-free water, typically 20 μ L.
- **large scale:** Precipitate 8 mL supernatant with 0.1 volume 3 M NaAc (pH 6.5) and 0.7 volume isopropanol overnight at -20°C . During the RNA precipitation procedure, residual SDS from the PK-buffer containing supernatant

may not be soluble at very low temperatures. Incubate the solution on a wheel at 4°C for 30 min. Afterwards, spin for 30 min at 20,000 \times g. Wash the pellet with 5 mL of 70% ethanol, spin for 5 min at 20,000 \times g, and take up RNA in 400 μ L RNase-free water. Use Costar Spin-X centrifuge tube filters to remove remaining gel fragments by centrifuging for 1 min at 20,000 \times g. Resulting artificial circular RNA sponges regularly yield up to 350 μ g, when preparation is conducted according to the large-scale protocol.

Measure the ciRS concentration. Assess the final circRNA quality, as mentioned previously, by loading 1% of the preparation onto denaturing polyacrylamide gels of various polyacrylamide contents, followed by ethidium bromide or SYBR Gold staining (Figure 3C). **II PAUSE STEP:** CiRS can be stored at -80°C . **▲ CRITICAL STEP:** Autohydrolysis of RNA is a stochastically occurring event causing a cleavage of RNA molecules at a random position. Subjection of linear RNA to autohydrolysis results in a fragmentation of the RNA molecule. The latter is detectable within analytic polyacrylamide-urea gels as a typical smear after ethidium bromide or SYBR Gold staining. CircRNAs are characterized by an elevated stability compared to their linear counterparts [19]. Nevertheless, circular RNA molecules are degraded, but in contrast to their linear counterparts, in a biphasic manner. Thus, stochastic autohydrolysis cleaves the circRNA into a re-linearized isoform. Next, the re-linearized circRNA

is in turn subjected to decay. Due to this fact, products of autohydrolytic degradation of efficiently purified circRNA sponges are detectable on analytic polyacrylamide-urea gels after ethidium bromide or SYBR Gold staining as faint bands of re-linearized RNA molecules within a circRNA preparation [16]. Therefore, excessive freezing and thawing of circRNAs should be avoided, as these may promote re-linearization by stochastic autohydrolysis.

6. *Validation of circularity by Ribonuclease R (RNase R) treatment.* Despite the differential mobilities of circular RNAs within polyacrylamide-urea gels of different acrylamide contents, circularity of the produced sponges should also be proven by RNase R treatment. Incubate ciRS with 1 U/ μ g RNase R, 10 \times RNase R Rxn Buffer to a final concentration of

1 \times and 40 U RNaseOUT, add to 40 μ L with RNase-free water, and incubate for 20 min at 37°C. Phenol/Chloroform/Isoamylalcohol extraction and ethanol or isopropanol precipitation are performed to purify the RNase R-treated circular RNAs. Assess circularity by loading 100 ng of the RNA onto a polyacrylamide-urea gel (Figure 4).

7. *Transfection of circRNA sponges in cell culture.* **OPTIONAL STEP:** CiRS can be transfected into any eukaryotic cell culture-based system. Typically, transfection is performed using lipid- or synthetic-nanoparticles such as Lipofectamine 2000 or poly-ethylenimine formulations as used for siRNA transfections following the manufacturer's instructions. Additionally, electroporation of circRNA sponges is possible. This procedure should use established protocols for the model system used.

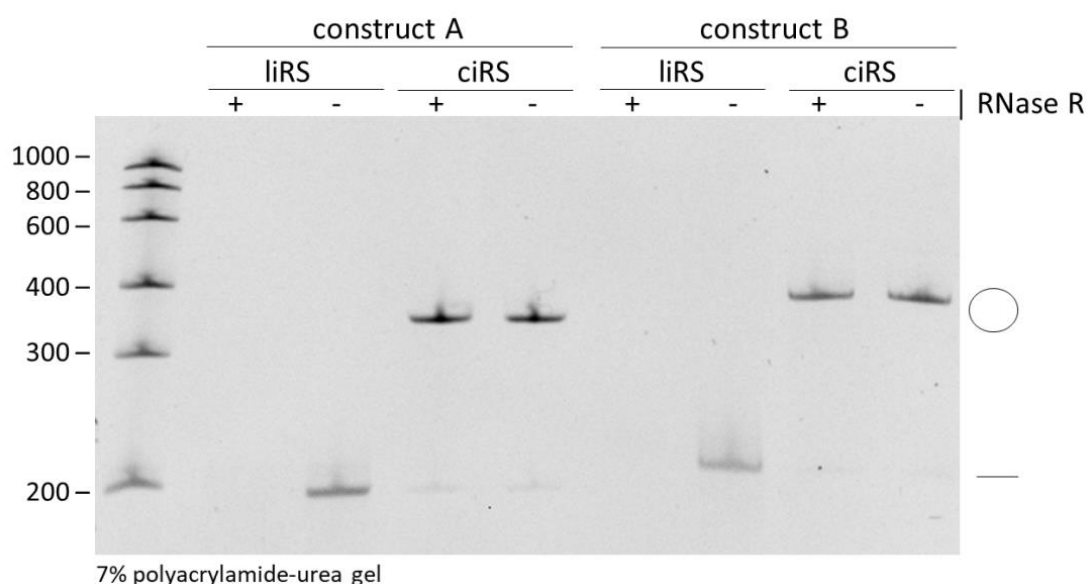


Figure 4. Validation of circularity by RNase R treatment. Both purified circular and linear RNA sponges (ciRS and liRS) of the two produced exemplary constructs with a length of 197 nt (construct A) and 208 nt (construct B) were subjected to RNase R exonuclease (+) or control (-) treatment and then analysed on 7% polyacrylamide-urea gel by ethidium bromide staining.

Author Contributions: All authors have read and agree to the published version of the manuscript. Conceptualization, J.B. and O.R.; methodology, O.R.; writing—original draft preparation, J.B. and O.R.; writing—review and editing, J.B. and O.R.; visualization, J.B.; supervision, O.R.; project administration, O.R. All authors have read and agreed to the published version of the manuscript.

Funding: This research was funded by the Deutsche Forschungsgemeinschaft DFG, Research Training Group (RTG) 2355 (project number 325443116).

Acknowledgments: We would like to thank Lyudmila A. Shalamova and Corinna Ulshöfer for critical discussion on the manuscript.

Conflicts of Interest: The authors declare no conflict of interest.

References

- [1] Jeck W.R., Sorrentino J.A., Wang K., Slevin M.K., Burd C.E., Liu J., Marzluff W.F., Sharpless N.E. (2013) Circular RNAs are abundant, conserved, and associated with ALU repeats. *RNA (New York, N.Y.)*, 19:141–157. DOI:10.1261/rna.035667.112.
- [2] Memczak S., Jens M., Elefsinioti A., Torti F., Krueger J., Rybak A., Maier L., Mackowiak S.D., Gregersen L.H., Munschauer M., Loewer A., Ziebold U., Landthaler M., Kocks C., Le Noble F., Rajewsky N. (2013) Circular RNAs are a large class of animal RNAs with regulatory potency. *Nature*, 495:333–338. DOI:10.1038/nature11928.
- [3] Chen L.-L. (2016) The biogenesis and emerging roles of circular RNAs. *Nature reviews. Molecular cell biology*, 17:205–211. DOI:10.1038/nrm.2015.32.
- [4] Starke S., Jost I., Rossbach O., Schneider T., Schreiner S., Hung L.-H., Bindereif A. (2015) Exon circularization requires canonical splice signals. *Cell reports*:103–111. DOI:10.1016/j.celrep.2014.12.002.
- [5] Kristensen L.S., Hansen T.B., Venø M.T., Kjems J. (2018) Circular RNAs in cancer: opportunities and challenges in the field. *Oncogene*:555–565. DOI:10.1038/onc.2017.361.
- [6] Cocquerelle C., Mascrez B., Héтуin D., Bailleul B. (1993) Mis-splicing yields circular RNA molecules. *FASEB journal : official publication of the Federation of American Societies for Experimental Biology*, 7:155–160. DOI:10.1096/fasebj.7.1.7678559.
- [7] Sanger H.L., Klotz G., Riesner D., Gross H.J., Kleinschmidt A.K. (1976) Viroids are single-stranded covalently closed circular RNA molecules existing as highly base-paired rod-like structures. *Proceedings of the National Academy of Sciences of the United States of America*, 73:3852–3856. DOI:10.1073/pnas.73.11.3852.
- [8] Nigro J.M., Cho K.R., Fearon E.R., Kern S.E., Ruppert J., Oliner J.D., Kinzler K.W., Vogelstein B. (1991) Scrambled exons. *Cell*, 64:607–613. DOI:10.1016/0092-8674(91)90244-S.
- [9] Cocquerelle C., Daubersies P., Majérus M.A., Kerckaert J.P.,

- Bailleul B. (1992) Splicing with inverted order of exons occurs proximal to large introns. *The EMBO Journal*, 11:1095–1098.
- [10] Capel B., Swain A., Nicolis S., Hacker A., Walter M., Koopman P., Goodfellow P., Lovell-Badge R. (1993) Circular transcripts of the testis-determining gene Sry in adult mouse testis. *Cell*, 73:1019–1030. DOI:10.1016/0092-8674(93)90279-Y.
- [11] Salzman J., Gawad C., Wang P.L., Lacayo N., Brown P.O. (2012) Circular RNAs are the predominant transcript isoform from hundreds of human genes in diverse cell types. *PLoS one*, 7:e30733. DOI:10.1371/journal.pone.0030733.
- [12] Salzman J., Chen R.E., Olsen M.N., Wang P.L., Brown P.O. (2013) Cell-type specific features of circular RNA expression. *PLoS genetics*, 9:e1003777. DOI:10.1371/journal.pgen.1003777.
- [13] Hansen T.B., Jensen T.I., Clausen B.H., Bramsen J.B., Finsen B., Damgaard C.K., Kjems J. (2013) Natural RNA circles function as efficient microRNA sponges. *Nature*:384–388. DOI:10.1038/nature11993.
- [14] Petkovic S., Müller S. (2015) RNA circularization strategies *in vivo* and *in vitro*. *Nucleic Acids Research*, 43:2454–2465. DOI:10.1093/nar/gkv045.
- [15] Litke J.L., Jaffrey S.R. (2019) Highly efficient expression of circular RNA aptamers in cells using autocatalytic transcripts. *Nature biotechnology*: 667–675. DOI:10.1038/s41587-019-0090-6.
- [16] Wesselhoeft R.A., Kowalski P.S., Anderson D.G. (2018) Engineering circular RNA for potent and stable translation in eukaryotic cells. *Nature communications*:2629. DOI:10.1038/s41467-018-05096-6.
- [17] Puttaraju M., Been M.D. (1992) Group I permuted intron-exon (PIE) sequences self-splice to produce circular exons. *Nucleic Acids Research*, 20:5357–5364. DOI:10.1093/nar/20.20.5357.
- [18] Ford E., Ares M. (1994) Synthesis of circular RNA in bacteria and yeast using RNA cyclase ribozymes derived from a group I intron of phage T4. *Proceedings of the National Academy of Sciences of the United States of America*, 91:3117–3121. DOI:10.1073/pnas.91.8.3117.
- [19] Jost I., Shalamova L.A., Gerresheim G.K., Niepmann M., Bindereif A., Rossbach O. (2018) Functional sequestration of microRNA-122 from Hepatitis C Virus by circular RNA sponges. *RNA biology*, 15:1032–1039. DOI:10.1080/15476286.2018.1435248.
- [20] Jeck W.R., Sharpless N.E. (2014) Detecting and characterizing circular RNAs. *Nature biotechnology*, 32:453–461. DOI:10.1038/nbt.2890.
- [21] Guo J.U., Agarwal V., Guo H., Bartel D.P. (2014) Expanded

- identification and characterization of mammalian circular RNAs. *Genome biology*, 15:409. DOI:10.1186/s13059-014-0409-z.
- [22] Ebbesen K.K., Kjems J., Hansen T.B. (2016) Circular RNAs: Identification, biogenesis and function. *Biochimica et biophysica acta*, 1859:163–168. DOI:10.1016/j.bbagr.2015.07.007.
- [23] Piwecka M., Glažar P., Hernandez-Miranda L.R., Memczak S., Wolf S.A., Rybak-Wolf A., Filipchyk A., Klironomos F., Cerda Jara C.A., Fenske P., Trimbuch T., Zywitzka V., Plass M., Schreyer L., Ayoub S., Kocks C., Kühn R., Rosenmund C., Birchmeier C., Rajewsky N. (2017) Loss of a mammalian circular RNA locus causes miRNA deregulation and affects brain function. *Science (New York, N.Y.)*, 357. DOI:10.1126/science.aam8526.
- [24] Zhang Y., Zhang X.-O., Chen T., Xiang J.-F., Yin Q.-F., Xing Y.-H., Zhu S., Yang L., Chen L.-L. (2013) Circular intronic long noncoding RNAs. *Molecular cell*, 51:792–806. DOI:10.1016/j.molcel.2013.08.017.
- [25] Ashwal-Fluss R., Meyer M., Pamudurti N.R., Ivanov A., Bartok O., Hanan M., Evtal N., Memczak S., Rajewsky N., Kadener S. (2014) circRNA biogenesis competes with pre-mRNA splicing. *Molecular cell*, 56:55–66. DOI:10.1016/j.molcel.2014.08.019.
- [26] Saetrom P., Heale B.S.E., Snøve O., Aagaard L., Alluin J., Rossi J.J. (2007) Distance constraints between microRNA target sites dictate efficacy and cooperativity. *Nucleic Acids Research*:2333–2342. DOI:10.1093/nar/gkm133.
- [27] Schirle N.T., Sheu-Gruttadauria J., MacRae I.J. (2014) Structural basis for microRNA targeting. *Science (New York, N.Y.)*, 346:608–613. DOI:10.1126/science.1258040.
- [28] Jinek M., Doudna J.A. (2009) A three-dimensional view of the molecular machinery of RNA interference. *Nature*, 457:405–412. DOI:10.1038/nature07755.
- [29] Ameres S.L., Horwich M.D., Hung J.-H., Xu J., Ghildiyal M., Weng Z., Zamore P.D. (2010) Target RNA-directed trimming and tailing of small silencing RNAs. *Science (New York, N.Y.)*, 328:1534–1539. DOI:10.1126/science.1187058.
- [30] La Mata M. de, Gaidatzis D., Vitanescu M., Stadler M.B., Wentzel C., Scheiffele P., Filipowicz W., Großhans H. (2015) Potent degradation of neuronal miRNAs induced by highly complementary targets. *EMBO reports*:500–511. DOI:10.15252/embr.201540078.
- [31] Barta T., Peskova L., Hampl A. (2016) miRNAsong: a web-based tool for generation and testing of miRNA sponge constructs in silico. *Scientific reports*:36625. DOI:10.1038/srep36625.
- [32] Khorshid M., Hausser J., Zavolan M., van Nimwegen E. (2013) A

biophysical miRNA-mRNA
interaction model infers canonical
and noncanonical targets. *Nature
methods*:253–255.
DOI:10.1038/nmeth.2341.

[33] Harris M.E., Christian E.L. (1999)
Use of circular permutation and end
modification to position
photoaffinity probes for analysis of
RNA structure. *Methods (San Diego,
Calif.)*, 18:51–59.
DOI:10.1006/meth.1999.0756.

[34] Petkovic S., Müller S. (2013) RNA
self-processing: formation of cyclic
species and concatemers from a
small engineered RNA. *FEBS letters*,
587:2435–2440.
DOI:10.1016/j.febslet.2013.06.013.

Synthetic circular miR-21 RNA decoys enhance tumor suppressor expression and impair tumor growth in mice

Simon Muller^{1,†}, Alice Wedler^{1,†}, Janina Breuer^{2,†}, Markus Glaß¹, Nadine Bley¹, Marcell Lederer¹, Jacob Haase¹, Claudia Misiak¹, Tommy Fuchs¹, Alina Ottmann², Tessa Schmachtel², Lyudmila Shalamova², Alexander Ewe³, Achim Aigner^{3,*}, Oliver Rossbach^{2,*} and Stefan Hüttelmaier^{1,*}

¹Institute of Molecular Medicine, Section for Molecular Cell Biology, Faculty of Medicine, Martin Luther University Halle-Wittenberg, 06120 Halle, Germany, ²Institute of Biochemistry, Faculty of Biology and Chemistry, Justus Liebig University of Giessen, 35392 Giessen, Germany and ³Department of Clinical Pharmacology, Rudolf Boehm Institute for Pharmacology and Toxicology, Faculty of Medicine, Leipzig University, 04107 Leipzig, Germany

*To whom correspondence should be addressed. Stefan Hüttelmaier Tel: +49 3455573957, Fax: +49 3455527126, Email: stefan.huettelmaier@medizin.uni-halle.de; Correspondence may also be addressed to Achim Aigner Tel: +49 341 9724 660, Fax: +49 3419724669, Email: achim.aigner@medizin.uni-leipzig.de; Correspondence may also be addressed to Oliver Rossbach Tel: +49 6419935422, Fax: +49 9935419, Email: oliver.rossbach@bc.jlug.de

†The first three authors should be regarded as Joint First Authors.

Abstract: Naturally occurring circular RNAs efficiently impair miRNA functions. Synthetic circular RNAs may thus serve as potent agents for miRNA inhibition. Their therapeutic effect critically relies on (i) the identification of optimal miRNA targets, (ii) the optimization of decoy structures and (iii) the development of efficient formulations for their use as drugs. In this study, we extensively explored the functional relevance of miR-21-5p in cancer cells. Analyses of cancer transcriptomes reveal that miR-21-5p is the by far most abundant miRNA in human cancers. Deletion of the *MIR21* locus in cancer-derived cells identifies several direct and indirect miR-21-5p targets, including major tumor suppressors with prognostic value across cancers. To impair miR-21-5p activities, we evaluate synthetic, circular RNA decoys containing four repetitive binding elements. In cancer cells, these decoys efficiently elevate tumor suppressor expression and impair tumor cell vitality. For their *in vivo* delivery, we for the first time evaluate the formulation of decoys in polyethylenimine (PEI)-based nanoparticles. We demonstrate that PEI/decoy nanoparticles lead to a significant inhibition of tumor growth in a lung adenocarcinoma xenograft mouse model via the upregulation of tumor suppressor expression. These findings introduce nanoparticle-delivered circular miRNA decoys as a powerful potential therapeutic strategy in cancer treatment.

This publication represents a component of my doctoral (Dr. rer. nat.) thesis in the Faculty of Biology and Chemistry at the Justus Liebig-University Giessen, Germany. Published in: *NAR Cancer*, doi: 10.1093/narcan/zcaa014 (2020). Received: May 04, 2020; Revised: July 03, 2020; Editorial Decision: July 06, 2020; Accepted: July 08, 2020

INTRODUCTION

MicroRNAs (miRNAs, miRs) are broadly conserved small (20–25 nt), non-coding RNAs (ncRNAs), which inhibit gene expression by inducing the degradation and/or suppressing the translation of target mRNAs [1,2]. Consistent with a plethora of mRNA targets, miRNAs have been implicated in the control of various biological and pathological processes, including the development and progression of cancer [3]. Oncogenic miRNAs (oncomiRs) are generally upregulated in cancer and inhibit the expression of tumor suppressor-encoding mRNAs. The opposite is considered for tumor-suppressive miRNAs. The duplicity of targeting both types of mRNAs, oncogenic or tumor suppressive, by a single miRNA is one reason why therapeutic approaches are proceeded with caution [4]. However, members of the let-7 miRNA family are prominent and well-described examples of largely tumor-suppressive miRNAs, inhibiting mRNAs encoding major oncogenes like RAS family members or HMGA2 [5]. In contrast, miR-21 is one of the earliest identified oncomiRs associated with proliferation and invasion during all stages of carcinogenesis. In a large-scale miRNome analysis of 540 tumor samples, miR-21 has been shown to be the most commonly upregulated miRNA in solid human carcinoma, including lung cancer [6]. This was confirmed for ovarian [7], thyroid [8], liver [9] and various other types of cancer. The oncogenic role of miR-21 was largely attributed to the inhibition of tumor suppressors, most notably PTEN [10] and PDCD4 [11]. MiR-21-

directed inhibition of these was proposed to promote the proliferation and metastatic potential of various cancer-derived cells. Its broad upregulation and highly conserved oncogenic properties, e.g. demonstrated for the inhibition of PDCD4 in a variety of cancers [12–17], suggest miR-21 as a prime target for RNA-based therapeutic approaches. However, despite a variety of clinical trials evaluating therapeutic inhibition of miRNA by antagomiRs, the silencing of miR-21 is only considered for the treatment of Alport syndrome [18]. In recent studies, artificial circular RNAs were developed to sequester mature miRs resulting in impaired biological function [19,20]. Sequestration of HCV-promoting miR-122 by an artificial circular RNA decoy inhibited viral protein synthesis in HCV cell culture systems [19]. The transfection of a circular RNA sequestering miR-21 in gastric cancer cells led to increased apoptosis and globally reduced protein synthesis [20]. However, in-depth analyses of affected tumor suppressor genes suitable for monitoring therapeutic efficacy, dose dependency and *in vivo* suitability of synthetic circular miR-21-directed decoys are still lacking [21].

MATERIALS AND METHODS

Plasmids and cloning

Plasmids including cloning strategies, oligonucleotides for annealing and restriction sites are summarized in Supplementary Table S9. All plasmids were verified by sequencing.

Cell culture and transfections

A549 (ATCC, RRID: CVCL_0023), H1975 (ATCC, RRID: CVCL_1511), ES-2 (ATCC, RRID: CVCL_3509), Huh-7 (ATCC, RRID: CVCL_0336), C643 (CLS, RRID: CVCL_5969) and HEK293T/17 (ATCC, RRID: CVCL_1926) were cultured in Dulbecco's modified Eagle medium supplemented with 10% fetal bovine serum at 37°C and 5% CO₂. The transfection of cells with DNA or decoys was performed using Lipofectamine 3000 (Thermo Fisher Scientific) according to manufacturer's protocols. Lentiviral particles were generated as previously described [22]. Lentiviral transductions were achieved at 10 MOI (multiplicity of infection). For luciferase reporter analyses, 1×10^5 cells were transfected with 100 ng pmirGLO plasmids, as described [22]. For CRISPR/Cas9-mediated genomic deletions, 5×10^5 cells were transfected with 1 µg Cas9-encoding plasmid and two sgRNA-encoding plasmids (500 ng each). Plasmids are summarized in Supplementary Table S9. For circular RNA stability analysis, 3×10^6 ES-2 cells were transfected with 750 ng of either circular or linear sponge RNAs by electroporation (GenePulser Xcell; Bio-Rad). Harvested cells were reconstituted in Cytomix (120 mM KCl, 0.15 mM CaCl₂, 10 mM K₂HPO₄/KH₂PO₄, pH 7.6, 25 mM HEPES, 2 mM EGTA, 5 mM MgCl₂, supplemented by 2 mM ATP and 5 mM glutathione directly before use) to 6×10^6 cells/ml. Electroporation was performed with 500 µl cell suspension in 4 mm cuvettes (Sigma) with the following settings: square wave, 270 V, 20 ms, single pulse. A total of 5×10^5

transfected cells were seeded per well in six-well plates.

Generation of MIR21 knockouts

Genomic deletions in the *MIR21* locus by CRISPR/Cas9 were achieved by transfection of two sgRNA-encoding plasmids (psg_RFP_miR-21_for, psg_RFP_miR-21_rev, expressing RFP) and the Cas9-encoding plasmid (pcDNA_Cas9-T2A-GFP, expressing GFP). Forty-eight hours post-transfection, single RFP- and GFP-positive cells were seeded by using a FACS Melody sorter (BD Biosciences). The deletion of ~200 nt in the locus was verified by PCR on isolated gDNA of single-cell clones and sequencing of amplicons. Plasmids and PCR primer are summarized in Supplementary Table S9.

Cell proliferation, spheroid growth and invasion, and anoikis resistance assays

Cell proliferation was determined in 2D and spheroid culture systems. A total of 1×10^3 cells were seeded in standard (2D) or round-bottom ultra-low attachment (Corning, spheroid) 96-well plates. Spheroid formation was induced by centrifugation at $300 \times g$ for 3 min. Cell confluency and spheroid growth were monitored for 5 days using an IncuCyte S3 system (Sartorius) with 4× (2D, whole well scan) or 10× magnification (spheroid). Confluence masks were generated by using the IncuCyte analysis software. CellTiter Glo (Promega) was used to determine cell viability according to manufacturer's protocols. For anoikis

resistance assays, 1×10^3 cells were seeded in flat-bottom ultralow-attachment plates (Corning) and cultured in media supplemented with 1% fetal bovine serum for 5 days. Colony formation was determined by bright-field microscopy (IncuCyte S3, 4 \times magnification) and cell viability by CellTiter Glo. Invasion assays were performed by monitoring tumor cell infiltration in Matrigel. Pre-formed spheroids of 1×10^3 cells were embedded in invasion matrix (Trevigen; 6 mg/ml) by centrifugation at $300 \times g$ for 3 min. Infiltration was monitored for 24 h using an IncuCyte S3 system. The relative invasive area and the invasive front were determined by using the IncuCyte analysis software.

Cell cycle analyses

For cell cycle analyses, A549 cells were harvested using trypsin and fixed overnight in 70% ethanol at -20°C . DNA staining was performed using propidium iodide (Miltenyi Biotec; dilution 1:1000) at 37°C for 30 min in phosphate-buffered saline supplemented with RNase A (Sigma-Aldrich; 2 $\mu\text{g}/\text{ml}$). The DNA content was measured by flow cytometry using a MACS Quant Analyzer (Miltenyi Biotec) and analyzed using FlowJo software.

Animal handling and xenograft analyses

Immunodeficient athymic nude mice (FOXN1^{nu/nu}) were held according to the guidelines of the Martin Luther

University and the University of Leipzig. Local ethical committees granted permissions.

For subcutaneous xenograft studies, 2.5×10^5 control or miR-21 knockout A549 cells, expressing iRFP by lentiviral transduction, were harvested in media and 50% Matrigel (ECM gel from Engelbreth-Holm-Swarm murine sarcoma; Sigma-Aldrich). Cell suspensions were injected into the left flank of 6-week-old nude mice, obtained from Charles River. Chlorophyll-free food *ad libitum* was used to avoid noise in iRFP imaging using a Pear Trilogy System (LICOR). Tumor growth and volumes were weekly measured and monitored by near-infrared imaging upon isoflurane anesthesia. Volumes were calculated using the following formula: $0.52 \times L_1 \times L_2 \times L_3$. Experiments were terminated when first tumors reached a maximal diameter of 1.5 cm. Tumors were excised to determine volume and weight.

Luciferase reporter assays

Complementary miRNA sequences or 48-nt regions of 3'-UTRs were cloned in the pmirGLO plasmid (Promega). Dual-GLO reporter analyses were performed according to manufacturer's instructions. Firefly and Renilla luciferase activities were determined 48 h post-transfection of reporters by using a GloMax Explorer Microplate Reader (Promega). Firefly activities were normalized to Renilla activities and to reporters with a minimal 3'-UTR (MCS), as previously described [22].

RNA isolation and RT-qPCR

Total RNA was isolated by using TRIzol (Thermo Fisher Scientific) according to manufacturer's instructions. Reverse transcription and quantitative PCR analyses on a Light Cycler 480 II (Roche) were performed as previously described [23]. Primers were selected using Primer-BLAST (www.ncbi.nlm.nih.gov/tools/primer-blast/). Genes and sequences are summarized in Supplementary Table S9. The $\Delta\Delta C_t$ method was used to determine relative RNA levels.

Northern blot

Infrared northern blotting of miRNAs and ncRNAs was essentially performed as described before [22]. In brief, 4 μ g of TRIzol-purified total RNA was separated in a 15% denaturing TBE-urea gel and transferred onto nylon membranes (Roche). After cross-linking (150 mJ/cm²), DY782- or DY682-labeled probes (MWG Biotech) were hybridized in PerfectHyb Plus (Sigma-Aldrich) at 20°C for 1 h and monitored using an Odyssey Scanner (LI-COR). Sequences of probes are indicated in Supplementary Table S9.

RNA sequencing and differential gene expression

Small RNA-seq libraries were prepared by using 50 ng of total RNA, isolated from parental cell lines, as input and the NEXTflex Small RNA Library Prep Kit v3 (Bio Scientific) or by Novogene (Hong Kong). Sequencing was performed on an Illumina HighSeq platform at the Deep Sequencing Group

(TU Dresden) or Novogene. For mRNA-seq libraries, polyA-RNA was enriched using oligo(dT) beads. Generation of libraries and sequencing were performed by Novogene on an Illumina HiSeq platform. RNA-seq and miRNA-seq data were analyzed as described previously [22,23]. RNA-seq data of the TCGA cohorts were obtained from the GDC portal (<https://portal.gdc.cancer.gov>).

Gene set enrichment analyses

Gene set enrichment analyses (GSEA) were performed using the GSEA software (v3.0) [24] with MSigDB (v7.0) gene sets for Hallmark pathways. For the generation of pre-ranked lists, protein-coding genes were ranked according to the correlation coefficient with miR-21 in TCGA lung adenocarcinoma (LUAD) RNA-seq data or the fold change determined upon miR-21 knockout by RNA-seq in A549 cells. Note that TCGA-derived data do not provide miR-21-5p/-3p distinguished information. For correlation analyses of protein-coding genes and miR-21, matching miRNA-seq and mRNA-seq information for each patient of the TCGA LUAD cohort was considered. Data sets were $\log_2(\text{RP(K)M} + 1)$ -transformed and the Pearson correlation coefficient (R) was determined. Genes were ranked from positive to negative R values.

MicroRNA-target predictions

For the prediction of miR-21-5p target genes, miRWalk v2.0 (<http://zmf.umm.uni-heidelberg.de/>)

apps/zmf/mirwalk2/) [25] was used. The following databases were considered for targeting 3'-UTRs of transcripts: miRWalk, miRDB, PITA, MicroT4, miRMap, RNA22, miRanda, miRNAMap, RNAhybrid, miRBridge, PICTAR2 and Targetscan. Prediction scores are indicated in Supplementary Table S6.

Western blot

Infrared western blotting analyses were performed as previously described [22]. In brief, cells were harvested by scraping and total protein was extracted by using lysis buffer (50 mM Tris-HCl, pH 7.4, 50 mM NaCl, 2 mM MgCl₂, 1% SDS) supplemented with protease inhibitor cocktails (Sigma-Aldrich). Proteins were separated in a NuPAGE 4–12% Bis-Tris gel (Thermo Fisher Scientific) and transferred to an Amersham Protran membrane (GE Healthcare). Protein expression was determined by using specific primary and fluorescence-coupled secondary antibodies and an infrared Odyssey Scanner (LI-COR). Antibodies are summarized in Supplementary Table S9.

Circular RNA production

Artificial circular RNAs were designed and produced as described in [19,26]. In brief, a plasmid backbone flanked by an EcoRI restriction site containing a T7 promoter, a stem-loop, a constant region and an XbaI restriction site was used to insert a double-stranded 5'-phosphorylated DNA oligonucleotide (Sigma-Aldrich)

containing four miRNA21 binding sites or control sequences (see Supplementary Figure S4). For *in vitro* transcription, a DNA template was excised using EcoRI, gel purified and 200 ng of the DNA template was used in a 1× *in vitro* transcription using HiScribe T7 High Yield RNA Synthesis Kit (NEB), according to the manufacturer's instructions for short transcripts. Notably, every transcription reaction was supplemented with a 10-fold molar excess of guanosine monophosphate (SigmaAldrich). This results in ~90% of transcripts with a 5'-monophosphate serving to facilitate circularization. The transcription reactions were upscaled 5-fold for production of large quantities of circRNA. DNA templates were digested by RQ1 DNase (Promega). Transcripts were purified by phenol extraction and precipitation, followed by removal of free nucleotides by gel filtration (mini Quick Spin RNA Columns; Roche). To enhance annealing of the stem-loop structure to favor intra- over intermolecular ligation, transcripts were heated to 95°C and cooled to room temperature over 20 min in a thermocycler in the presence of 10 mM Tris-HCl, pH 7.5, and 50 mM NaCl in 100–200 µl. The circularization protocol was modified from [27]. Circularization reactions were conducted in 250 or 500 µl volume using T4 RNA ligase 1 (Thermo Scientific or NEB), as described [19]. One percent of the total ligation reaction was analyzed on 5%, 6%, 7% or 8% analytical polyacrylamide-urea gel by ethidium bromide staining. Remaining 99% of the total ligation

reaction was loaded on a 6% or 8% preparative polyacrylamide–urea gel to excise circular and linear monomer RNAs. The latter were eluted in 1× proteinase K buffer containing 1% SDS for 1 h at 50°C. The elution volume varied between 0.8 and 8 ml depending on the circularization efficiency and therefore on the size of the gel area excised. Eluted RNAs were purified by phenol extraction and precipitation and dissolved in an appropriate amount of RNase-free water. Remaining gel fragments were removed by Costar Spin-X centrifuge tube filters (Corning). The circular RNA production and purification procedure is documented in Supplementary Figure S4B and E. To prove circularity, the RNA preparations were treated using the exonuclease RNase R as described before [26].

RNA affinity purification

In vitro and *in vivo* RNA affinity purification was performed using NeutrAvidin Agarose Beads (Thermo Fisher Scientific). Beads were blocked overnight at 4°C with bovine serum albumin (BSA), tRNA and glycogen (blocking buffer: 4 mM HEPES, pH 7.5, 0.2 mM DTT, 2 mM MgCl₂, 20 mM KCl, 0.002% NP-40, 0.2 mg/ml tRNA, 1 mg/ml BSA, 0.2 mg/ml glycogen).

For *in vitro* affinity purification, 25 µl packed beads were washed [wash buffer (WB): 20 mM HEPES, pH 7.5, 1 mM DTT, 10 mM MgCl₂, 0.01% NP-40, 150 or 600 mM KCl] and incubated with 800 fmol biotinylated circular RNA in 800 µl WB-600 for 30 min at room temperature. After washing, beads were incubated with ES-2 cell

extract lysed using 4-fold excess RIPA buffer (50 mM Tris–Cl, pH 7.4, 1% NP40, 0.1% SDS, 150 mM NaCl, 5 mM EDTA, 1× HALT protease inhibitor; Thermo Fisher Scientific) for 1 h at 37°C.

For *in cellulo* affinity purification, 1.6×10^7 A549 cells were transfected with 16 pmol biotinylated circular RNA by using Lipofectamine 2000 Reagent (Thermo Fisher Scientific) and harvested 3 h post-transfection. A549 cellular extracts was generated using 4-fold excess RIPA buffer as described above, and incubated with 50 l blocked NeutrAvidin Agarose Beads (Thermo Fisher Scientific) for 1 h at room temperature.

For both *in vitro* and *in vivo* RNA affinity purification, beads were washed (4× WB-600, 1× WB-150) afterward and RNA was isolated using TRIzol. Isolated RNA was analyzed by small RNA northern blot using 15% polyacrylamide gels, EDC cross-linking [28], DigoxigeninLNA-miR-21 probes (Qiagen) and visualized by DIG-FabFragment/CDP-Star-based detection (Sigma-Aldrich).

Circular RNA stability

For cellular decay analyses, the first time point was represented by directly harvested input material. For other time points [8, 24, 48 and 72 h], medium was exchanged 8 h post-electroporation. Total RNA was isolated by TRIzol and 50% of isolated RNA was analyzed by 7% denaturing polyacrylamide gel electrophoresis. Northern blotting was performed by transfer to nylon membrane (GE

Healthcare) and hybridization at 59°C with an internally labeled *in vitro* transcribed ³²P-riboprobe (71 nt) directed against the constant region of the linear and circular RNAs. In addition, as an internal control, hybridization with a ³²P-labeled riboprobe against the U1 snRNA (163 nt) was performed. Results were visualized by Typhoon FLA 9500-based phosphorimaging (GE Healthcare). Quantification was conducted using ImageQuantTL software and normalization to inputs. Half-lives of indicated RNA species were derived by fitting to an exponential decay function using OriginPro8 software (ExpDec1 function).

PEI complexation of circRNA decoys and analysis of physicochemical complex properties

Circular RNA sponges were complexed with low molecular weight polyethylenimine (PEI) F25-LMW [29], as described previously for small RNAs [30]. Briefly, 10 µg RNA was complexed in 5% glucose/10 mM HEPES, pH 7.4, by mixing both components at a PEI:RNA mass ratio of 7.5 prior to incubation for 45 min. When preparing larger amounts, complexes were then aliquoted and stored frozen [31]. Complexation efficacy at different PEI amounts was determined by agarose gel electrophoresis using 0.5 µg RNA. The complexes were mixed with 10× loading dye and separated onto a 2% agarose gel prestained with 1× SybrTM Gold in TAE buffer running buffer. Complex stabilities were measured by a

heparin displacement assay. PEI F25/RNA complexes were mixed with increasing amounts of heparin as shown in the figure. After an incubation of 30 min, the samples were analyzed by agarose gel electrophoresis as above.

Zeta potentials and particle sizes of complexes were measured as described previously [32]. Briefly, complexes containing 20 µg RNA were diluted to 1.5 ml pure water prior to phase analysis light scattering (PALS) and photon correlation spectroscopy, using a Brookhaven ZetaPALS system (Brookhaven Instruments, Holtsville, NY, USA). The data were analyzed using the manufacturer's software and applying a viscosity and refractive index of pure water at 25°C. Zeta potentials were measured in 10 runs, with each run containing 10 cycles, and applying the Smoluchowski model. For size determination, the complexes were analyzed in five runs with a run duration of 1 min. Results are expressed as intensity-weighted mean diameter from different experiments. Additionally, sizes were analyzed by nanoparticle tracking analysis (NTA) using a NanoSight LM10 (Malvern) equipped with a 640 nm sCMOS camera, software NTA 3.0 and a circRNA concentration of 1 µg/ml.

PEI/circRNA-based xenograft treatment

For PEI/circRNA therapy studies, 1 × 10⁶ A549 cells in 150 µl medium supplemented with 50% Matrigel were subcutaneously injected into both flanks of nude mice. When tumor

volumes reached sizes between 40 and 110 mm³, mice were randomized into negative control and specific treatment groups. PEI-based nanoparticles containing

10 µg miR-21-5p or control decoys were intraperitoneally injected over 6 weeks (days 1, 4, 7, 25 and 39). Tumor volumes were regularly monitored and experiments were terminated after 43 days of treatment. Tumors were excised and flash-frozen in liquid nitrogen upon determining volume and mass.

Statistics

All experiments were performed at least in biological triplicates as indicated. For equally distributed data sets, a parametric Student's t-test was used for statistical significance. Otherwise, a non-parametric Mann-Whitney test was performed as indicated. For RNA-seq false discovery rates (FDRs) were calculated upon TMM normalization. Overall survival analyses were performed using KMplotter (<https://kmplot.com/analysis/>) [33]. Patients were split by auto select best cutoff. For protein-coding genes, the LUAD cohort (n = 865 patients) based on gene chips was considered. For miRNAs, miR power based on the TCGA LUAD cohort (n = 513 patients) was used. Log-rank analyses were used for statistical significance of Kaplan–Meier plots.

RESULTS

MicroRNA 21 is the most conserved and abundant miRNA in cancer

The microRNA 21-5p (miR-21) has been reported as a potent oncomiR in various cancers [34,35]. Inspection of miRNA expression in 33 TCGA-provided tumor cohorts, including miRNome data of 9891 tumor patients, revealed that miR-21 is the most abundant miRNA with a median percentage of 33% across cancers (Figure 1A and B; Supplementary Table S1). Other miRs with still high, but substantially lower median abundance than miR-21 are miR-22 (12%), miR-143 (7%), miR-148a (5%) and miR-99b (3%). In LUAD, median miR-21 abundance was even further pronounced to 41% and substantially upregulated compared to normal lung tissue (Figure 1B, right panel, and C). Although miRs 22, 148a and 99b were significantly increased as well, their degree of upregulation and total abundance falls way behind miR-21. In agreement with a tumorsuppressive role of miR-143 [36], this miRNA was significantly downregulated in LUAD. Importantly, significant association with adverse prognosis in LUAD was only observed for miR-21 (Figure 1D). For the other most abundant miRs (miRs 22, 148a and 99b), elevated expression, surprisingly, was associated with a rather good prognosis, as expected for miR-143. Collectively, these findings

independent, oncogenic roles of miR-21-5p/3p in squamous cell carcinoma stem cells [37,38]. In this study, miRNA sequencing in LUAD-derived A549 cells identified an exceedingly high abundance of miR-21-5p, representing ~68% of all miRNAs (Supplementary Figure S1A; Supplementary Table S7). In contrast, miR-21-3p was substantially less abundant representing only ~0.08% of the cellular miRNome. To evaluate the oncogenic potency of miR-21-5p in LUAD-derived cells, the *MIR21* locus was deleted in A549 as well as H1975 cells by CRISPR/Cas9 using two sgRNAs (Figure 2A). PCR on genomic DNA and northern blotting confirmed homozygous deletion of *MIR21* and loss of miR-21-5p expression (Figure 2B). In agreement, the repression (~98%) of luciferase reporter comprising one miR-21-5p complementary targeting site in the 3'-UTR was completely abrogated in *MIR21*-KO cells (Figure 2C; Supplementary Figure S1B). The activity of corresponding miR-21-3p reporters remained largely unaffected in parental cells, supporting the low abundance of this miRNA (Supplementary Figure S1C). This obviously suggested that miR-21-3p activity is largely irrelevant in LUAD-derived cells and that *MIR21*-deleted cells are a suitable model to study the role of miR-21-5p. *MIR21* silencing significantly decreased 2D proliferation, 3D spheroid growth, anoikis resistance and self-renewal in both LUAD-derived cell lines (Figure 2D–F; Supplementary Figure S1D). These findings implied that *MIR21*

deletion also impairs tumor growth *in vivo*. This was analyzed in nude mice subcutaneously injected with A549 cells stably expressing iRFP (infrared fluorescent protein) to trace tumor formation. The deletion of *MIR21* significantly impaired tumor growth and resulted in substantially diminished final tumor volume and mass (Figure 2G and H). In summary, these studies indicated that miR-21-5p is a potent oncogenic driver in LUAD tumor models.

MiR-21-5p is a major inhibitor of tumor suppressor expression promoting tumor cell vitality

Both mature miR-21 ncRNAs, 21-5p as well as 21-3p, have been reported to be involved in the regulation of key oncogenic and tumor-suppressive pathways as well as cancer stem cell properties, in particular self-renewal capacity [38,39]. However, in LUAD-derived cells miR-21-3p was found largely irrelevant. Therefore, major cancer-associated pathways controlled by miR-21-5p in LUAD-derived cells were analyzed by monitoring transcriptome changes in *MIR21*-deleted A549 cells by RNA-seq (Supplementary Table S2). GSEA of genes ranked by their fold change of expression upon *MIR21* deletion indicated a striking downregulation of proliferation-associated gene sets, e.g. E2F target and G2M checkpoint, as well as other cancer-associated hallmark gene sets like MTORC1-signaling (Figure 3A; Supplementary Table S3). GSEA of genes ranked by their association (Pearson correlation) with

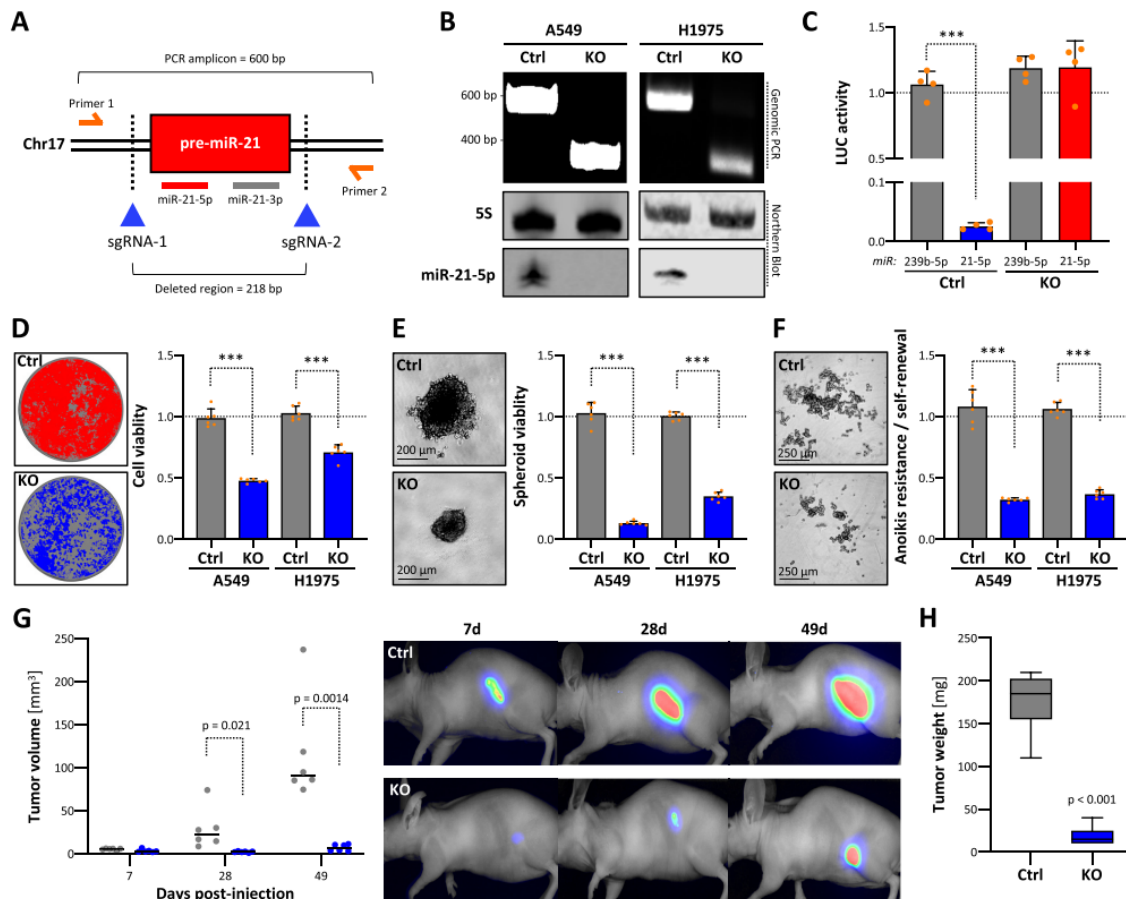


Figure 2. Genomic deletion of *MIR21* in cancer impairs tumor growth. (A) Schematic showing the experimental strategy to delete the *MIR21* locus by using Cas9 nuclease and indicated CRISPR guide RNAs (sgRNAs). Primers for PCR on genomic DNA (gDNA) and amplicon/deleted region sizes are indicated. (B) Representative PCR analysis on gDNA of parental (Ctrl) and *MIR21*-deleted (KO) A549 and H1975 cells (top panel). Representative northern blot analysis of miR-21-5p expression in Ctrl or KO A549 and H1975 cells (bottom panel). 5S served as a normalization control. (C) miRNA reporter analyses in A549 Ctrl or miR-21 KO cells. The activity of indicated miRNAs (cel-miR-239b-5p and hsa-miR-21-5p) was analyzed by using antisense luciferase reporters. Luciferase activities, normalized to a control reporter comprising a minimal 3'-UTR, were determined in four experiments. Viability in 2D (D) or 3D spheroid growth (E) and anoikis resistance (F) analyses of parental (Ctrl) or miR-21 KO A549 and H1975 cells. Representative images of A549 cells are shown (left panels). Viability and anoikis resistance were determined by CellTiter Glo in six median-normalized experiments (right panels). (G) Ctrl and miR-21 KO A549 cells expressing iRFP were injected (s.c.) into nude mice ($n = 6$ per condition). Xenograft tumor volumes were measured (left panel) and monitored by near-infrared imaging (right panel) at indicated time points upon injection. (H) Box plots showing final tumor mass 49 days post-injection. Statistical significance, indicated by P-values, was determined by the Mann-Whitney test: *** $P < 0.001$.

miR-21 expression in LUAD (Supplementary Table S4) suggested that gene sets found overall decreased upon *MIR21* deletion tended to show

expression patterns positively associated with miR-21 abundance (Supplementary Table S5). For instance, E2F target genes were largely

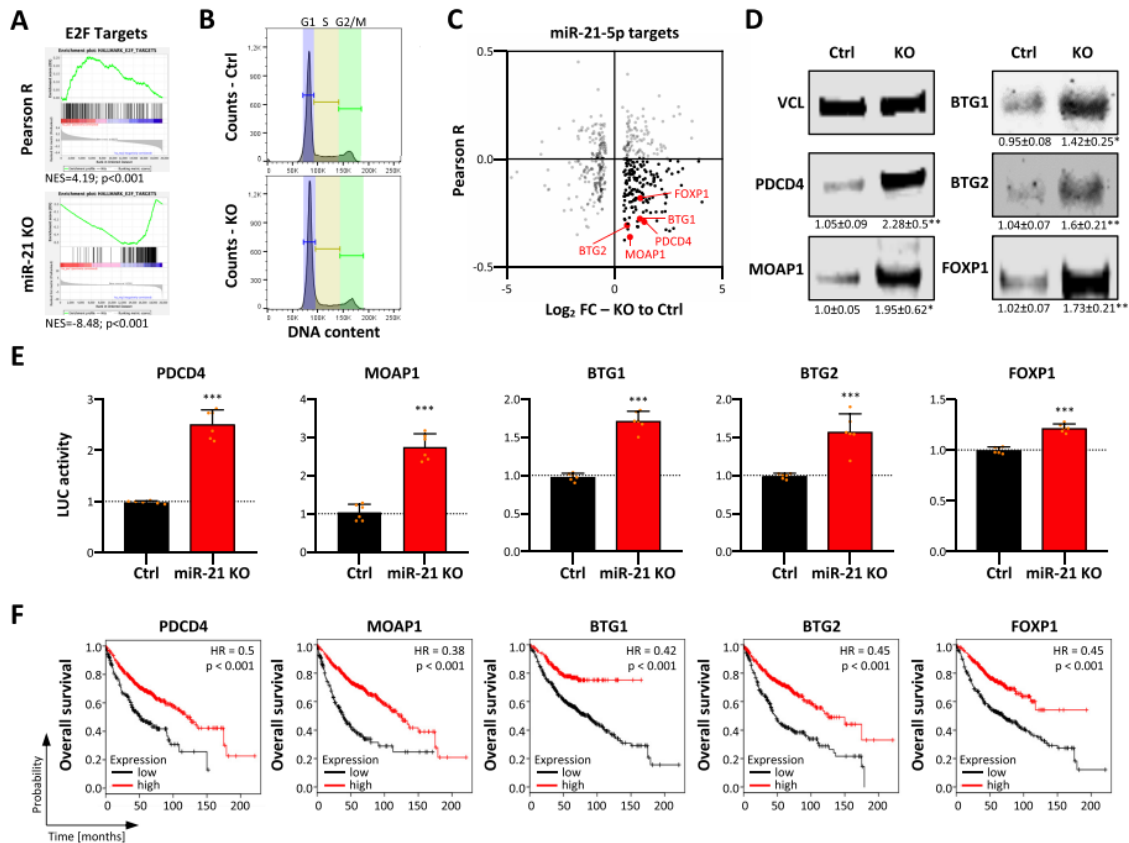


Figure 3. Loss of miR-21 enforces tumor suppressor expression. (A) E2F target GSEA of protein-coding genes ranked by the determined Pearson correlation coefficient determined for their associated expression with miR-21 in the LUAD tumor cohort (upper panel). E2F target GSEA of genes ranked according to their fold change (FC) of expression in *MIR21*-KO in A549 cells compared to parental cells, as determined by RNA-seq (lower panel). (B) Cell cycle phase distribution of A549 Ctrl and *MIR21*-KO cells determined by PI labeling and flow cytometry. (C) Scatter plots showing the Pearson correlation of miR-21 expression in LUAD (Pearson R) and differential expression of predicted miR-21 target genes ($n = 444$) differentially expressed ($FDR < 0.01$) upon *MIR21*-KO, as determined in (A). Correlation coefficients were analyzed over 526 LUAD patient samples with matched polyA- and miRNA-seq data sets. MiR-21 target genes were considered when predicted by 5 out of 11 databases analyzed via miRWalk (v2.0). (D) Representative western blot analysis of indicated proteins in parental A549 (Ctrl) and *MIR21*-KO cells. VCL served as a loading and normalization control. Relative expression values and standard deviation (SD) were determined in three analyses. (E) Luciferase reporter analyses in parental and miR-21 KO A549 cells. The activity of reporters was analyzed by using luciferase reporters comprising 48-nt-long regions of indicated 3'-UTRs including miR-21-5p seed regions. Reporter activities in KO cells were median-normalized to parental cells in six experiments. Statistical significance was determined by Student's *t*-test: * $P < 0.05$; ** $P < 0.01$; *** $P < 0.001$. (F) Kaplan–Meier plots of overall survival analyses based on expression (best cutoff) of indicated mRNAs in LUAD patient samples. HR, hazard ratio; *p*, log-rank *P*-value.

downregulated by *MIR21* deletion and were mainly positively associated with miR-21 expression in LUAD, as

indicated by an NES (normalized enrichment score) of 4.2 (Supplementary Table S5). Consistent with

impaired E2F activity, *MIR21* deletion led to an accumulation of cells in G1 suggesting impaired G1/S transition (Figure 3B; Supplementary Figure S1E). The mRNA levels of positive, e.g. E2F1, CDK2 and CCNE1, but also negative regulators, e.g. E2F5, RB1 and RBL1, of G1/S transition were found largely downregulated upon *MIR21* loss (Supplementary Table S2). This downregulation was associated with marked upregulation of TGFB1 and other facilitators of TGFB signaling like TGFBR2. In view of the substantial downregulation of CDC25A expression and upregulation of SKP2, this suggested that the loss of miR-21 promotes a TGFB signaling-dependent impairment of G1/S transition, as previously proposed [40]. To identify key tumor-suppressive factors directly inhibited by miR-21-5p in primary tumors and LUAD-derived cells, the correlation of mRNA expression with miR-21 in LUAD was determined for mRNAs with predicted miR-21-5p target sites that were differentially expressed in A549 cells upon deletion of *MIR21* (Figure 3C; Supplementary Table S6). This identified various validated tumor suppressors upregulated upon *MIR21* deletion. These showed substantial negative association with miR-21 expression in LUAD (Figure 3C, black and red dots). The respective tumor suppressors included the previously reported miR-21-5p targets BTG2 and PDCD4 [14,41,42], as well as BTG1, FOXP1 and MOAP1 [43–45], not previously described as miR-21-5p targets. In agreement with their significantly

elevated mRNA abundance in A549 and H1975 *MIR21* knockout cells (Supplementary Figure S2A and B), the protein levels of all five tumor suppressors were upregulated by the loss of miR-21 expression (Figure 3D). Direct miR-21-5p effects were evaluated by testing the regulation of luciferase reporters containing predicted targeting sites with flanking sequences in their 3-UTRs (Supplementary Figure S2C). The activity of all five tested reporters was significantly increased by *MIR21* loss, indicating the repression of all five tumor suppressors by miR-21-5p in LUAD-derived A549 cells (Figure 3E). Notably, the analysis of overall survival probability revealed the prognostic relevance of all five miR-21-5p regulated tumor suppressors in LUAD. For each of them, a negative correlation with miR-21 expression was observed (Supplementary Figure S2D) and their low abundance was associated with significantly reduced overall survival probability (Figure 3F). Taken together, these findings demonstrated that miR-21-5p is a key inhibitor of tumor suppressors impairing major pro-proliferative oncogenic pathways.

MIR-21-5p indirectly enhances the expression of oncogenic factors repressed by let-7 miRNAs

MiRNA-seq confirmed the severe reduction (to ~38% of parental cells) of total miRNA abundance in A549 cells upon deletion of *MIR21* due to the essential loss of miR-21-5p and -3p (Supplementary Table S7). However,

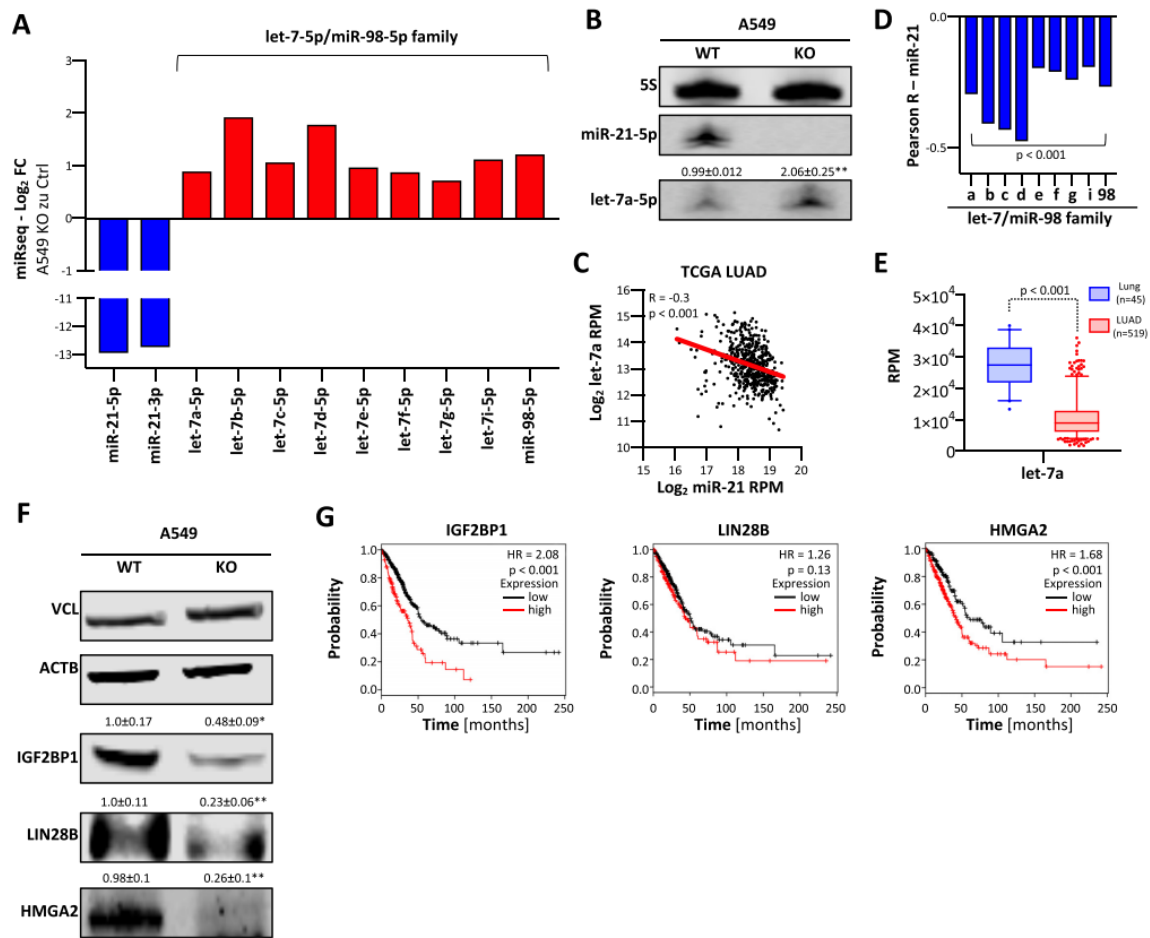


Figure 4. Loss of miR-21 reduces the expression of oncogenic let-7 targets. (A) Expression changes of indicated miRNAs in *MIR21*-KO A549 cells, as determined by miRNA-seq. (B) Representative northern blot of three analyses for miR-21-5p and let-7a-5p in parental (WT) and *MIR21*-KO A549 cells. 5S served as a loading and normalization control. (C) Scatter plots showing the expression of miR-21 and let-7a in TCGA LUAD patients ($n = 519$). Pearson correlation coefficient (R) and P -value are indicated. (D) Pearson correlation coefficients of miR-21 with members of the let-7/miR-98 family in the TCGA LUAD cohort. (E) Box plots indicating the expression of let-7a in normal lung tissue ($n = 45$) and LUAD ($n = 519$). Statistical significance was determined by the Mann-Whitney test. (F) Representative western blot of three analyses for IGF2BP1, LIN28B and HMGA2 protein expression in parental and *MIR21*-KO A549 cells. VCL and ACTB served as loading and normalization controls. Statistical significance was determined by Student's t -test: * $P < 0.05$; ** $P < 0.01$. (G) Kaplan-Meier plots of overall survival analyses based on expression (best cutoff) of IGF2BP1, LIN28B and HMGA2 mRNAs in LUAD patient samples. HR, hazard ratio; p , log-rank P -value.

total miRNA abundance remained ~6% higher than expected (to ~32% of parental cells) upon *MIR21* deletion, suggesting an upregulation of some miRNAs. Intriguingly, miRNAseq indicated elevated expression of the complete, tumorsuppressive let-7

miRNA family in *MIR21*-KO cells (Figure 4A and B; Supplementary Table S7). Concomitantly, let-7 miRNA family members like let-7a were significantly downregulated in LUAD and showed an inverse association with miR-21 expression. This suggested that miR-21

interferes with the suppression of oncogenic factors by let-7 miRNAs (Figure 4C–E). In support of this, the loss of *MIR21* was associated with reduced expression of the three major oncofetal let-7-5p target proteins IGF2BP1, LIN28B and HMGA2 (Figure 4F) [5]. Notably, these three proteins form an oncogenic triangle antagonizing tumor-suppressive functions of let-7 in cancer cells [46]. In LUAD, a prooncogenic role of these oncofetal proteins is supported by their significant upregulation and association with reduced survival probability (Figure 4G). LIN28B is a key inhibitor of let-7 expression [47], suggesting that its downregulation upon *MIR21* loss is a key driver of let-7 upregulation. In conclusion, our results indicated that, beyond the direct inhibition of protein-coding tumor suppressors, miR-21 indirectly promotes the expression of pro-oncogenic factors like LIN28B by downregulating miRNAs of the let-7 family expression via mechanisms yet to be characterized in detail.

MiR-21 is a conserved oncomiR in cancer

The consistently high abundance of miR-21 expression in human cancers, its validated role in directly inhibiting the expression of conserved tumor suppressors and the indirect enhancement of conserved pro-oncogenic factors suggested that its oncogenic roles are highly conserved as well. This was analyzed by deleting *MIR21* in three additional cancer cell lines: ES-2 (ovarian cancer), C643 (anaplastic thyroid carcinoma) and

Huh-7 (hepatocellular carcinoma) cells. In all these cell lines, miR-21-5p was the most abundant single miRNA, as revealed by miRNA-seq (Figure 5A; Supplementary Table S8). Moreover, miR-21-5p showed strong biological activity in all these cancer cell lines, as indicated by the nearly complete repression of luciferase reporters comprising one complementary miR-21-5p targeting site (Supplementary Figure S3A). Deletion of *MIR21* in these cells abolished miR-21-5p expression (Figure 5B). This was associated with substantially impaired cell proliferation (Supplementary Figure S3B), spheroid growth in all three cell lines and markedly reduced Matrigel invasion of ES-2 cells (Figure 5C and D; Supplementary Figure S3C and D). In sum, these findings confirmed the high conservation of miR-21-5p's oncogenic roles in cancer cells supporting the initial hypothesis that targeting miR-21, specifically miR-21-5p, is likely beneficial in a broad variety of cancers.

Inhibition of miR-21-5p by circular RNA decoys impairs the oncogenic potential of tumor cells

Inspired by the efficient miR sponging by naturally occurring circular RNAs [48,49], miR-21-5p-directed circular RNA decoys (ciRs), recently described to disturb gastric carcinoma cell vitality [20], were explored in LUAD-derived cells and 3D cell models. Two miR-21-5p-directed ciRs were generated. Beyond previous studies, exclusively describing decoys containing five bulged miR-21-5p targeting sites, we extended our studies

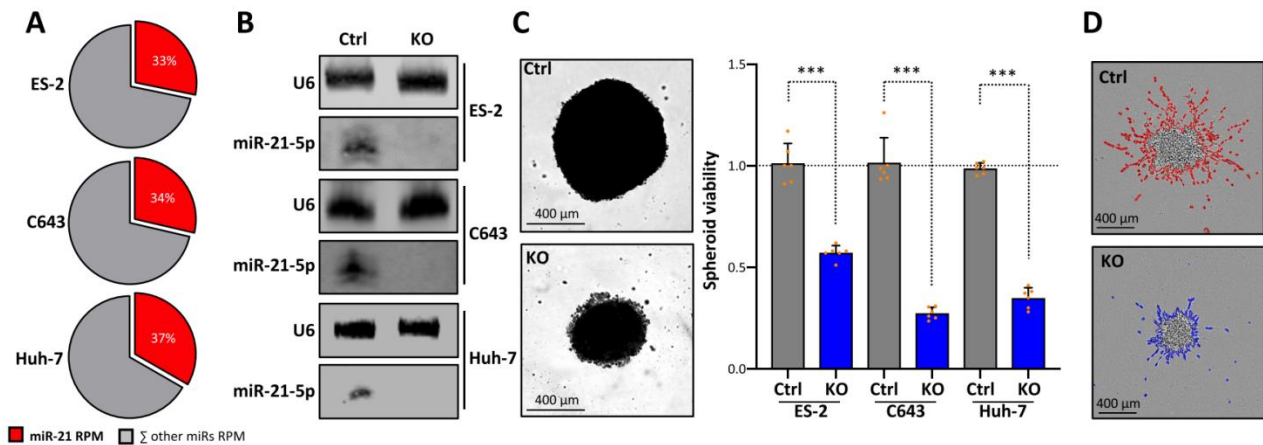


Figure 5. *MIR21*-KO concisely reduces proliferation and invasion in distinct cancer-derived cells. (A) Pie charts showing the percentage of miR-21-5p (red) and all other miRNAs in ES-2, C643 and Huh-7 cells, as determined by miRNA-seq. (B) Representative northern blot ($n = 3$ experiments) of miR-21-5p in parental and *MIR21*-KO ES-2, C643 and Huh-7 cells. U6 served as a loading control. (C) Proliferation of parental and *MIR21*-KO ES-2-, C643- and Huh-7-derived spheroids ($n = 6$ each) was determined by using CellTiter Glo (right). Statistical significance was determined by Student's t -test: *** $P < 0.001$. Representative images of ES-2 spheroids are shown (left). (D) Representative bright-field image ($n = 3$ analyses) of ES-2 spheroid invasion in Matrigel. The invasive front is shown in red (Ctrl, parental) or blue (*MIR21*-KO).

toward shorter decoys with either four perfectly complementary or four bulged miR-21-5p sites (Figure 6A; Supplementary Figure S4A). Upon synthesis of linear RNAs (Supplementary Figure S4B) by *in vitro* transcription as well as circular RNA decoys by subsequent ligation and purification (Supplementary Figure S4C and D), the efficiency of decoys in binding miR-21-5p was evaluated by affinity purification of biotinylated RNA in ES-2 cell lysates (Figure 6B and C). Irrespective of circularization or bulging, all decoys efficiently associated with miR-21-5p. To evaluate the stability of circular versus linear miR-21-5p decoys, their decay in transfected ES-2 cells was monitored by northern blotting (Figure 6D). These studies revealed that circularization substantially increased the intracellular stability of miR-21-5p decoys, as

indicated by a >2-fold increase in the half-life of circular decoys ($t_{1/2} \sim 21$ h) when compared to linear counterparts ($t_{1/2} \sim 10$ h). This elevated stability resulted from a two-step decay of circular decoys with a relinearized intermediate [50]. In sum, these studies revealed that circularization substantially increased the cellular stability of miR-21-5p decoys and thus suggested ciRs as effective inhibitors of miR-21-5p *in cellulo*. This was evaluated further by monitoring the viability of A549 cells transfected with increasing amounts of negative control versus perfectly complementary circular miR-21-5p decoys. The latter strongly impaired cell viability at low doses (Supplementary Figure S5A). Notably, control decoys did not affect viability at any tested concentration, excluding non-specific RNA effects. The circularity of purified and transfected

RNAs was monitored by exonuclease treatment and northern detection (Supplementary Figures S4E and S5B), and interaction of miR-21-5p in the transfected cells was validated by affinity purification of transfected biotinylated circRNAs (Supplementary Figure S5C). To evaluate whether growth inhibition is preserved in 3D cell models and among distinct tumor cells, both types of decoys, perfectly complementary or bulged, were analyzed in LUAD-derived A549 cells and ovarian cancer-derived ES-2 cells. Both types of decoys impaired 3D spheroid growth and 2D proliferation at similar efficiency (Figure 6E; Supplementary Figure S5D). Moreover, they substantially interfered with the Matrigel invasion of ES-2 cells, which could not be tested in A549 cells due to insufficient invasive potential (Figure 6F; Supplementary Figure S5E). Strikingly, the growth of A549- or H1975-derived spheroids was unaffected by transfecting corresponding linear RNAs (Supplementary Figure S5G) indicating the importance of circularization and elevated decoy stability. Decreased spheroid growth upon transfection of circular RNAs was associated with a significant upregulation of all prior evaluated tumor suppressors that had been found repressed by miR-21-5p in A549 and H1975 cells (Figure 6G; Supplementary Figure S5F and H). In conclusion, the presented findings revealed that miR-21-5p decoys show high intracellular stability in tumor-derived cells and effectively impair oncogenic roles of miR-21-5p in tumor

cells, irrespective of being perfectly complementary or bulged.

PEI nanoparticles loaded with circular mir-21-5p decoys impair tumor growth in vivo

The high inhibitory potency and *in cellulo* stability of circular miR-21-5p decoys suggested them as potential candidates for therapeutic intervention, i.e. for inhibiting tumor growth *in vivo*. This was tested in an A549-derived subcutaneous (s.c.) tumor xenograft model in mice. For therapeutic application and *in vivo* delivery, bulged miR-21-5p decoys were formulated in PEI-based nanoparticles. For this, decoys were complexed with the low molecular weight branched PEI F25-LMW [29], as described previously for small RNAs [30]. Efficient complexation was achieved already at a low polymer:mass ratio of 2.5, as demonstrated by the absence of the free decoy band in gel electrophoresis (Supplementary Figure S6A). These PEI/decoy complexes were found very stable, requiring 1 unit heparin per 0.2 g RNA for complex decomposition in heparin displacement assays (Supplementary Figure S6B). Dynamic light scattering revealed complex sizes in the range of ~130 nm, which was also confirmed by NTA (Supplementary Figure S6C). Finally, PALS revealed a positive zeta potential of ~20 mV. Taken together, this confirmed the formation of polymeric nanoparticles for decoy delivery and cellular internalization. Previous studies on the *in vivo* biodistribution

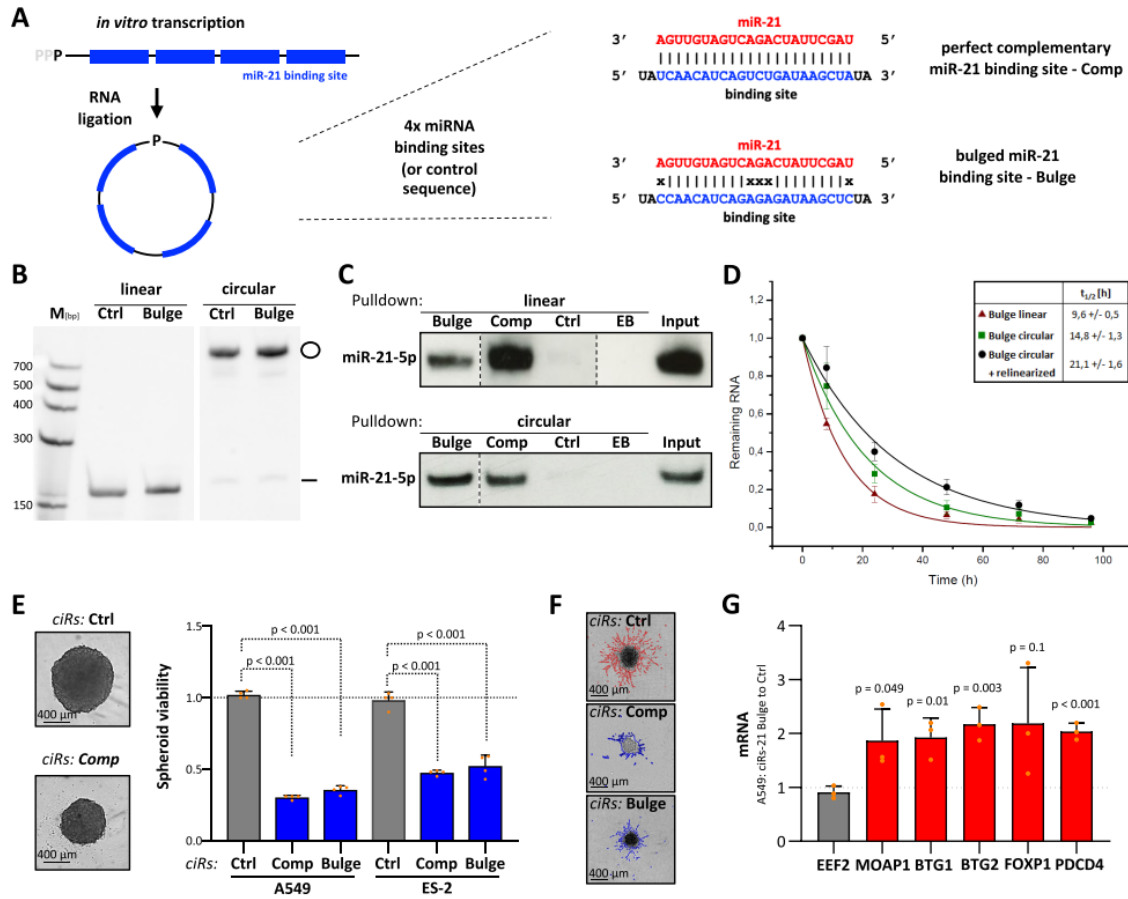


Figure 6. Circular miR-21-5p RNA decoys impair cancer cell proliferation and invasion. (A) Schematic showing the synthesis strategy of ciRs containing four miRNA-binding or control sequences. Single, perfectly complementary and bulged miR-21-5p binding sites are depicted (right panel). (B) Representative northern blot analysis ($n = 3$ experiments) of linear and circular RNAs before (left) and upon RNA ligation (right). (C) Representative northern blot analysis of miR-21-5p associated with linear (top panel) or circular (bottom panel) immobilized miRNA decoys in transfected ES-2 cells. EB, empty beads. (D) Decay of linear (red) and circular (green) bulged miR-21-5p decoys was determined by northern blotting upon transfection in ES-2 cells. The biphasic degradation (circular + relinearized) of circular RNA decoys is shown in black. Half-lives of indicated RNA species are indicated ($n = 3$ experiments). (E) Proliferation of A549 or ES-2 spheroids was determined by using CellTiter Glo upon transfection with indicated ciRs in four experiments. Representative bright-field images of ES-2 spheroids (left panel). (F) Representative bright-field images of ES-2 spheroids invading Matrigel upon transfection of indicated ciRs ($n = 5$ experiments). The invasive fronts are shown in red (Ctrl) or blue (miR-21-5p decoys complementary and bulged). (G) RT-qPCR analysis of mRNA levels in A549 cells transfected with bulged miR-21-5p ciRs normalized to Ctrl ciRs. RPLP0 served as a normalization and EE2 as a negative control in three experiments. Error bars indicate SD. Statistical significance, indicated by P -values, was determined by Student's t -test.

of PEI/siRNA complexes upon systemic application had identified intraperitoneal (i.p.) injection as more suited over intravenous injection for

complex delivery into s.c. tumor xenografts [51]. Thus, PEI nanoparticles containing 10 g miR-21-5p or control decoy were injected five times over 6

weeks (days 1, 4, 7, 25 and 39) in nude mice with A549- derived s.c. tumors. The monitoring of tumor sizes revealed substantially diminished tumor growth in the specific treatment group, becoming obvious already at day 12 of treatment. This trend was further pronounced at the time of termination (day 43), as indicated by a significant and nearly 2-fold decrease in tumor size in miR-21-5p decoy-treated mice (Figure 7A and B). Notably, we observed no obvious side effects upon PEI/decoy nanoparticle treatment in the course of 6 weeks. How decoy treatment influenced gene expression in the lung and s.c. xenograft tumors was analyzed for the five prior identified tumor suppressors targeted by miR-21-5p. Despite isolation of tissue samples 4 days after the last injection of PEI nanoparticles, robust upregulation of all five tumor suppressors was observed in tumors isolated from animals treated with miR-21-5p decoys (Figure 7D, upper panel). In contrast, expression remained essentially unaffected in the lung of animals (Figure 7D, lower panel). Northern blotting clearly indicated that circular and linearized decoys were substantially more abundant in lung tissue (Supplementary Figure S7A). However, consistent with the severe upregulation of miR-21 expression in LUAD compared to healthy lung tissue, northern blotting demonstrated that miR-21-5p levels are substantially lower, actually non-detectable by northern blotting, in mouse lung tissue when compared to xenograft tumors (Figure 7C). These preclinical findings provide strong evidence that the

systemic application of circular miR-21-5p decoys delivered by PEI nanoparticles has a high therapeutic potency in impairing tumor growth in mice.

DISCUSSION

This study demonstrates for the first time the inhibition of the major oncomiR, miR-21-5p, by nanoparticle-delivered circular RNA decoys, leading to efficient impairment of tumor growth in an experimental mouse model. Our results as well as previous findings reported in the literature identify miR-21-5p as a direct or indirect regulator of major tumor suppressor genes. This combined regulation of several targets may provide a substantial advantage for therapies based on miRNA inhibition, with their broader action also addressing the notion of cancer as a pathway disease [52]. Concomitantly, miR-21-5p offers a strong predictive value, for example, with regard to overall patient survival, as also seen for the protein tumor suppressors, e.g. BTGs and PDCD4, identified or confirmed here to be regulated by this miRNA. Interestingly, *MIR21* deletion also leads to an upregulation of non-protein tumor suppressors, most prominently an increase of all let-7 miRNA family members. This supports the substantial impact of miR-21 on broad repression of tumor suppressors. Whereas elevated expression of protein tumor suppressors upon *MIR21* deletion is an obvious result of mRNA upregulation, the elevated expression

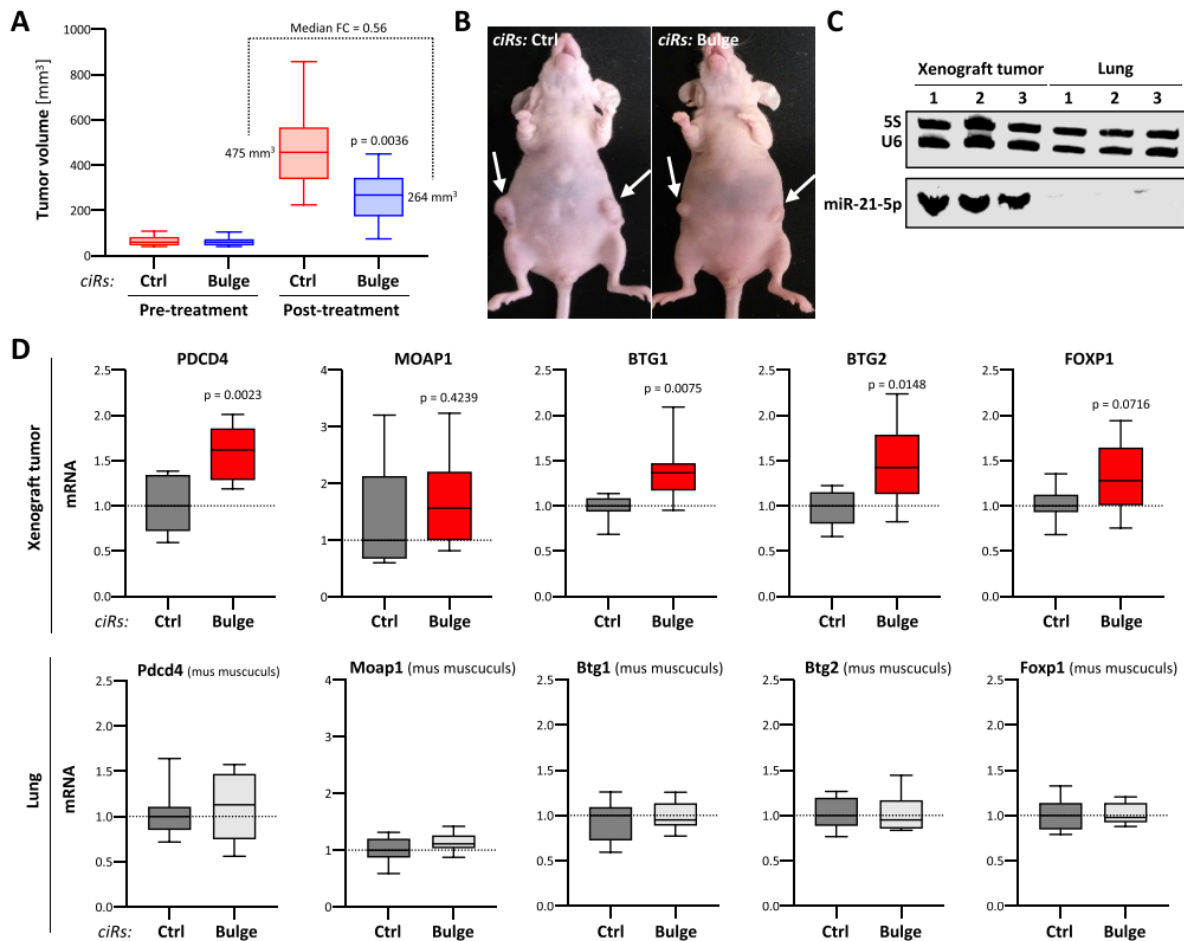


Figure 7. Nanoparticle-delivered miR-21-5p ciRs inhibit tumor growth and enforce tumor suppressor expression in murine LUAD models. (A) A549 cells were injected into the left and right flanks of nude mice. Mice were randomized when reaching tumor volume threshold volume (40–110 mm³). PEI nanoparticles loaded with Ctrl or bulged miR-21-5p ciRs were i.p. injected five times in 43 days and tumor volume was monitored (post-treatment, Ctrl $n = 8$, bulge $n = 13$). Statistical significance, indicated by P -values, was determined by the Mann-Whitney test. (B) Representative images of mice treated with Ctrl (left) or bulged miR-21-5p (right) ciRs. Arrows indicate primary tumors. (C) Northern blot analysis of miR-21-5p in xenograft tumors and murine lung tissue. 5S and U6 served as loading controls. (D) The expression of indicated mRNAs in tumors ($n = 8$, upper panel) and lung tissues ($n = 7$, bottom panel) derived from mice treated with miR-21-5p or control (Ctrl) ciRs is shown by box plots. RNA levels in miR-21-5p ciR-treated samples were normalized to median mRNA abundance in samples treated with Ctrl ciRs, as depicted by dashed lines. Statistical significance, as indicated by P -values, was determined using Student's t -test.

of let-7 miRNAs most likely indicates secondary regulation. This potentially relies on changes in transcription, the processing of precursor RNAs and/or altered turnover of mature or intermediate miRNA precursors. Although requiring further in-depth

analyses, upregulation of let-7 miRNAs in *MIR21-KO* cells is expected to largely result from downregulation of the oncogenic RNA-binding protein LIN28B. This destabilizes let-7 miRNAs by oligouridylation [53]. Most importantly, however, the substantial

abundance across cancers and comprehensive inhibition of tumor suppressors by miR-21-5p indicate this miRNA as a potent and broadly applicable therapeutic strategy in cancer treatment. Such strategies, however, require the development of potent inhibitors as well as their efficient delivery to the desired site of action. Here, we present the first evidence that targeting of miR-21-5p by circular miRNA decoys is effective in distinct tumor cells and impairs tumor growth in xenograft mouse models when delivered by nanoparticles.

Naturally occurring circular RNAs with miR decoy activity have been identified to serve essential roles in controlling gene expression [54–56]. In 2018, the first artificial circRNA decoy has been established to target miR-122 that is crucial for hepatic HCV expansion [19]. Recently, synthetic circular RNA sponges harboring five bulged miR-21 binding elements have been shown to suppress the proliferation of gastric cancer cells [20], although the circRNA design and production was substantially different from the earlier miR-122/HCV study and this study, as discussed elsewhere [21]. In this study, we designed ciRs containing only four either complementary or bulged miR-21-5p binding motifs. The bulged configuration is derived from the natural incorporation of any cellular miRNA into the Ago2 protein. In this complex, positions 10–12 of the miRNA are not required for base pairing with its target sequence [57]. These circRNAs proved to be substantially more stable than linear analogues with a cellular

half-life of ~20 h when transfected into cells in this and former studies. This elevated stability apparently results from a biphasic decay mechanism of circular RNA decoys, where the first and rate-limiting step is relinearization by either autohydrolysis or a yet to be determined endonucleolytic activity. In a second step, relinearized ciRs seem to undergo standard RNA decay. Considering the availability of functional miR-21-5p binding sites within the cell after transfection of circular RNA sponges, the detectable amounts of circular and linear RNA sponges have to be added up resulting in an elevated decoy half-life [19]. The efficient sequestration of miR-21-5p by these ciRs in cancer cells increased the expression of tumor suppressors targeted by miR-21-5p and, concomitantly, impaired tumor cell vitality. In agreement, the first reported *in vivo* application of ciR-21-loaded PEI nanoparticles efficiently inhibited tumor growth in a subcutaneous LUAD xenograft mouse model. Notably, this was associated with the de-repression of tumor suppressors, otherwise inhibited by miR-21-5p in tumors. While this demonstrates the specificity of this therapeutic intervention on the molecular level, it cannot be excluded that de-repression of other miR-21-5p targets may be involved in the antitumor effects as well, thus adding to the overall efficacy of miR-21-5p inhibition. Notably, although largely accumulated in healthy lungs, the expression of tumor suppressors remained unaffected by ciRs, most likely due to exceedingly low miR-21 levels in healthy lung tissue. This

underscores the specificity of the circular miR-21 decoys used here. In a related approach, Wang and colleagues transfected a human adenocarcinoma cell line with circular miR-21 decoys using lipofection before implanting these cells into mice [58]. Although this supports the notion of effective inhibition of tumor cell growth by miR-21-5p-directed decoys *in vivo*, the here presented studies present the first evidence that therapeutic delivery of ciRs by nanoparticles impairs growth of preformed tumors. PEIs have been shown previously to deliver plasmid DNA as well as small RNA molecules *in vitro* and *in vivo* (see e.g. [29,59–62]). In this study, we extend the use of PEI nanoparticles for the first time toward circRNAs and demonstrate high efficacy. This is particularly noteworthy since several liposomal and polymeric nanoparticle systems, including PEI complexes, have been found rather inefficient for mRNA delivery, which is generally considered more challenging than that of small oligonucleotides [see e.g. [63,64] and references therein]. In the case of PEI, it has been tempting to speculate that poor intracellular complex decomposition may be an underlying reason for this inefficacy, due to long, linear RNA molecules forming more stable complexes based on intramolecular cooperativity in electrostatic PEI/RNA interactions. This study, however, demonstrates the capability of PEIs for efficient *in vivo* delivery and activity of circular RNAs. In combination with its favorable biocompatibility, the low molecular weight PEI F25-LMW thus provides a platform for the therapeutic use of

circRNAs as well as for further improvement of nanoparticle properties. This may well include even shorter PEIs and/or their chemical modifications (see e.g. [65]). It has been controversially discussed whether artificial circular RNAs trigger the innate immune response as RNA viruses [66,67]. The Huh-7.5 cell line used in the earlier study is defective in RNA sensory pathways triggered by RIG-I or TLR-3 [19], but this may be relevant in antitumor approaches. It remains to be elucidated whether and how circular RNAs are recognized by the cell or in the context of the whole organism. Since RNA recognition largely relies on the detection of RNA ends, circRNAs may avoid innate immunity [67]. In summary, this study provides a proof of principle that circular miRNA decoys are suitable and effective tools for the *in cellulo* as well as *in vivo* inhibition of miR-directed gene silencing. Notably, substantial inhibition was demonstrated for miR-21-5p, the by far most abundant miRNA in cancer cells. This indicates ciRs as easily and costeffectively produced miR inhibitors, providing high flexibility by rapidly introducing variable miR-binding motifs depending on cellular miRNA expression patterns. Thus, the here presented findings unravel a new, exciting perspective in RNA-based drug development.

DATA AVAILABILITY

Total RNA-seq as well as small RNA-seq data were deposited at NCBI GEO (GSE148736).

ACKNOWLEDGEMENTS

The authors thank the Core Facility Imaging (CFI) of the Martin Luther University, the Deep Sequencing Group (TU Dresden) and Novogene (Hong Kong) for the support with all analyses.

AUTHOR CONTRIBUTIONS

S.M., S.H., O.R. and A.A. designed the experiments. S.M., A.W., J.B., N.B., M.L., C.M., A.O., T.S., L.S. and A.E. performed and interpreted the experiments. S.M., A.W. and J.H. generated *MIR21* knockout cells. S.M., A.E. and A.A. performed and T.F. supported animal experiments. M.G. analyzed RNA sequencing data. S.H., S.M., A.A. and O.R. conceived and wrote the manuscript.

FUNDING

DFG, Research Training Groups (RTGs) [2467 to S.H., 2355 to O.R.]; LOEWE program Medical RNomics (State of Hessen) [to O.R.].

CONFLICT OF INTEREST STATEMENT

None declared.

REFERENCES

- [1] Bartel,D.P. (2009) MicroRNAs: target recognition and regulatory functions. *Cell*, 136, 215–233.
- [2] Jonas,S. and Izaurralde,E. (2015) Towards a molecular understanding of microRNA-mediated gene silencing. *Nat. Rev. Genet.*, 16, 421–433.
- [3] Peng,Y. and Croce,C.M. (2016) The role of microRNAs in human cancer. *Signal Transduct. Target. Ther.*, 1, 15004.
- [4] Svoronos,A.A., Engelman,D.M. and Slack,F.J. (2016) OncomiR or tumor suppressor? The duplicity of microRNAs in cancer. *Cancer Res.*, 76, 3666–3670.
- [5] Boyerinas,B., Park,S.M., Shomron,N., Hedegaard,M.M., Vinther,J., Andersen,J.S., Feig,C., Xu,J., Burge,C.B. and Peter,M.E. (2008) Identification of let-7-regulated oncofetal genes. *Cancer Res.*, 68, 2587–2591.
- [6] Volinia,S., Calin,G.A., Liu,C.G., Ambs,S., Cimmino,A., Petrocca,F., Visone,R., Iorio,M., Roldo,C., Ferracin,M. et al. (2006) A microRNA expression signature of human solid tumors defines cancer gene targets. *Proc. Natl Acad. Sci. U.S.A.*, 103, 2257–2261.
- [7] Iorio,M.V., Visone,R., Di Leva,G., Donati,V., Petrocca,F., Casalini,P., Taccioli,C., Volinia,S., Liu,C.G., Alder,H. et al. (2007) MicroRNA signatures in human ovarian cancer. *Cancer Res.*, 67, 8699–8707.
- [8] Sondermann,A., Andreghetto,F.M., Moulatlet,A.C., da Silva Victor,E., de Castro,M.G., Nunes,F.D., Brandao,L.G. and Severino,P. (2015) MiR-9 and miR-21 as prognostic biomarkers for recurrence in papillary thyroid cancer. *Clin. Exp. Metastasis*, 32, 521–530.
- [9] Braconi,C., Henry,J.C., Kogure,T., Schmittgen,T. and Patel,T. (2011) The role of microRNAs in human liver cancers. *Semin. Oncol.*, 38, 752–763.

- [10] Liu,Z.L., Wang,H., Liu,J. and Wang,Z.X. (2013) MicroRNA-21 (miR-21) expression promotes growth, metastasis, and chemo- or radioresistance in non-small cell lung cancer cells by targeting PTEN. *Mol. Cell. Biochem.*, 372, 35–45.
- [11] Yang,Y., Meng,H., Peng,Q., Yang,X., Gan,R., Zhao,L., Chen,Z., Lu,J. and Meng,Q.H. (2015) Downregulation of microRNA-21 expression restrains non-small cell lung cancer cell proliferation and migration through upregulation of programmed cell death 4. *Cancer Gene Ther.*, 22, 23–29.
- [12] Zhou,L., Yang,Z.X., Song,W.J., Li,Q.J., Yang,F., Wang,D.S., Zhang,N. and Dou,K.F. (2013) MicroRNA-21 regulates the migration and invasion of a stem-like population in hepatocellular carcinoma. *Int. J. Oncol.*, 43, 661–669.
- [13] Wu,Y., Song,Y., Xiong,Y., Wang,X., Xu,K., Han,B., Bai,Y., Li,L., Zhang,Y. and Zhou,L. (2017) MicroRNA-21 (Mir-21) promotes cell growth and invasion by repressing tumor suppressor PTEN in colorectal cancer. *Cell. Physiol. Biochem.*, 43, 945–958.
- [14] Asangani,I.A., Rasheed,S.A., Nikolova,D.A., Leupold,J.H., Colburn,N.H., Post,S. and Allgayer,H. (2008) MicroRNA-21 (miR-21) post-transcriptionally downregulates tumor suppressor Pcd4 and stimulates invasion, intravasation and metastasis in colorectal cancer. *Oncogene*, 27, 2128–2136.
- [15] Frankel,L.B., Christoffersen,N.R., Jacobsen,A., Lindow,M., Krogh,A. and Lund,A.H. (2008) Programmed cell death 4 (PDCD4) is an important functional target of the microRNA miR-21 in breast cancer cells. *J. Biol. Chem.*, 283, 1026–1033.
- [16] Nagao,Y., Hisaoka,M., Matsuyama,A., Kanemitsu,S., Hamada,T., Fukuyama,T., Nakano,R., Uchiyama,A., Kawamoto,M., Yamaguchi,K. et al. (2012) Association of microRNA-21 expression with its targets, PDCD4 and TIMP3, in pancreatic ductal adenocarcinoma. *Mod. Pathol.*, 25, 112–121.
- [17] Pennelli,G., Galuppini,F., Barollo,S., Cavedon,E., Bertazza,L., Fassan,M., Guzzardo,V., Pelizzo,M.R., Rugge,M. and Mian,C. (2015) The PDCD4/miR-21 pathway in medullary thyroid carcinoma. *Hum. Pathol.*, 46, 50–57.
- [18] Bonneau,E., Neveu,B., Kostantin,E., Tsongalis,G.J. and De Guire,V. (2019) How close are miRNAs from clinical practice? A perspective on the diagnostic and therapeutic market. *eJIFCC*, 30, 114–127.
- [19] Jost,I., Shalamova,L.A., Gerresheim,G.K., Niepmann,M., Bindereif,A. and Rossbach,O. (2018) Functional sequestration of microRNA-122 from hepatitis C

- virus by circular RNA sponges. *RNA Biol.*, 15, 1032–1039.
- [20] Liu,X., Abraham,J.M., Cheng,Y., Wang,Z., Wang,Z., Zhang,G., Ashktorab,H., Smoot,D.T., Cole,R.N., Boronina,T.N. et al. (2018) Synthetic circular RNA functions as a miR-21 sponge to suppress gastric carcinoma cell proliferation. *Mol. Ther. Nucleic Acids*, 13, 312–321.
- [21] Rossbach,O. (2019) Artificial circular RNA sponges targeting MicroRNAs as a novel tool in molecular biology. *Mol. Ther. Nucleic Acids*, 17, 452–454.
- [22] Muller,S., Glass,M., Singh,A.K., Haase,J., Bley,N., Fuchs,T., Lederer,M., Dahl,A., Huang,H., Chen,J. et al. (2019) IGF2BP1 promotes SRF-dependent transcription in cancer in a m6A- and miRNA-dependent manner. *Nucleic Acids Res.*, 47, 375–390.
- [23] Muller,S., Bley,N., Glass,M., Busch,B., Rousseau,V., Misiak,D., Fuchs,T., Lederer,M. and Huttelmaier,S. (2018) IGF2BP1 enhances an aggressive tumor cell phenotype by impairing miRNA-directed downregulation of oncogenic factors. *Nucleic Acids Res.*, 46, 6285–6303.
- [24] Subramanian,A., Tamayo,P., Mootha,V.K., Mukherjee,S., Ebert,B.L., Gillette,M.A., Paulovich,A., Pomeroy,S.L., Golub,T.R., Lander,E.S. et al. (2005) Gene set enrichment analysis: a knowledge-based approach for interpreting genome-wide expression profiles. *Proc. Natl Acad. Sci. U.S.A.*, 102, 15545–15550.
- [25] Dweep,H. and Gretz,N. (2015) miRWalk2.0: a comprehensive atlas of microRNA–target interactions. *Nat. Methods*, 12, 697.
- [26] Breuer,J. and Rossbach,O. (2020) Production and purification of artificial circular RNA sponges for application in molecular biology and medicine. *Methods Protoc.*, 3, 42.
- [27] Pan,T. (2000) Probing RNA structure and function, by circular permutation. *Methods Enzymol.*, 317, 313–330.
- [28] Pall,G.S., Codony-Servat,C., Byrne,J., Ritchie,L. and Hamilton,A. (2007) Carbodiimide-mediated cross-linking of RNA to nylon membranes improves the detection of siRNA, miRNA and piRNA by northern blot. *Nucleic Acids Res.*, 35, e60.
- [29] Werth,S., Urban-Klein,B., Dai,L., Hobel,S., Grzelinski,M., Bakowsky,U., Czubyko,F. and Aigner,A. (2006) A low molecular weight fraction of polyethylenimine (PEI) displays increased transfection efficiency of DNA and siRNA in fresh or lyophilized complexes. *J. Control. Release*, 112, 257–270.
- [30] Hobel,S. and Aigner,A. (2010) Polyethylenimine (PEI)/siRNA-

- mediated gene knockdown *in vitro* and *in vivo*. *Methods Mol. Biol.*, 623, 283–297.
- [31] Hobel,S., Prinz,R., Malek,A., Urban-Klein,B., Sitterberg,J., Bakowsky,U., Czubayko,F. and Aigner,A. (2008) Polyethylenimine PEI F25-LMW allows the long-term storage of frozen complexes as fully active reagents in siRNA-mediated gene targeting and DNA delivery. *Eur. J. Pharm. Biopharm.*, 70, 29–41.
- [32] Ewe,A., Przybylski,S., Burkhardt,J., Janke,A., Appelhans,D. and Aigner,A. (2016) A novel tyrosine-modified low molecular weight polyethylenimine (P10Y) for efficient siRNA delivery *in vitro* and *in vivo*. *J. Control. Release*, 230, 13–25.
- [33] Nagy,A., Lanczky,A., Menyhart,O. and Gyorfy,B. (2018) Validation of miRNA prognostic power in hepatocellular carcinoma using expression data of independent datasets. *Sci. Rep.*, 8, 9227.
- [34] Calin,G.A. and Croce,C.M. (2006) MicroRNA signatures in human cancers. *Nat. Rev. Cancer*, 6, 857–866.
- [35] Esquela-Kerscher,A. and Slack,F.J. (2006) Oncomirs: microRNAs with a role in cancer. *Nat. Rev. Cancer*, 6, 259–269.
- [36] Wu,X.L., Cheng,B., Li,P.Y., Huang,H.J., Zhao,Q., Dan,Z.L., Tian,D.A. and Zhang,P. (2013) MicroRNA-143 suppresses gastric cancer cell growth and induces apoptosis by targeting COX-2. *World J. Gastroenterol.*, 19, 7758–7765.
- [37] Chen,B., Chen,X., Wu,X., Wang,X., Wang,Y., Lin,T.Y., Kurata,J., Wu,J., Vonderfecht,S., Sun,G. et al. (2015) Disruption of microRNA-21 by TALEN leads to diminished cell transformation and increased expression of cell–environment interaction genes. *Cancer Lett.*, 356, 506–516.
- [38] Ge,Y., Zhang,L., Nikolova,M., Reva,B. and Fuchs,E. (2016) Strand-specific *in vivo* screen of cancer-associated miRNAs unveils a role for miR-21* in SCC progression. *Nat. Cell Biol.*, 18, 111–121.
- [39] Sekar,D., Krishnan,R., Panagal,M., Sivakumar,P., Gopinath,V. and Basam,V. (2016) Deciphering the role of microRNA 21 in cancer stem cells (CSCs). *Genes Dis.*, 3, 277–281.
- [40] Massague,J., Blain,S.W. and Lo,R.S. (2000) TGFbeta signaling in growth control, cancer, and heritable disorders. *Cell*, 103, 295–309.
- [41] Duriez,C., Falette,N., Audouyand,C., Moyret-Lalle,C., Bensaad,K., Courtois,S., Wang,Q., Soussi,T. and Puisieux,A. (2002) The human BTG2/TIS21/PC3 gene: genomic structure, transcriptional regulation and evaluation as a candidate tumor suppressor gene. *Gene*, 282, 207–214.

- [42] Liu,M., Wu,H., Liu,T., Li,Y., Wang,F., Wan,H., Li,X. and Tang,H. (2009) Regulation of the cell cycle gene, BTG2, by miR-21 in human laryngeal carcinoma. *Cell Res.*, 19, 828–837.
- [43] Rouault,J.P., Rimokh,R., Tessa,C., Paranhos,G., Ffrench,M., Duret,L., Garoccio,M., Germain,D., Samarut,J. and Magaud,J.P. (1992) BTG1, a member of a new family of antiproliferative genes. *EMBO J.*, 11, 1663–1670.
- [44] Banham,A.H., Beasley,N., Campo,E., Fernandez,P.L., Fidler,C., Gatter,K., Jones,M., Mason,D.Y., Prime,J.E., Trougouboff,P. et al. (2001) The FOXP1 winged helix transcription factor is a novel candidate tumor suppressor gene on chromosome 3p. *Cancer Res.*, 61, 8820–8829.
- [45] Baksh,S., Tommasi,S., Fenton,S., Yu,V.C., Martins,L.M., Pfeifer,G.P., Latif,F., Downward,J. and Neel,B.G. (2005) The tumor suppressor RASSF1A and MAP-1 link death receptor signaling to Bax conformational change and cell death. *Mol. Cell*, 18, 637–650.
- [46] Busch,B., Bley,N., Muller,S., Glass,M., Misiak,D., Lederer,M., Vetter,M., Strauss,H.G., Thomssen,C. and Huttelmaier,S. (2016) The oncogenic triangle of HMGA2, LIN28B and IGF2BP1 antagonizes tumor-suppressive actions of the let-7 family. *Nucleic Acids Res.*, 44, 3845–3864.
- [47] Viswanathan,S.R., Daley,G.Q. and Gregory,R.I. (2008) Selective blockade of microRNA processing by Lin28. *Science*, 320, 97–100.
- [48] Hansen,T.B., Jensen,T.I., Clausen,B.H., Bramsen,J.B., Finsen,B., Damgaard,C.K. and Kjems,J. (2013) Natural RNA circles function as efficient microRNA sponges. *Nature*, 495, 384–388.
- [49] Memczak,S., Jens,M., Elefsinioti,A., Torti,F., Krueger,J., Rybak,A., Maier,L., Mackowiak,S.D., Gregersen,L.H., Munschauer,M. et al. (2013) Circular RNAs are a large class of animal RNAs with regulatory potency. *Nature*, 495, 333–338.
- [50] Wesselhoeft,R.A., Kowalski,P.S. and Anderson,D.G. (2018) Engineering circular RNA for potent and stable translation in eukaryotic cells. *Nat. Commun.*, 9, 2629.
- [51] Hobel,S., Koburger,I., John,M., Czubyko,F., Hadwiger,P., Vornlocher,H.P. and Aigner,A. (2010) Polyethylenimine/small interfering RNA-mediated knockdown of vascular endothelial growth factor *in vivo* exerts anti-tumor effects synergistically with bevacizumab. *J. Gene Med.*, 12, 287–300.
- [52] Bader,A.G., Brown,D. and Winkler,M. (2010) The promise of microRNA replacement therapy. *Cancer Res.*, 70, 7027–7030.

- [53] Balzeau,J., Menezes,M.R., Cao,S. and Hagan,J.P. (2017) The LIN28/let-7 pathway in cancer. *Front. Genet.*, 8, 31.
- [54] Hsiao,K.Y., Lin,Y.C., Gupta,S.K., Chang,N., Yen,L., Sun,H.S. and Tsai,S.J. (2017) Noncoding effects of circular RNA CCDC66 promote colon cancer growth and metastasis. *Cancer Res.*, 77, 2339–2350.
- [55] Hsiao,K.Y., Sun,H.S. and Tsai,S.J. (2017) Circular RNA: new member of noncoding RNA with novel functions. *Exp. Biol. Med. (Maywood)*, 242, 1136–1141.
- [56] Zheng,Q., Bao,C., Guo,W., Li,S., Chen,J., Chen,B., Luo,Y., Lyu,D., Li,Y., Shi,G. et al. (2016) Circular RNA profiling reveals an abundant circHIPK3 that regulates cell growth by sponging multiple miRNAs. *Nat. Commun.*, 7, 11215.
- [57] Schirle,N.T., Sheu-Gruttadauria,J. and MacRae,I.J. (2014) Structural basis for microRNA targeting. *Science*, 346, 608–613.
- [58] Wang,Z., Ma,K., Cheng,Y., Abraham,J.M., Liu,X., Ke,X., Wang,Z. and Meltzer,S.J. (2019) Synthetic circular multi-miR sponge simultaneously inhibits miR-21 and miR-93 in esophageal carcinoma. *Lab. Invest.*, 99, 1442–1453.
- [59] Aigner,A., Fischer,D., Merdan,T., Brus,C., Kissel,T. and Czubayko,F. (2002) Delivery of unmodified bioactive ribozymes by an RNA-stabilizing polyethylenimine (LMW-PEI) efficiently down-regulates gene expression. *Gene Ther.*, 9, 1700–1707.
- [60] Urban-Klein,B., Werth,S., Abuharbeid,S., Czubayko,F. and Aigner,A. (2005) RNAi-mediated gene-targeting through systemic application of polyethylenimine (PEI)-complexed siRNA *in vivo*. *Gene Ther.*, 12, 461–466.
- [61] Ibrahim,A.F., Weirauch,U., Thomas,M., Grunweller,A., Hartmann,R.K. and Aigner,A. (2011) MicroRNA replacement therapy for miR-145 and miR-33a is efficacious in a model of colon carcinoma. *Cancer Res.*, 71, 5214–5224.
- [62] Thomas,M., Lange-Grunweller,K., Dayyoub,E., Bakowsky,U., Weirauch,U., Aigner,A., Hartmann,R.K. and Grunweller,A. (2012) PEI-complexed LNA antiseeds as miRNA inhibitors. *RNA Biol.*, 9, 1088–1098.
- [63] Kowalski,P.S., Rudra,A., Miao,L. and Anderson,D.G. (2019) Delivering the messenger: advances in technologies for therapeutic mRNA delivery. *Mol. Ther.*, 27, 710–728.
- [64] Jarzebinska,A., Pasewald,T., Lambrecht,J., Mykhaulyk,O., Kummerling,L., Beck,P., Hasenpusch,G., Rudolph,C., Plank,C. and Dohmen,C. (2016) A single methylene group in

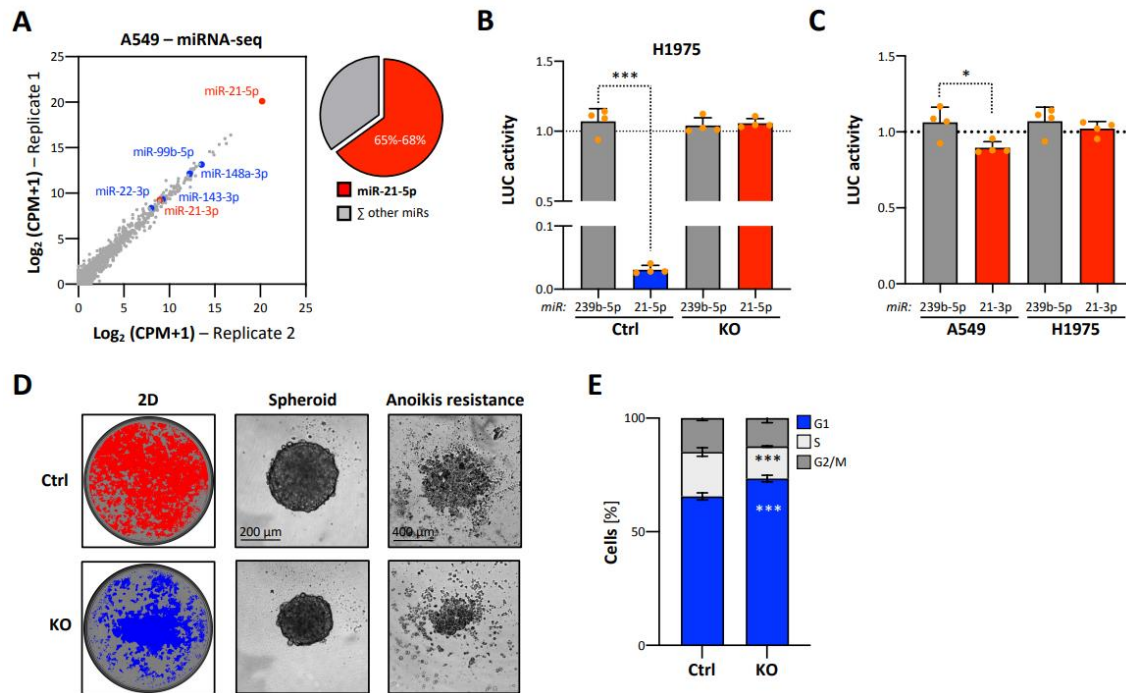
oligoalkylamine-based cationic polymers and lipids promotes enhanced mRNA delivery. *Angew. Chem., Int. Ed.*, 55, 9591–9595.

[65] Ewe,A., Noske,S., Karimov,M. and Aigner,A. (2019) Polymeric nanoparticles based on tyrosine-modified, low molecular weight polyethylenimines for siRNA delivery. *Pharmaceutics*, 11, 600.

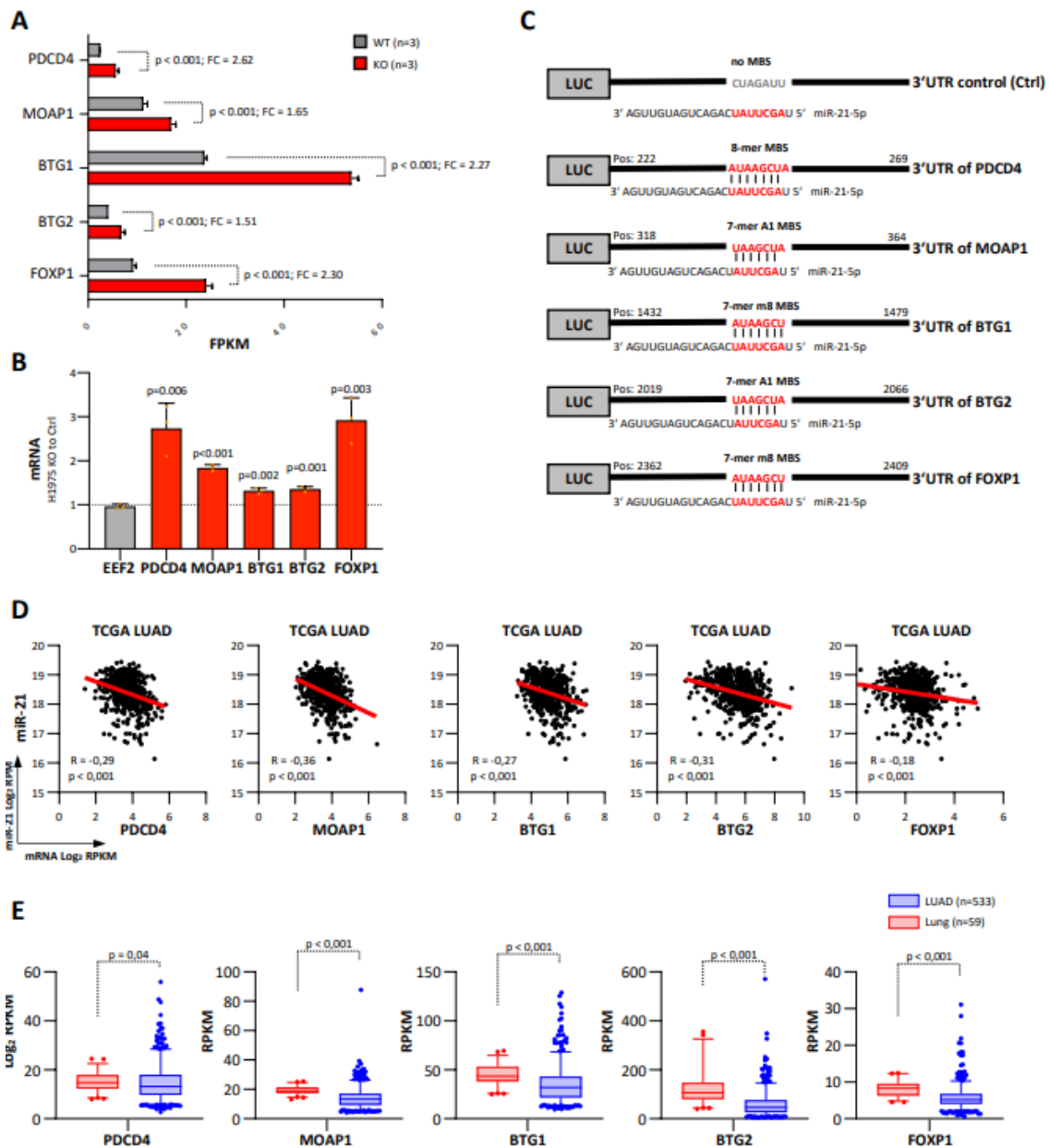
[66] Chen,Y.G., Kim,M.V., Chen,X., Batista,P.J., Aoyama,S., Wilusz,J.E., Iwasaki,A. and Chang,H.Y. (2017) Sensing self and foreign circular RNAs by intron identity. *Mol. Cell*, 67, 228–238.

[67] Wesselhoeft,R.A., Kowalski,P.S., Parker-Hale,F.C., Huang,Y., Bisaria,N. and Anderson,D.G. (2019) RNA circularization diminishes immunogenicity and can extend translation duration *in vivo*. *Mol. Cell*, 74, 508–520.

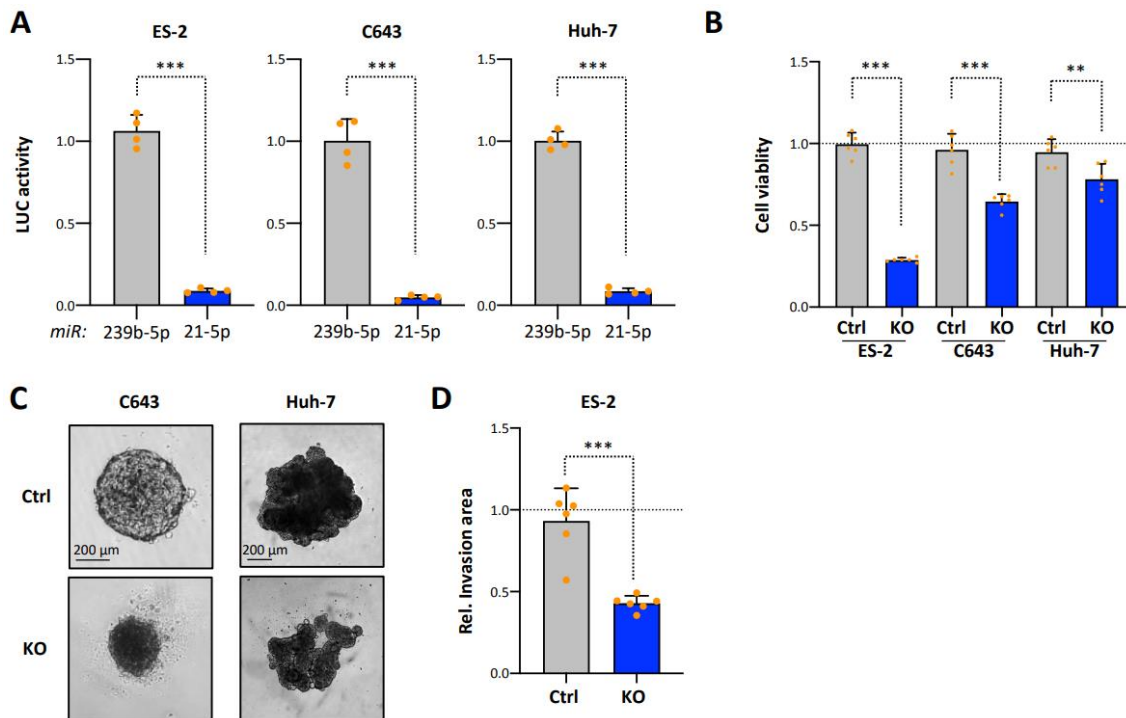
SUPPLEMENTARY DATA



Supplementary Figure S1. Loss of miR-21 impairs proliferation of LUAD-derived cancer cells. (A) Scatter plot (left panel) showing miRNA expression in two A549 miRNA-seq data sets. Selected miRNAs of Figure 1 are indicated. Pie chart (right panel) indicating the distribution of miR-21-5p/3p and all other annotated miRNAs in A549 cells determined by miRNA-seq. (B) miRNA-reporter analyses in H1975 Ctrl or miR-21 KO cells. The activity of the miRNAs (cel-miR-239b-5p and hsa-miR-21-5p) was analyzed as in Figure 1C in four independent experiments. (C) Reporter analysis showing the activity of miR-21-3p in A549 and H1975 cells. Analyses were performed as in Figure 2C in four independent experiments. (D) Representative images of H1975 Ctrl and *MIR21*-KO cells from Figure 2D-F are shown. (E) Fractions of A549 Ctrl and miR-21 KO cells in each cell cycle phase were quantified in five independent analyses. Statistical significance was determined by Student's *t*-test: *, $p < 0.05$; ***, $p < 0.001$

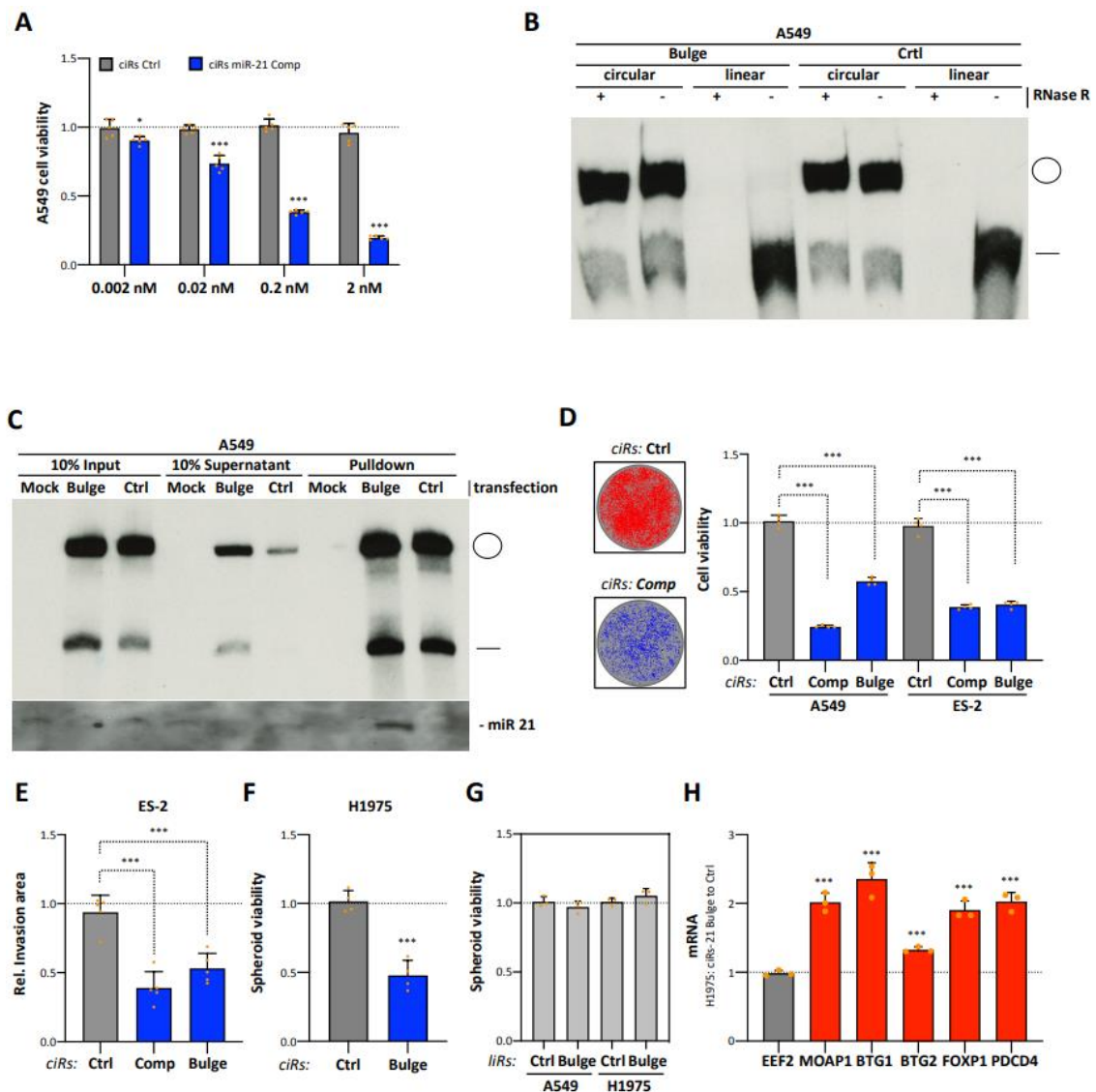


Supplementary Figure S2. Tumor suppressor-encoding mRNAs are repressed by miR-21 in LUAD-derived cells. (A) Abundance of indicated mRNAs in A549 Ctrl and miR-21 KO cells determined by RNAseq. Fold changes and p-values derived from 3 independent samples are shown. (B) RT-q-PCR analysis of mRNA levels in H1975 miR-21 KO cells normalized to Ctrl cells. RPLP0 served as normalization and EEF2 as negative control. Statistical significance was determined by using Student's *t*-test. (C) Schematic presenting luciferase reporters as in Figure 3E. Luciferase reporters comprise 48nt regions of the indicated 3'UTRs, including miR-21-5p seed regions (highlighted in red). (D) Scatter plots showing the expression of miR-21-5p (log2 RPM) and tumor suppressor-encoding mRNAs (log2 RPKM) in matched TCGA LUAD patients as in Figure 3C. Pearson correlation coefficient (*R*) and p-value are indicated. (E) Box plots of mRNA expression in lung (red, n=59) or LUAD (blue, n=533) RNA-seq data sets. Statistical significance was determined by using Mann-Whitney test.



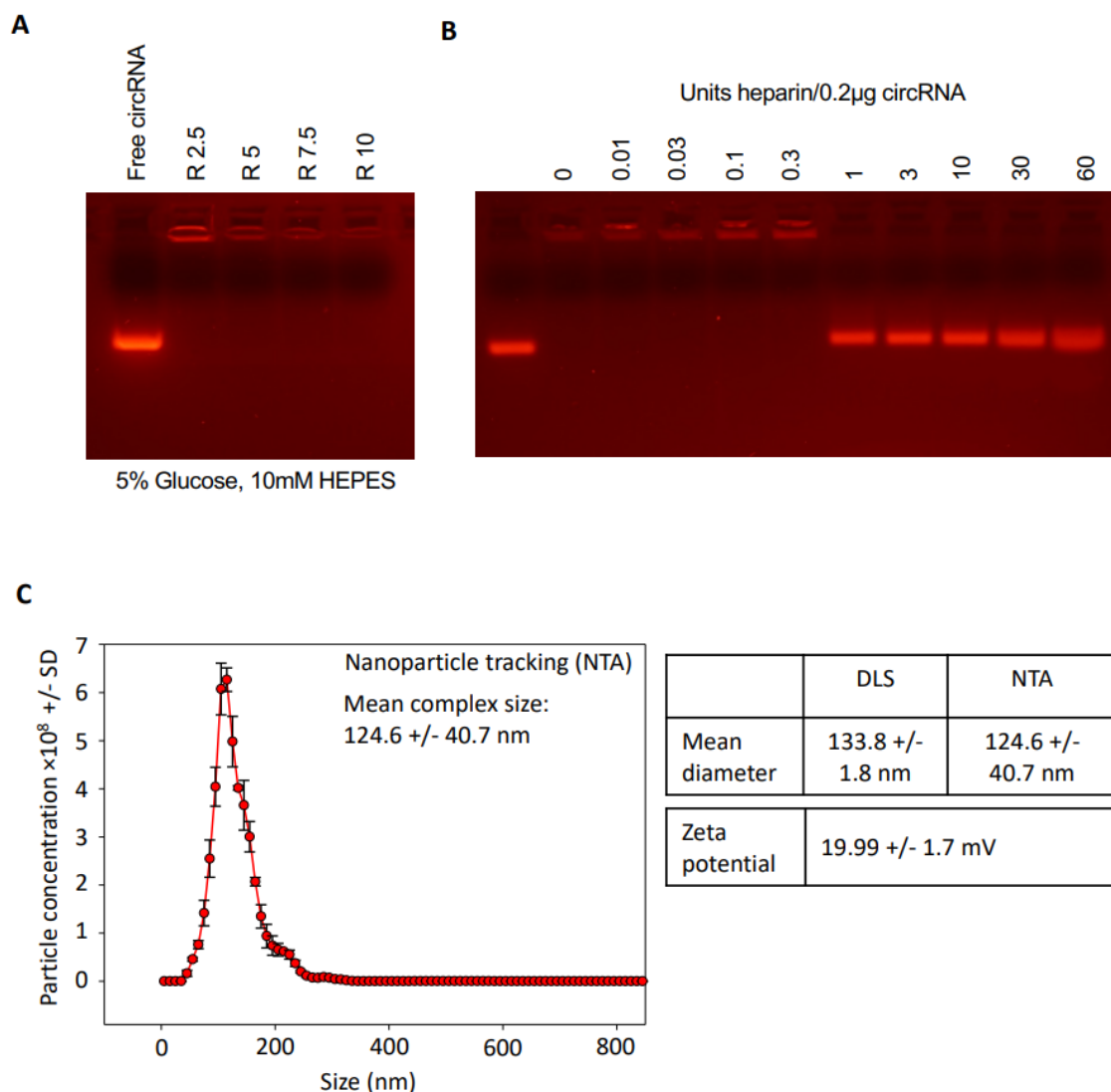
Supplementary Figure S3. MiR-21 promotes the proliferation of cancer-derived cells. (A) MiRNAreporter analyses in Ctrl or miR-21 KO ES-2, C643 and Huh-7 cells. Activities of miRNAs (cel-miR-239b5p and hsa-miR-21-5p) were determined and normalized as in Figure 2C. (B) Proliferation in 2D cultures of Ctrl or miR-21 KO ES-2, C643 and Huh-7 cells was determined by CellTiter GLO and mediannormalized in six independent experiments. (C) Representative images of Ctrl and *MIR21*-KO C643- and Huh-7-derived spheroids as in Figure 5C. (D) Quantification of the relative invasion area of Ctrl and *MIR21*-KO ES-2 spheroids from Figure 5D in six independent experiments. Statistical significance was determined by Student's *t*-test: **, $p < 0.01$; ***, $p < 0.001$

binding sites; Bulge: bulged miR-21 binding sites; Ctrl: control sequence without miR-21 binding sites) were produced by *in vitro* transcription following the protocol given in (Breuer, Rosbach 2020). The DNA template was removed by DNase treatment. Transcripts were analyzed on a 7% polyacrylamide-urea gel and visualized by ethidium bromide staining. (C) *In vitro* transcribed RNAs were ligated using T4 RNA ligase, resulting in a mixture of linear monomers (indicated by a dash), circular monomers (circle), linear dimers (double dash), linear trimers (triple dash) and circular dimers (large circle). To identify circularized miR-21 decoy RNAs the ligation reaction was analyzed using three different polyacrylamide-urea gels with 5, 6 and 7% polyacrylamide, respectively. Note that while the mobility of linear RNAs within polyacrylamide gels is proportionally to the size marker, circular RNAs show a decreased mobility within higher percentage polyacrylamide gels, which is detectable as a size shift comparing 5, 6 and 7% polyacrylamide-urea gels. (D) Linear and circular monomers from the ligation reaction in (C) were purified from a preparative 6% polyacrylamide gel, and analyzed as described above. Note that the minor linear monomer band in the circular RNA preparations is derived from stochastically occurring autohydrolysis of purified circular RNA molecules rather than co-purified linear monomer transcripts. (E) Purified linear and circular monomer RNA molecules were incubated in the presence or absence of RNase R (indicated by “+” and “-”). Afterwards the reaction was analyzed on a 7% polyacrylamide-urea gel and visualized by ethidium bromide staining. Note that the amount of the minor linear monomeric RNA in the circular RNA reactions is not changed with or without RNase R treatment, indicating that the linear monomer detected here are derived from stochastically occurring autohydrolysis of the circular RNA following RNase R treatment rather than RNase R resistant species.



Supplementary Figure S5. Artificial circular miR-21 RNA sponges reduce cell proliferation and enhance tumor suppressor expression. (A) Proliferation in 2D cultures of A549 cells transfected with increasing concentrations of Ctrl or miR-21-5p complementary circular RNA decoys (ciRS). Viability was determined by CellTiter GLO in five independent experiments and normalized to the Ctrl median with 0.002 nM ciRS. (B) RNase R treatment of total RNA isolated from A549 cells transfected with 200 ng of either circular or linear isoforms of the described artificial miR-21 sponges. Total RNA was isolated and incubated in the presence or absence of RNase R (indicated by “+” and “-”). Processed samples were analyzed on a 7% polyacrylamide-urea gel followed by visualization of circular and linear RNAs using Northern blotting. Note that the amount of the minor linear monomeric RNA in the circular RNA reactions remains unaffected by RNase R treatment, indicating that the linear monomer detected here are derived from stochastically occurring autohydrolysis of the circular RNA following RNase R treatment rather than RNase R-resistant species. (C) *In vivo* miR-21 affinity purification assay of artificial circular miR-21 sponges. A549 cells were transfected with biotinylated, circular miR-21 decoys. Upon affinity purification of decoys, co-purified RNA was analyzed by 7% and 15% polyacrylamide-urea gels. Decoys (upper panel) and mature miR-21-5p (lower panel) were analyzed by Northern blotting. Note that miR21-5p is only enriched with circular miR-21 decoys. (D) 2D proliferation of A549 and ES-2 cells transfected with 2nM Ctrl or miR-21-5p

targeting ciRS. Cell viability was determined by CellTiter Glo in four independent experiments and normalized to the Ctrl median (right panel). Representative brightfield images with overlaying confluence masks of ES-2 cells are shown (left panel). (E) Quantification of the relative invasion area of ES-2 spheroids transfected with 2nM Ctrl or miR-21-5p targeting ciRS, as depicted in Figure 6F, was performed in five independent experiments. (F) Proliferation of H1975- derived spheroids transfected with 2 nM Ctrl or miR-21 ciRs was determined by CellTiter GLO. Four independent experiments were normalized to the Ctrl median. (G) Proliferation of A549- and H1975- derived spheroids transfected with 2 nM Ctrl or miR-21 bulge linear RNAs (liRs) was determined by CellTiter GLO in three independent experiments normalized to the Ctrl median. (H) RT-q-PCR analysis of mRNA levels in H1975 cells transfected with bulged miR-21 circular RNA sponges normalized to Ctrl ciRS in three independent experiments. RPLP0 served as normalization and *EEF2* as negative control. Statistical significance was determined by Student's *t*-test: *, $p < 0.05$; *** $p < 0.001$



Supplementary Figure S6. Physicochemical characterization of PEI/circRNA complexes, with regard to complexation efficacy (A), complex stability (B) and complex properties (C).

What goes around comes around: Artificial circular RNAs bypass cellular antiviral responses

Janina Breuer¹, Patrick Barth², Yannic Noe¹, Lyudmila Shalamova³, Alexander Goesmann², Friedemann Weber³, and Oliver Rossbach^{1*}

¹Institute of Biochemistry, Faculty of Biology and Chemistry, Justus-Liebig-University of Giessen, Heinrich-Buff-Ring 17, 35392 Giessen, Germany; ²Bioinformatics and Systems Biology, University of Giessen, Heinrich-Buff-Ring 58, 35392 Giessen, Germany; ³Institute for Virology, Faculty of Veterinary Medicine, University of Giessen, Schubertstr. 81, 35392 Giessen, Germany

*To whom correspondence should be addressed. Oliver Rossbach, E-mail: oliver.rossbach@bc.jlug.de

Abstract: Natural circular RNAs have been found to sequester microRNAs and suppress their function. We have used this principle as a molecular tool and produced artificial circular RNA sponges in a cell-free system by *in vitro* transcription and ligation. Formerly, we were able to inhibit hepatitis C virus propagation by applying a circular RNA decoy strategy against microRNA-122, which is essential for the viral life cycle. In another proof-of-principle study, we used circular RNAs to sequester microRNA-21, an oncogenic and pro-proliferative microRNA. This strategy slowed tumor growth in a 3D cell culture model system, as well as in xenograft mice upon systemic delivery. In the wake of the global use of an *in vitro* transcribed RNA in coronavirus disease 2019 (COVID-19) vaccines, the question arose whether therapeutic circular RNAs trigger cellular antiviral defense mechanisms when delivered systemically. In this study, we present data on the cellular innate immune response as a consequence of liposome-based transfection of the circular RNA sponges we previously used to inhibit microRNA function. We find that circular RNAs produced by the presented methodology do not trigger the antiviral response and do not activate innate immune-signaling pathways.

This publication represents a component of my doctoral (Dr. rer. nat.) thesis in the Faculty of Biology and Chemistry at the Justus Liebig-University Giessen, Germany. Published in: *Molecular Therapy Nucleic Acids*, <https://doi.org/10.1016/j.omtn.2022.04.017> (2022). Received: January 04, 2022; Accepted: April 21, 2022

INTRODUCTION

Research on circular RNA (circRNA) has been underestimated and neglected for a long period but has become increasingly important for molecular biology, medicine, and pharmaceutical science in the recent years. Harboring neither a 5' cap nor a 3' poly(A) tail, circRNA molecules belong to a class of mainly non-coding

RNAs [1–5]. Naturally occurring circRNAs arise by an alternative splicing mechanism termed “back splicing” [3] or “head-to-tail splicing” [2]. This process is characterized by joining a splice donor to an upstream instead of a downstream splice acceptor site, relying on canonical splicing signals [1–5]. This results in a covalently closed and therefore

circularized structure, which is characterized by resistance to exonucleolytic degradation and an elevated stability compared with linear RNAs [3,6–9].

Even though naturally occurring circRNAs appear to be highly abundant, found in diverse species throughout the eukaryotic Tree of Life, and strictly regulated, the molecular function of most endogenous circRNAs is still unknown [2,3,6,10–12]. Nevertheless, there are several lines of evidence showing that circRNAs have important regulatory roles in cell biology and development [2,11,13–15]. As described by Holdt et al. [16] in 2017, circRNAs function in two general ways. First underlies the process of circRNA generation itself, and second, following their formation, their function as *trans*-acting molecule. Considering the latter, recent studies demonstrate that naturally occurring circRNAs have at least three major functions in eukaryotic cells: circRNAs can function as microRNA (miRNA) sponges, interact with RNA-binding proteins (RBPs), and act as nuclear transcriptional regulators—all together illustrating the impact of circRNAs on the regulatory networks governing gene expression [15,17,18].

When binding cytoplasmic miRNAs as molecular sponges, circRNAs are able to regulate and neutralize endogenous miRNA levels. In this context, two initial studies, published simultaneously in 2013 by the groups of Nikolaus Rajewsky and Jørgen Kjems, focused on the *cerebellar degeneration-related protein 1 transcript*

(CDR1as) gene, which expresses the cellular circRNA CDR1as/ciRS-7. CDR1as/ciRS-7 acts as a molecular sponge sequestering the cytoplasmic miRNA-7 via 70 highly conserved binding sites, hence its alternative name circRNA sponge for miRNA-7 (miR-7) (ciRS-7) [2,12]. Co-expressed with miRNA-7 in neocortical and hippocampal neurons, CDR1as/ciRS-7 leads to a sequestration of the miRNA, a suppression of miR-7 functions, and thereby a de-repression of natural miR-7 targets [2,12]. CDR1as/ciRS-7 knockout mice showed deregulated miRNAs, dysfunctional synaptic transmission, and symptoms associated with human neuropsychiatric disorders [19]. These exemplary results not only delay the sequestration of miRNAs by circRNAs and therefore the biological availability and function but also indicate the importance of circRNAs for normal cell functions [16].

The described characteristics, functions, and importance of naturally occurring circRNAs imply the increasing relevance of artificially produced circRNAs as potential tool for molecular biology and medicine [2,8,11,13–15,20]. In 2020, our group developed and published an optimized method for the engineering, *in vitro* production, and stringent purification of artificial ciRSs as novel agents for miRNA inhibition [20]. This technique was firstly utilized in the hepatitis C virus (HCV) model system to provide a proof-of-principle study that artificial ciRSs are capable of the sequestration of mature miRNAs to impair their biological functions [8]. Binding of miR-

122 at two distinct binding sites at the 5' end of the positive-sense, single-stranded RNA genome of the hepatocyte-specific virus results in the protection of the viral RNA from exonucleolytic degradation and enhancement of viral translation [21–24]. Miravirsen, a locked nucleic acid (LNA)-containing DNA oligonucleotide antisense to miR-122, inhibits viral propagation by sequestration of the miRNA [25]. In this context, engineered ciRSs efficiently bound and sequestered the cellular miR-122 *in vitro* and *in vivo*, thereby reducing viral intracellular protein levels similar to Miravirsen [8].

Moreover, the concept of artificial circRNA sponges was used to target miR-21. miR-21 is one of the earliest identified oncogenic miRNAs [26]. When upregulated in cancer cells, miR-21 inhibits numerous tumor suppressor mRNAs, which is associated with proliferation, apoptosis, and invasion [26–28]. As miR-21 is the most abundant miRNA across cancer transcriptomes, and *MIR21* knockout resulted in a reduced tumor growth, ciRSs were designed to impair miR-21 activities *in vivo* [9]. In addition to causing a significant reduction in cell proliferation and invasion of 3D spheroid model systems, artificial ciRS sequestering miR-21 significantly inhibited tumor growth in a lung adenocarcinoma xenograft mouse model via the upregulation of tumor-suppressor expression [9]. Furthermore, the transfection of related circRNAs sequestering miR-21 led to induced apoptosis and increased expression of miR-21-

regulated proteins in gastric cancer cell lines in another study [29].

Two fundamental parameters determine the fate of any pharmaceutical: (1) the efficacy and (2) the toxicity [30]. Considering the described findings, the past few years have witnessed the advent of artificial circRNA sponges as a novel and powerful antisense approach to inhibit miRNA activities in the context of human diseases, e.g., caused by viral infections or cancer [8,9,29,30]. What remained controversial, however, was the question whether circRNAs may provoke innate immunity responses. The cellular innate immune system is able to detect foreign RNA via sensory molecules like RIG-I, PKR, or TLR7/8. This leads to the activation of various signaling pathways, resulting in the induction of cytokines, chemokines, and interferons [31]. As recently also seen in the context of mRNA vaccines, the bypassing of the cellular immunity is crucial for the success of a clinical application [32]. Several groups have tested circRNAs that have been artificially produced and purified by different procedures for their capability to stimulate RNA recognition pathways, with varying and controversial results [33,34].

In this study, we demonstrate that artificial circRNAs can be utilized as miRNA sponges, if produced in a cell-free system by *in vitro* transcription and ligation, and stringently purified by gel extraction, can bypass the cellular RNA sensors, and are not recognized by the innate immune system.

RESULTS

Artificial circular RNA sponges can be produced and purified in vitro

Encouraged by naturally occurring circRNAs containing binding sites that are able to sequester specific miRNAs, artificial ciRSs were designed to target the oncogenic miR-21 [2,9,12]. Together with a doublestranded 11-nt stem loop and a 63-nt constant region, the engineering process resulted in ciRS containing either four bulged miR-21-binding sites (ciRS-21-bulge (ciRS-21-bu)) or a randomized sequence with the exact same nucleotide composition (ciRS-21-random (ciRS-21-rnd)) as negative control for miRNA binding. Our earlier studies demonstrated that sequestration of miR-21 was highly efficient, resulting in an impaired oncogenic potential of cancer cells in cell culture and in a xenograft mouse model, as published in Müller et al. [9] in 2020. Inspired by rising questions on the immunogenicity of circRNAs, this study focuses on the innate immune responses triggered by the same artificial ciRS.

Our *in vitro* circRNAs production procedure, as described in detail elsewhere [20], includes three main steps: (1) the T7 RNA polymerase-mediated *in vitro* transcription and transcript purification, (2) the transcript ligation based on the T4 RNA ligase, and (3) the gel purification of circular and linear constructs (Figure 1A). RNA quality and purity was controlled after each step of the production procedure (Figures 1B and 1C). After *in vitro* ligation, transcripts either remain linear

monomers; are ligated inter-molecularly, forming linear dimers or multimers; or are ligated intra-molecularly into circular monomers (Figures 1A and 1B). As already reported in 1988 by Tabak et al. [35], the aberrant mobility of circRNA molecules within 6%, 7%, and 8% polyacrylamide-urea gels allows specific identification and separation and therefore enables gel purification of circular and linear isoforms of the RNA sponges (ciRSs and liRSs). While the relative mobility of linear RNAs remains unchanged compared with the respective RNA ladder, the mobility of circRNAs appears lower in higher percentage polyacrylamide-urea gels, resulting in a shift of the circRNA compared with marker bands (Figures 1B and 1C). ciRS-21-bu and ciRS-21-rnd show circularization efficiencies of 70%–80%. Other isoforms, as linear transcript monomers or dimers, were detectable but at substantially lower abundance (Figure 1B). RNase R exonuclease treatment of gel-purified circular and linear isoforms of ciRS-21-bu and ciRS-21-rnd verified circularity (Figure 1D).

Differential expression analysis after ciRS transfection

Foreign RNA, e.g., viral RNA, is efficiently detected by the host antiviral innate immune system [36]. The array of RNA sensors includes single- and double-stranded RNA-binding proteins, such as RIG-I, PKR, and the TLRs (Figure 2) [37,38]. However, despite several publications discussing roles of RIG-I and PKR in detection of

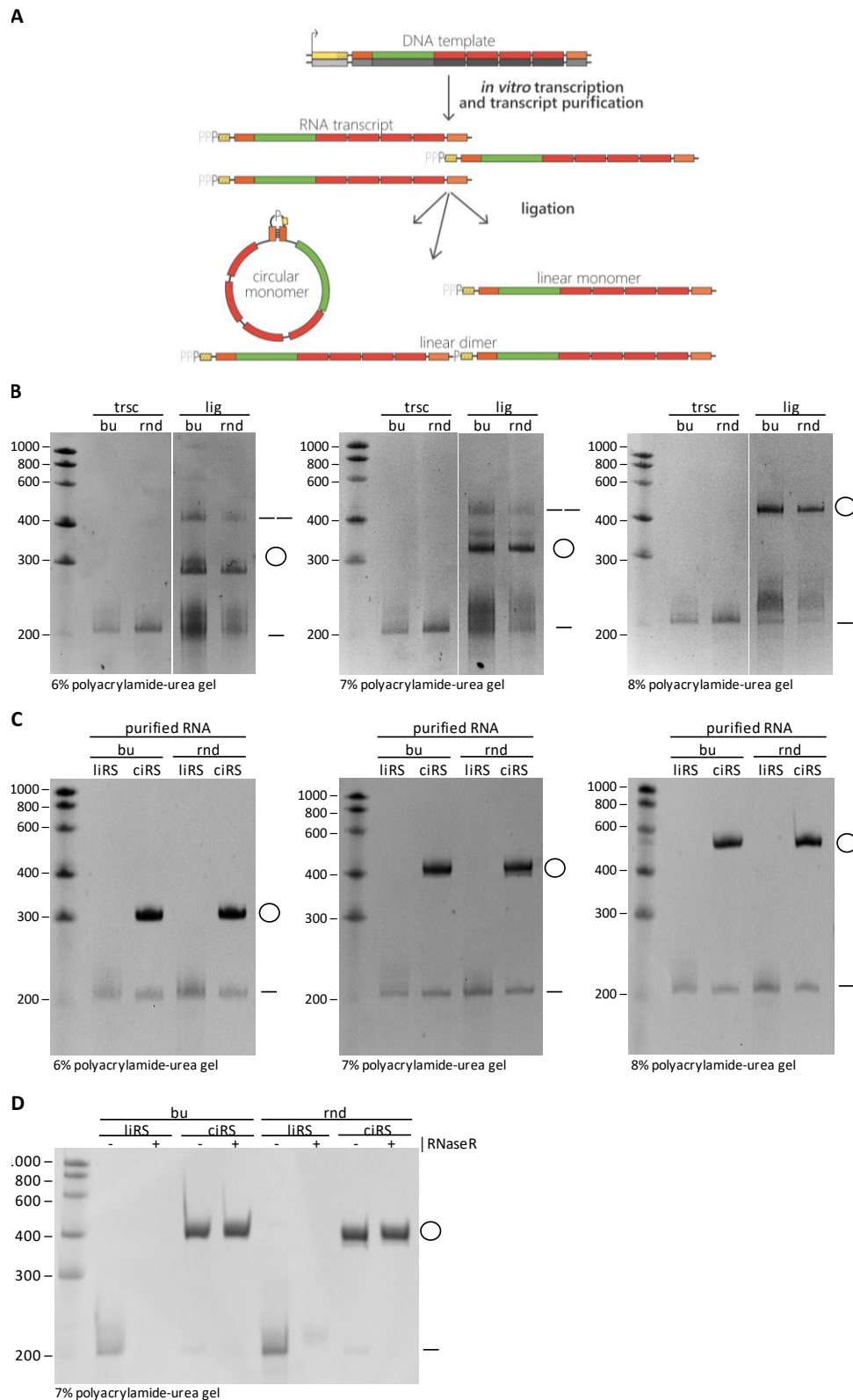


Figure 1: In vitro production of artificial circular RNA sponges. (A) Schematic workflow of the ciRS production procedure—including an *in vitro* transcription from a DNA template, followed by transcript purification and ligation. Considering the activity of the T4 RNA ligase, transcript ligation resulted in both linear monomers and dimers of the transcript and circularized transcripts (indicated by the dash and double dash or the circle in B, C, and D). (B) *In vitro* transcription (trsc) and circularization (lig) reaction of constructs ciRS-21-bulge (bu) and ciRS-

21-random (rnd) were analyzed by 6%, 7%, and 8% polyacrylamideurea gel electrophoresis, followed by ethidium bromide staining. Linear and circular isoforms of the 208-nt transcripts show a circularization efficiency of ~40%– 80%, and only small amounts of linear dimers are detectable. While the mobility of linear RNAs remains unchanged compared with the RNA ladder, the mobility of circular RNA appears lower in higher percentage polyacrylamide-urea gels, resulting in a shift of the circular RNA when comparing the polyacrylamide-urea gels with different concentrations and allowing circRNAspecific gel purification. (C) Circular and linear isoforms of the RNA sponges (ciRS and liRS) were purified, and quality was verified on analytic 6% and 7% polyacrylamide-urea gels by ethidium bromide staining. (D) Both purified ciRS and liRS were subjected to RNase R exonuclease (+) or control (-) treatment and analyzed on 7% polyacrylamide-urea gel by ethidium bromide staining to validate circularity.

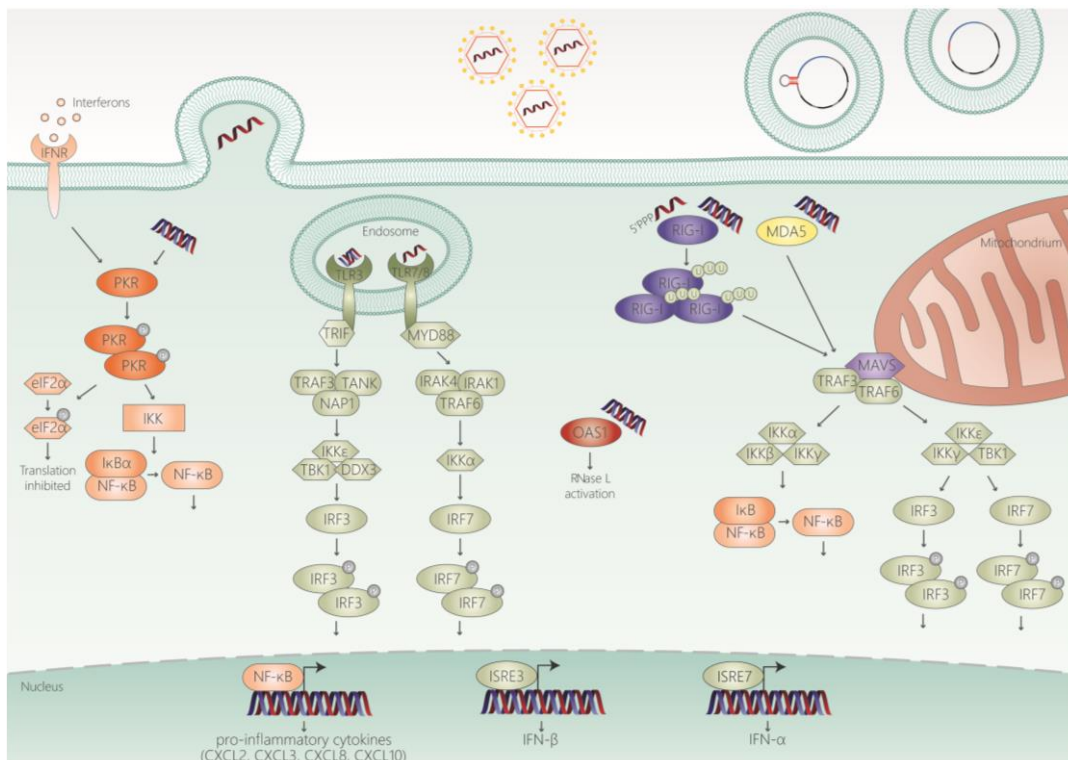


Figure 2: Cellular mechanisms for identifying foreign RNAs. The innate immunity is the first line of defense against invading pathogens entering a cell. In this context, cell-associated pattern recognition receptors are crucial for the detection of pathogen-associated molecular patterns (PAMPs), including, for example, viral single- or doublestranded RNA within the endosome or cytoplasm of a cell. Consequently, these intracellular sensory molecules like PKR, TLR3, TLR7, TLR8, OAS1, RIG-I, and MDA5 lead to an activation of a cascade of downstream signaling pathways, triggering an inflammatory response by inducing cytokines, chemokines, and interferons. However, the mechanism detecting foreign circular RNA is still unclear.

foreign circRNA molecules, the cellular mechanisms of discrimination and detection of foreign circRNAs are largely unknown [33,34,39,40]. Aiming to identify pathways activated after transfection of the linear and circular

miR-21 (liRS/ciRS-21-bu) and control RNAs (liRS/ciRS-21-rnd) into A549 cells, transcriptome analysis was performed via RNA sequencing (Figure 3). Gene ontology (GO) enrichment analysis of genes more than 4-fold

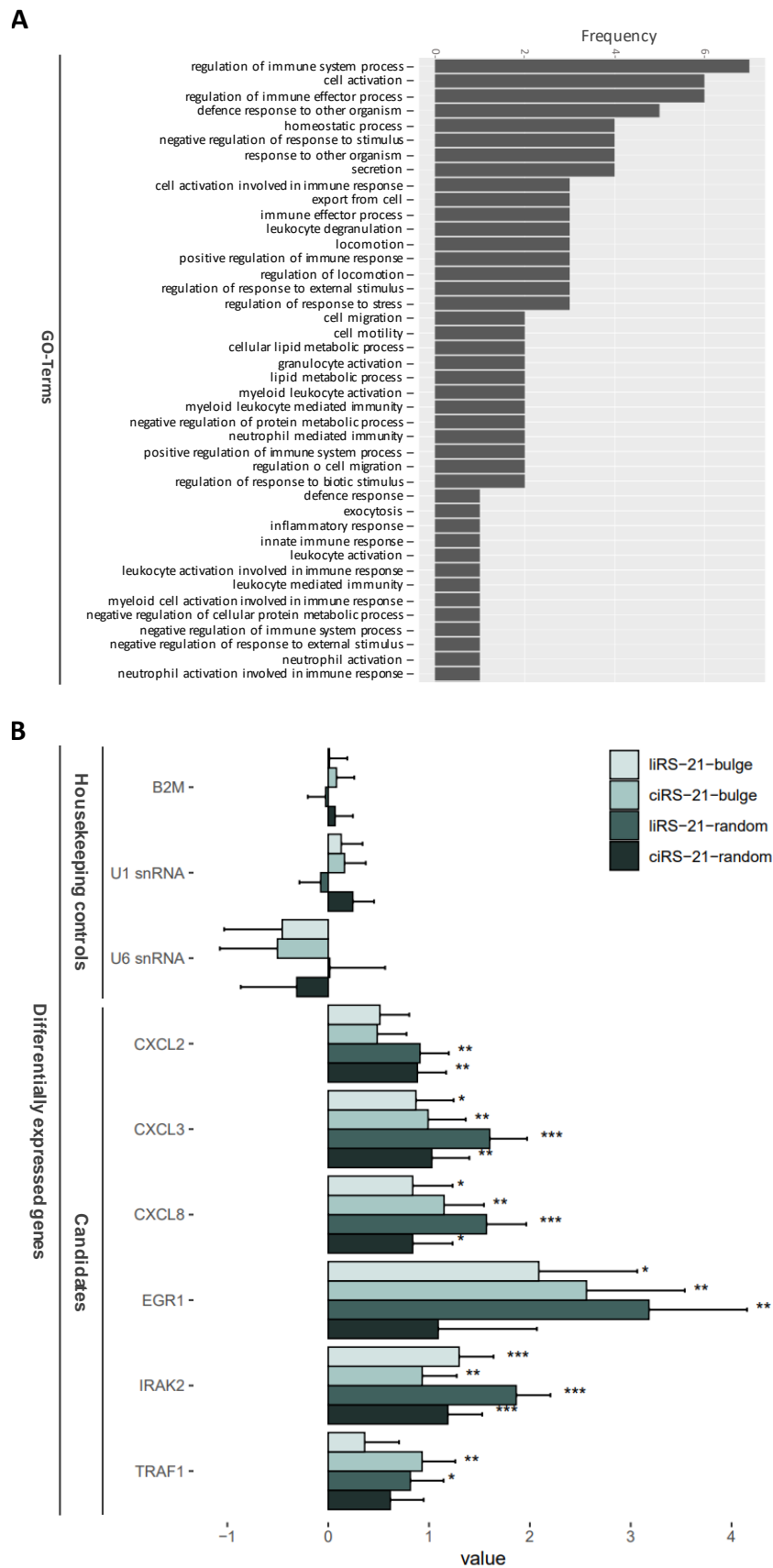


Figure 3: RNA sequencing revealed low immunogenic potential of ciRS-21-bu and ciRS-21-rnd and their linear counterparts. A549 cells were transfected with 250 ng of the artificial linear and circular RNA sponges ciRS-21-bu and ciRS-21-rnd. At 3 h posttransfection, A549 cells were

harvested, total RNA was isolated, and RNA sequencing was performed. Upregulated mRNAs upon ciRS-21-bu transfection were subjected to (A) Gene Ontology (GO) term analysis. (B) Furthermore, *CXCL2*, *CXCL3*, *CXCL8*, *EGR1*, *IRAK2*, and *TRAF1* were identified as differentially expressed candidate mRNAs upon ciRS-21-bu and ciRS-21-rnd transfection relative to mock-treated cells incubated with the transfection reagent only. *B2M* mRNA, U1 snRNA, and U6 snRNA were used as housekeeping controls. Statistical significance indicated by p values (*p < 0.05; **p < 0.01; ***p < 0.001).

upregulated after ciRS21-bu treatment indicated a variety of processes, such as the regulation of immune system process, cell activation, and secretion (Figure 3A). Differential expression analysis revealed that the transcriptome of cells transfected with ciRS/liRS-21-bu or ciRS/liRS-21-rnd was very similar to cells without RNA transfection, with only a few differentially expressed mRNAs detectable. Nevertheless, six potential candidates upregulated after ciRS transfection could be determined in context of the innate immune response: *CXCL2*, *CXCL3*, *CXCL8*, *EGR1*, *IRAK2*, and *TRAF1* (Figure 3B), although the increase in expression was moderate (2- to 4-fold) in the differential expression analysis.

Innate immune responses can be stimulated with an extensively double-stranded circRNA

As the sequencing results indicated a surprisingly low extent of innate immunity activation, we included a set of control RNA molecules for immune activation. Apart from using only known immunostimulants, such as high- and low-molecular-weight polyinosinic-polycytidylic acid (HMW and LMW poly(I:C)), which mimic long double-stranded RNAs (dsRNAs), and single-stranded poly uridine (ssPolyU), we created an extensively double-

stranded circRNA. In more detail, we engineered an artificial ciRS sharing the same basic structure as ciRS-21-bu and ciRS-21-rnd (stem loop and constant region) but containing a randomized self-complementary sequence of 50 bp, resulting in ciRS-21-doublestranded (ciRS-21-ds) (Figure 4A). The reverse-complementary sequence element of ciRS-21-ds was designed based on the nucleotide composition of the randomized ciRS-21-rnd circRNA (Figure 4A). Compared with ciRS-21-bu and ciRS-21-rnd, RNAfold secondary structure prediction for ciRS-21-ds showed the highconfidence base-pairing interaction within the sequence, with a maximum of 50 bp, resulting in a secondary structure formation (Figure 4B). As reported for ciRS-21-bu and ciRS-21-rnd, ciRS21-ds was produced via *in vitro* transcription, ligation of the transcripts, and gel purification of linear and circular isoforms (Figures 1A, 4C, and 4D). Contrary to previously illustrated *in vitro* ligations (Figure 1) [8,9,20], production of ciRS-21-ds was less efficient. The highly double-stranded sequence of this construct affected the transcription efficiency and altered the mobility within polyacrylamide-urea gels. As seen in Figures 4C and 4D, not only circular but also linear constructs of ciRS-21-ds showed a size shift compared with the RNA ladder within 6%, 7%, and 8%

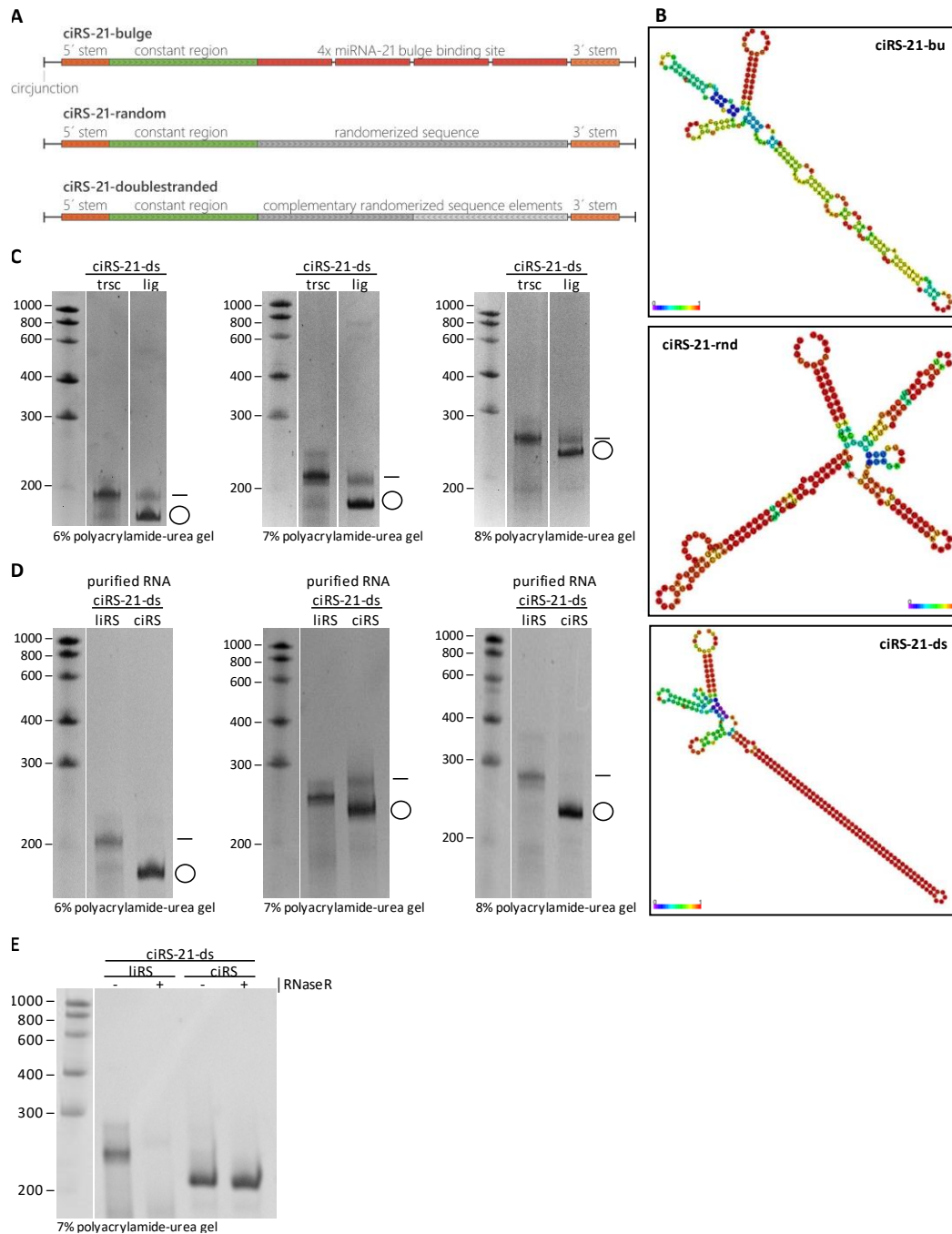


Figure 4: Design and *in vitro* production of a highly double-stranded artificial circular RNA sponge. (A) Schematic overview of structure and sequence properties of the analyzed artificial circular RNA sponges with a length of 208 nt. Conventionally, all transcripts share several sequence elements: a 5' and 3' stem (orange) sequence forming an 11-nt double-stranded stem-loop structure and a 63-nt "constant region" (green), which serves as binding site for, e.g., PCR primers or antisense probes in northern blotting. The ciRS-21-bu includes four miR-21-binding sites (red) containing a bulge between nucleotides 10 and 12 and a spacing of 4 nt between binding sites. Contrastingly, ciRS-21-rnd is characterized by a randomized sequence (dark gray), and based on the latter, ciRS-21-ds contains a doublestranded randomized sequence (dark and light gray) as central element. Vertical bars (|) mark the circular junctions. Less than (<) and greater than (>) symbols indicate complementary sequence elements. (B) Secondary structure of ciRS-21-bu, ciRS-21-rnd, and ciRS-21-ds predicted by RNAfold 2.4.18 online tool by

calculation of the minimum free energy of the RNA sequence. Predicted strong secondary structure interactions are indicated in red; low probability interactions are indicated in blue. (C) Analysis of the *in vitro* transcription (trsc) and ligation (lig) of the highly double-stranded ciRS-21-ds via 6%, 7%, and 8% polyacrylamide-urea gel electrophoresis, followed by ethidium bromide staining. Linear and circular transcripts (indicated by the dash or the circle, respectively) display an aberrant mobility of the 208 nt comprising construct, and a circularization efficiency is estimated at ~80%. (D) Circular and linear isoforms of the RNA sponge (ciRS-21-ds and liRS-21-ds) were gel purified, and RNA integrity was verified on analytic 6% and 7% polyacrylamide-urea gels by ethidium bromide staining. (E) Both purified ciRS and liRS were subjected to RNase R exonuclease (+) or control (-) treatment and analyzed on 7% polyacrylamide-urea gel by ethidium bromide staining to validate circularity.

polyacrylamide-urea gels, making it difficult to distinguish linear and circular isoforms. Surprisingly, highly double-stranded ciRS-21-ds migrated even faster than liRS-21-ds in 6%, 7%, and 8% polyacrylamide-urea gels (Figure 4C). Notably, no linear dimers of intermolecularly ligated transcripts were detected and the observed circularization efficiency was 90% compared with remaining linear transcript monomers (Figure 4C). Analytic polyacrylamide-urea gels and RNase R exonuclease treatment of purified liRS and ciRS confirmed that, despite the difficulties in identification of circular and linear isoforms within polyacrylamide-urea gels, the purification of ciRS-21-ds was successful (Figures 4D and 4E).

ciRS-21-bu and ciRS-21-rnd do not trigger the cellular innate immune response

Next, effects of ciRS-21-bu, ciRS-21-rnd, and ciRS-21-ds transfections of A549 cells were analyzed compared with cells treated with immunostimulants, such as HMW or LMW poly(I:C) and ssPolyU, or liposome transfected control (mock) cells (Figures 5, 6, and

7). We analyzed mRNA levels of the candidate regulated mRNAs of *CXCL2*, *CXCL3*, *CXCL8*, *EGR1*, *IRAK2*, and *TRAF1* identified in RNA sequencing (Figure 3) via qRT-PCR (Figures 5A, 6A, and 7A). Immunogenicity of transfected constructs was additionally assessed via the chemokine *CXCL10* and the interferon *INFB1* mRNA levels (Figures 5B, 6B, and 7C). After normalization to mock-treated control cells, only a global, unspecific response was observed in all transfections after 0.5 h, regardless of the agents used. However, a more specific response to ciRS-21-ds and both poly(I:C) controls manifested within 2–24 h (Figure 5). In addition, cellular response to treatment with increasing doses of the different constructs varying from 21 ng to 7,000 ng was analyzed 3 h after transfection of A549 cells. Even minimal amounts of ciRS-21-ds, HMW poly(I:C), and LMW poly(I:C) led to a potent increase in the levels of mRNAs associated with innate immunity signaling, as detected by qRT-PCR (Figure 6). However, treatment of A549 cells with ciRS-21-bu resulted in minimal upregulation of these mRNAs and only after treatment with high doses of the circRNA (Figure 6).

In all experiments performed, cellular response to the highly doublestranded ciRS-21-ds was found to mimic immunogenicity of poly(I:C) treatment (Figures 5, 6, and 7). Therefore, within this study, we reveal a time- and dose-dependent immunogenicity of ciRS-21-

ds, but not of ciRS-21-bu or ciRS-21-rnd—as evident from an upregulation of *CXCL2*, *CXCL3*, *CXCL8*, *EGR1*, and *TRAF1* mRNAs, as well as *CXCL10* and *IFNB1* (Figures 5, 6, and 7). However, *IRAK2* mRNA levels remained unchanged.

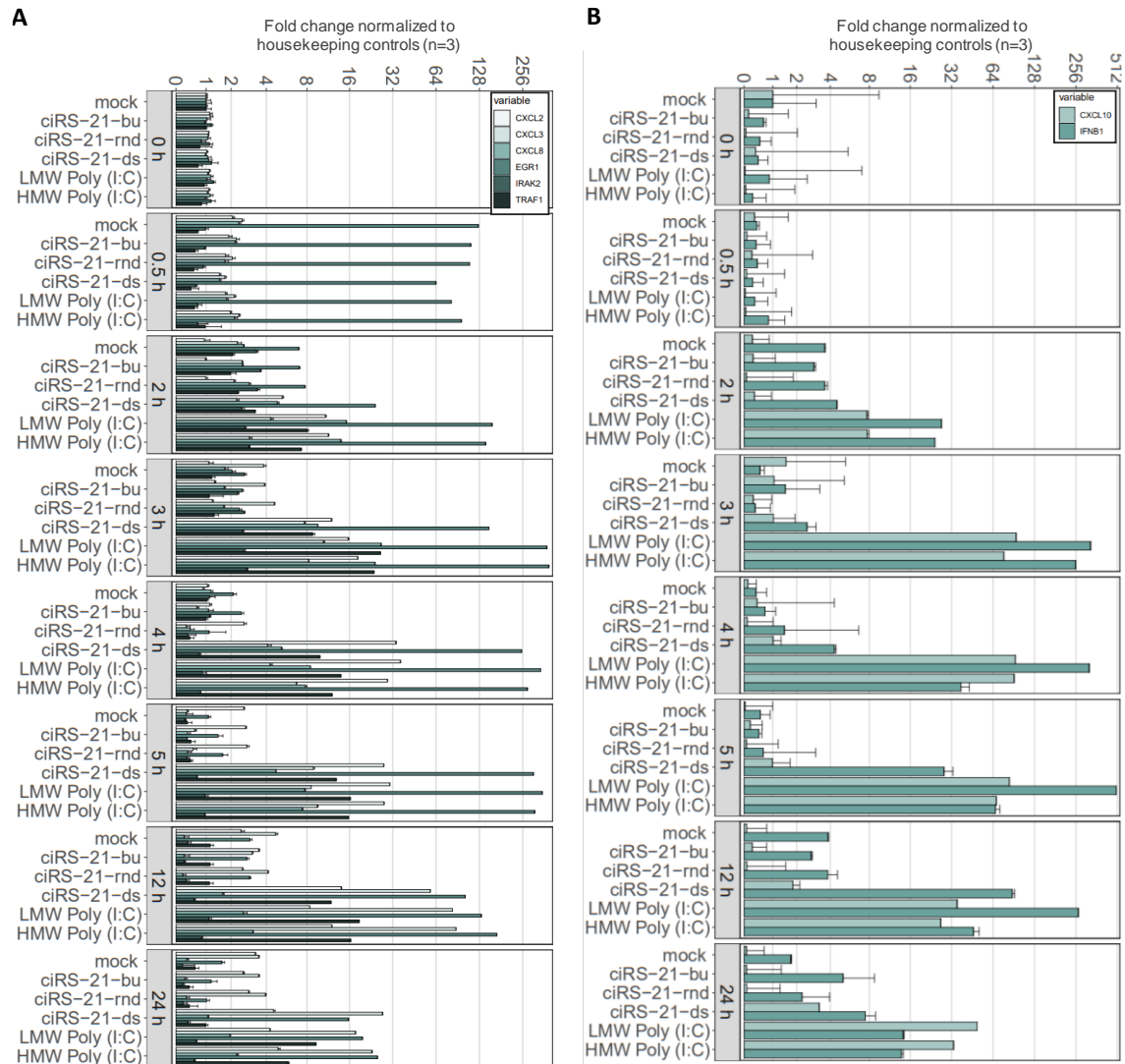


Figure 5: Time-dependent immune response to ciRS-21-ds and poly(I:C) in contrast to ciRS-21-rnd and ciRS-21-bu treatment. A549 cells were transfected with 250 ng of either the artificial circular RNA sponges, ciRS-21-bu, ciRS-21-rnd, and ciRS-21-ds or with the immunostimulants low-molecular-weight and high-molecular-weight polyinosinic:polycytidylic acid (LMW poly(I:C) and HMW poly(I:C)). As control, cells were only treated with the transfection reagent (mock) but no circular RNA or immunostimulant. We harvested A549 cells 0, 0.5, 2, 3, 4, 5, 12, and 24 h post transfection, and total RNA was isolated. qRT-PCR was performed for the candidates upregulated in RNA sequencing: (A) *CXCL2*, *CXCL3*, *CXCL8*, *IRAK2*, *EGR1*, and *TRAF1* as well as for (B) *CXCL10* and *IFNB1*. Data were normalized to mean value of B2M mRNA, U1 snRNA, and U6 snRNA housekeeping controls. Error bars represent SD (n=3). Data shown are representative of three independent experiments. Statistical

significance, indicated by p values, was determined by Student's t test (Tables S2 and S3). The numeric fold change of the mRNA expression of candidate genes is displayed using a logarithmic scale.

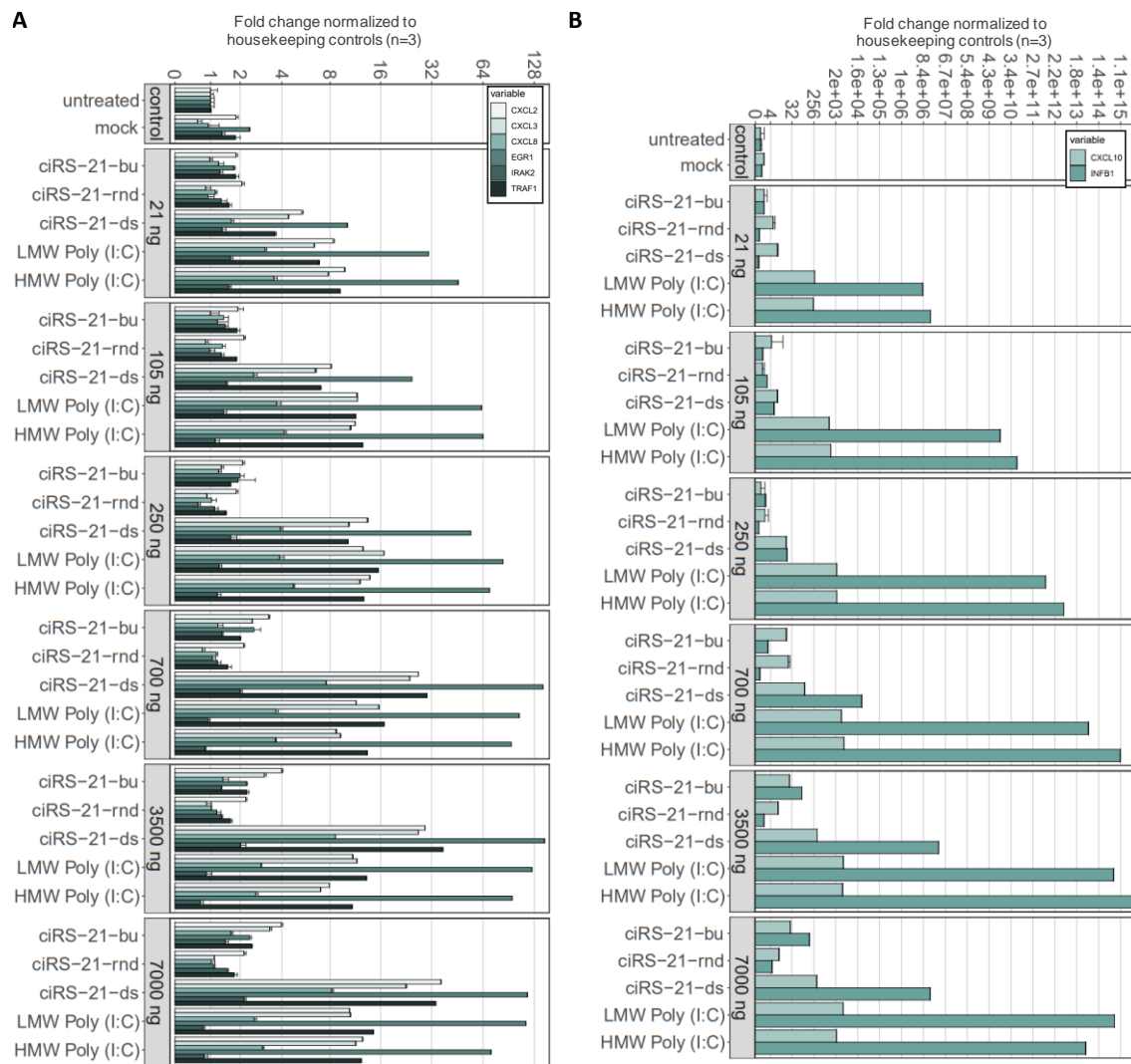


Figure 6: Dose-dependent immune activation to ciRS-21-ds and poly(I:C) in contrast to ciRS-21-rnd and ciRS-21-bu treatment. A549 cells were transfected with 21, 105, 250, 700, 3,500, or 7,000 ng of either the artificial circular RNA sponges, ciRS-21-bu, ciRS-21-rnd, and ciRS-21-ds or with the immunostimulants LMW poly(I:C) and HMW poly(I:C). As control, cells were only treated with the transfection reagent (mock) but no circular RNA or immunostimulant. Three hours post-transfection, A549 cells were harvested and total RNA was isolated. qRT-PCR was performed for the candidate mRNAs derived from RNA sequencing: (A) *CXCL2*, *CXCL3*, *CXCL8*, *IRAK2*, *EGR1*, and *TRAF1* as well as for (B) *CXCL10* and *IFNβ1*. Data were normalized to mean value of *B2M* mRNA, *U1* snRNA, and *U6* snRNA housekeeping controls. Error bars represent SD (n = 3). Data shown are representative of three independent experiments. Statistical significance, indicated by p values, was determined by Student's t test (Tables S4 and S5). The numeric fold change of the mRNA expression of candidate genes is displayed using a logarithmic scale.

To identify a potential upregulation of sensory molecules involved in circRNA sensing (Figure 2), we performed qRT-PCR to analyze the mRNA levels of *MDA5*, *PKR*, *OAS1*, *TLR3*, *TLR7*, *TLR8*, and *RIG-I* after transfection (Figure 7B). Despite an increase of *MDA5* and *RIG-I* mRNA levels upon HMW poly(I:C) and LMW poly(I:C) treatment, no transcriptional upregulation of RNA sensors could be detected after circRNA transfection (Figure 7B). Nonetheless, immunoblotting analysis of PKR in A549 cells revealed PKR activation by detection of phosphorylated PKR (Thr446 p-PKR) 3 h after transfection with 250 ng of ciRS-21-ds, HMW poly(I:C), and LMW poly(I:C), but not of ciRS-21-bu, ciRS-21-rnd, or ssPolyU. We conclude that our artificial circRNAs produced by *in vitro* transcription and purified by gel extraction do not trigger cellular RNA sensors and their downstream innate immune-signaling pathways when transfected in cell culture.

DISCUSSION

As a potential therapeutic tool, circRNAs have attracted the attention of many scientists in recent years. This has sparked a discussion about the immunogenicity of circRNAs [33,34]. Initially reported in 2017, Chen et al. [33] proposed that exogenous circRNAs, produced using a cell-free permuted intron-exon (PIE) system, led to potent immune activation when transfected into HeLa cells. Furthermore, they showed that the virus RNA sensor RIG-I is necessary and sufficient for sensing of exogenous

circRNA and, contrary to previous data, rather independent of RNA 5' triphosphate ends or bluntended double-stranded RNA [41]. RIG-I recognition was thereby dependent on the intron that facilitates circularization, since RNA-binding proteins are deposited on the circRNA, reflecting its origin and biogenesis [33]. In contrast, 2 years later, Wesselhoeft et al. [34] demonstrated that exogenous, PIE-derived circRNAs are able to bypass RNA sensors, including RIG-I, thereby circumventing the induction of cellular antiviral defense mechanisms. They conclude that the initially described immunogenicity of circRNAs result from 5'-triphosphorylated linear RNA contaminants that induce innate immune responses through RIG-I and TLRs. In general, artificial circRNA-mediated immune activation critically relies on (1) the production strategy (*in vivo* or *in vitro*) and purification method or purity of the final product, (2) RNA modifications, (3) secondary structure, and (4) the dose of the circRNA administered. However, in-depth analyses of cellular fate and immunogenicity of relatively short, highly purified artificial circRNAs produced in cell-free systems are still lacking.

Production strategies and purity of artificial circRNAs

To not only identify but also rather increase the functional understanding of circRNAs, a broad range of artificial circRNA expression systems was established. Relying on specifically designed overexpression vectors,

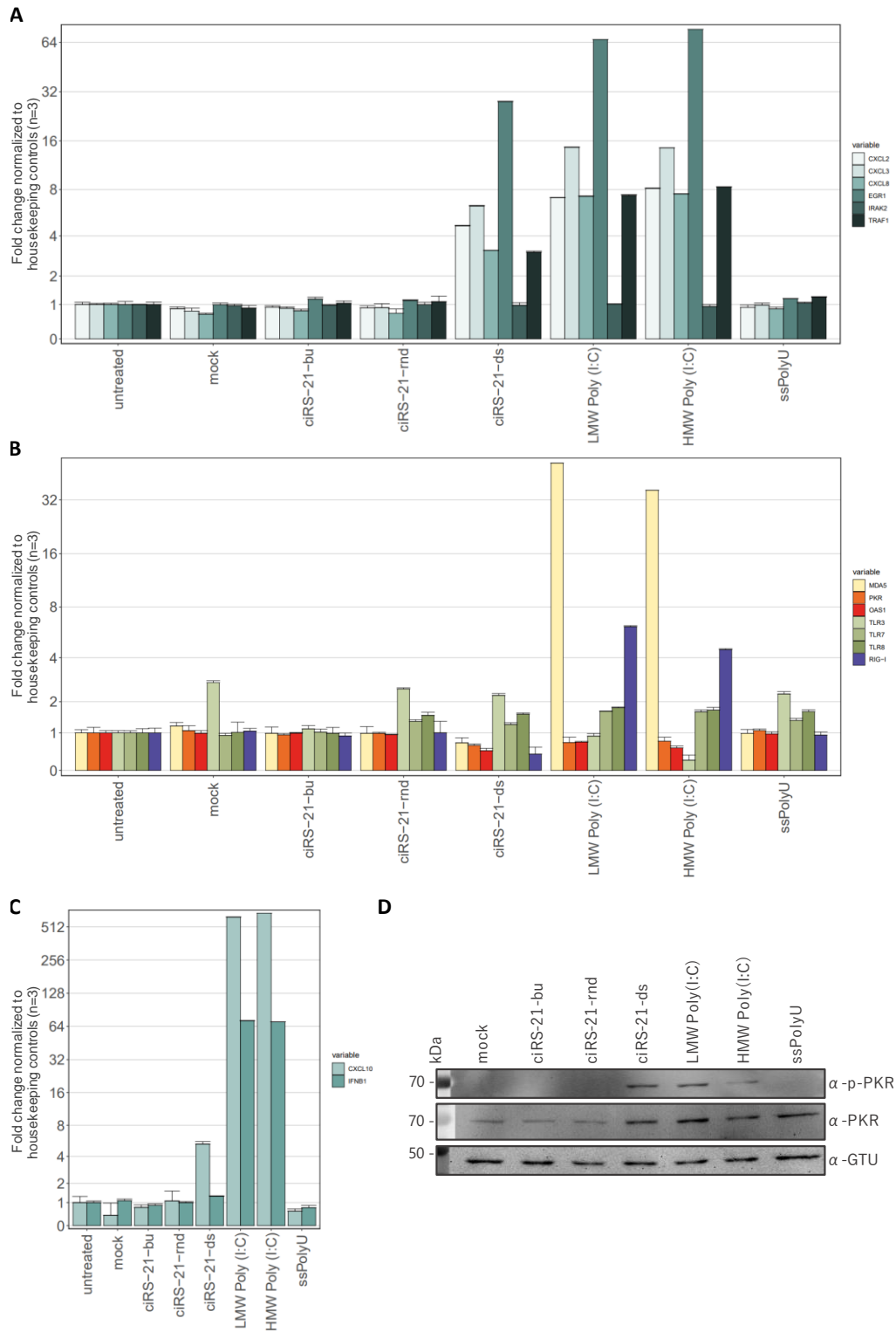


Figure 7: PKR is activated after ciRS-21-ds or poly(I:C) treatment. A549 cells were transfected with 250 ng of either the artificial circular RNA sponges, ciRS-21-bu, ciRS-21-rnd, and ciRS-21-ds or with the immunostimulants LMW poly(I:C) and HMW poly(I:C). As control, cells were only treated with the transfection reagent (mock) but no circular RNA or immunostimulant. Three hours posttransfection, A549 cells were harvested and total RNA was isolated. qRT-PCR was performed for the candidates upregulated in RNA sequencing: (A) *CXCL2*, *CXCL3*, *CXCL8*, *IRAK2*, *EGR1*, and *TRAF1* as well as for mRNAs of cellular RNA sensors (B) *MDA5*, *PKR*, *OAS1*, *TLR3*, *TLR7*, *TLR8*, and *RIG-I* and the known downstream components of immune response (C)

CXCL10 and *IFNB1*. Data were normalized to mean value of *B2M* mRNA, U1 snRNA, and U6 snRNA housekeeping controls. Error bars represent SD (n=3). Statistical significance, indicated by p values, was determined by Student's t test (Table S6). (D) A549 cells were harvested 3 h post-transfection with 250 ng of ciRS-21-bu, ciRS21-rnd, ciRS-21-ds, LMW poly(I:C), HMW poly(I:C), or single-stranded PolyU (ssPolyU), and total protein was isolated. Activated Thr466-phosphorylated PKR (p-PKR) and total PKR as well as γ -tubulin as housekeeping control were analyzed by immunoblotting. Data shown are representative of three independent experiments. The numeric fold change of the mRNA expression of candidate genes is displayed using a logarithmic scale.

circRNAs can be produced in cell culture (here termed "*in vivo*") both by spliceosome-dependent exon circularization strategy [2,12,42] and independent of the spliceosome based on engineered ribozymes derived from the tRNA splicing machinery (e.g., the "tornado" system) [43]. In addition, strategies relying on circRNA production via cell-free systems (here termed "*in vitro*") using recombinant T7-phage RNA-polymerase-mediated transcription and circularization by either employing genetically engineered autocatalytic group I introns (e.g., the PIE system) [42,44–46] or enzymatic intramolecular ligation using recombinant RNA ligases [8,9,20,42] gained importance for further characterization of circRNA utilities. The increasing knowledge on production strategies of artificial circRNAs leads to a rapid development of the potential range of application— e.g., in the context of viral infections [8,47], cancer [9,29], and cardiovascular disease [48].

In this respect, the purity of the isolated artificial circRNAs is crucial for avoidance of triggering innate immune responses with contaminants from the circRNA production process. In this study, we analyzed the cellular innate

immune response of A549 cells treated with *in vitro* produced and polyacrylamide-urea-gel-purified artificial circRNA sponges. We have used the same circRNAs that were applied in Müller et al. [9], with miRNA-21-binding sites ("bulged" binding configuration, abbreviated "bu") and a randomized control sequence based on the nucleotide composition of the miRNA-21 sponge construct ("rnd"). Interestingly, ciRS-21-rnd and ciRS-21-bu did not trigger the cellular innate immunity, as evident from mRNA levels of its downstream components. Although several GO terms related to immune activation are enriched, the selected candidate mRNAs show very moderate increase (2- to 4-fold) in differential expression (Figure 3) and in qRT-PCR analyses (Figures 5 and 6) when the circular RNAs ciRS-21-bu and ciRS-21-rnd are transfected, similar to mock (liposome-) transfected cells. In contrast, when the innate immune response is triggered by poly(I:C)-positive controls or a long double-stranded circRNA (ciRS-21-ds), candidate mRNA levels increase by 10- to 500-fold in a time- and dose-dependent manner (Figures 5 and 6). Therefore, we conclude that both ciRS-21-bu and ciRS-21-rnd are not immunogenic when produced by in

vitro transcription and circularization and purified by gel purification, as described in detail by Breuer and Rossbach [20].

While HPLC and preparative phosphatase RNase R digestion [49] may increase the purity of the circRNA, gel purification appears the most efficient method to obtain homogeneity of the preparation. As shown in Figure 1B, the choice of specific polyacrylamide concentrations during the purification gel run can “shift” the circular product to a region that is spatially separated from any other molecule species. This excludes contamination by linear mono- and dimers that may contain 5'-triphosphate ends, as well as by aberrant transcription products caused by formation of dsRNA region [50] as well as remaining protein or nucleoside triphosphates (NTPs) from the transcription reaction.

RNA modifications

Furthermore, nucleoside isomers and RNA modifications in foreign RNAs are discussed in the context of immune-stimulatory or -suppressing effects. For instance, linear RNAs with nucleobase modifications like, e.g., pseudouridine or N1-methylpseudouridine did not stimulate TLR3, TLR7, and/or TLR8, in contrast to nonmodified RNAs [51,52]. Such approach of masking an RNA therapeutic from the innate immune system has successfully been used in the severe acute respiratory syndrome coronavirus 2 (SARS-CoV-2) mRNA

vaccines (summarized in Morais et al. [32]).

In 2019, Chen et al. [53] identified N6 -methyladenosine (m6 A) as marker of cellular circRNAs, which do not induce the known innate immune pathways, whereas unmodified circRNAs activated RIG-I and innate immune signaling. Interestingly, in a cell-free system for ciRS production by *in vitro* transcription, ligation, and stringent purification via gel extraction, and the given length of about 200 nt, our ciRSs (ciRS-21-bu and ciRS-21-rnd) were found to be non-immunogenic, even without any RNA modifications. This may be different with longer RNAs that are, e.g., constructed for translation purposes and not only miRNA sequestration. Nonetheless, when necessary for longer circRNAs, modified NTPs (e.g., pseudo-UTP) can be used in *in vitro* transcription reactions, replacing the respective unmodified NTP, as it is common practice in mRNA vaccine production.

Secondary structure

Surprisingly, the highly double-stranded construct ciRS-21-ds (with a 50-bp perfectly double-stranded region) did not only upregulate the analyzed chemokine-, interferon-, and other innate-immuneresponse-associated mRNAs but also PKR, a key RNA sensor in cellular immunity. The autophosphorylation of threonine at position 446 in PKR is an indicator of PKR dimerization and activation [54]. The latter suggests that sequence composition and especially extensive

secondary structure elements may play a role in induction of the antiviral defense, since the ciRS-21-ds harboring the long double-stranded region not only fails to bypass detection by cellular innate immunity but even induces the latter to a comparable extent as the poly(I:C) dsRNA controls.

In summary, the entirety of all properties of an artificial circRNA may be crucial regarding the recognition and RNA-sensor-mediated immune activation and thus the cellular fate of a potential therapeutic – from design, production strategy, and stringent purification to the extent of double-stranded regions in a ciRS. The latter provides opportunities and possibilities for immunomodulatory effects. Thus, it could be useful in certain applications to either specifically trigger or bypass the innate immune system with an artificial circRNA therapeutic.

MATERIALS AND METHODS

ciRS design and production

The circRNAs used here were designed as initially described in Jost et al. [8] and contain a region at both ends enabling formation of an 11-nt stem region with a 10-nt open loop. Located in proximity of the stem loop, a 63-nt constant region is shared between all constructs and serves as a binding site for northern-detection probes and PCR primers. The miRNA sponge construct ciRS-21-bu carries four consecutive miR-21-binding sites, each separated by a 4-nt spacing. Note that the terminal 5'- and 3'-nt of miRNA-21 cannot base pair with the sponge sequence. Also,

nucleotides 11–13, directly adjacent to the “seed” sequence of the miRNA, cannot base pair and form the eponymous “bulge.” The construct ciRS-21-rnd is characterized by the same nucleotide composition as ciRS-21-bu, but instead of miRNA-21-binding sites, it harbors a randomized negative control sequence. Identical circRNA sponges were used in Müller et al. [9] and are described in detail in Breuer et al. [20]. Based on these ciRSs, within this study, we also designed a highly double-stranded circRNA sponge containing a randomized self-complementary sequence of 50 bp: ciRS-21-ds.

Template sequences were chemically synthesized and cloned into the multipurpose vector backbone containing the sequence elements described above, excised by flanking *EcoRI* restriction sites and gel purified via agarose gel electrophoresis. The purified template was used for *in vitro* transcription using the HiScribe T7 High Yield RNA Synthesis Kit (New England Biolabs; cat. no. E2040S) with additional 10-fold molar excess of guanosine monophosphate (GMP) over NTPs (Merck KGaA; cat. no. G8377). Transcripts were treated by RQ1 DNase (Promega; cat. no. M6101) digestion to remove the DNA template. Next, excess NTPs were removed by size-exclusion chromatography (mini Quick Spin RNA Columns; Merck KGaA; cat. no. 11814427001). *In vitro* circularization was performed at 16°C overnight using the T4 RNA Ligase I (Thermo Fisher Scientific; cat. no. EL0021). Ligation reaction was analyzed on analytic 6%,

7%, and 8% polyacrylamide-urea gels enabling distinguishment of linear and circular products. Using preparative 7% polyacrylamide-urea gels, circular and linear sponges (ciRS/liRS) were visualized and excised using UV shadowing and purified by gel extraction within PK Buffer at 50°C. Phenol and chloroform extraction was performed to purify RNA followed by ethanol precipitation. Purified sponges were analyzed on 6%, 7%, and 8% polyacrylamide-urea gels as described above. Find detailed information and protocol elsewhere [20].

RNase R treatment

Circularity was proven by RNase R treatment. Therefore, 200 ng of the RNA was incubated with 2 U RNase R (Lucigen; cat. no. RNR07250) for 30 min at 37°C. Afterward, 50% of the reaction was analyzed via polyacrylamide-urea gel electrophoresis and ethidium bromide staining.

Cell culture and transfection

A549 cells were cultured in Dulbecco's modified Eagle medium supplemented with 10% fetal bovine serum at 37°C and 5% CO₂. Twenty-four hours prior transfection 4.2×10^5 cells were seeded on 6-well plates. The transfection of cells was performed using Lipofectamine 2000 (Thermo Fisher Scientific; cat. no. 11668019) according to manufacturer's instructions. Depending on the approach, 21 ng to 7 mg of the circular RNA sponges, LMW poly(I:C) (InvivoGen; cat. no. tlrl-picw), HMW

poly(I:C) (InvivoGen; cat. no. tlrl-pic), or single-stranded (ss) PolyU (InvivoGen; cat. no. tlrl-lpu) were added to the transfection reaction. If not harvested beforehand, cells were washed with PBS and medium was exchanged 4 h post-transfection.

RNA isolation and qRT-PCR

Cells were lysed and total RNA was isolated using TRIzol (Thermo Fisher Scientific; cat. no. 15596026) reagent. Two micrograms of total RNA served as template for reverse transcription using the qScript cDNA Synthesis Kit (QuantaBio; cat. no. 733-1174) according to manufacturer's protocols. Two-step qRT-PCR with an annealing temperature of 58°C was performed utilizing Luna Universal qPCR Master Mix (New England Biolabs; cat. no. M3003E) based on SYBR green technology in both a QuantStudio 3 and StepOnePlus Real-Time PCR cycler (Thermo Fisher Scientific). Primer pairs were selected using the Primer Blast designing tool (<https://www.ncbi.nlm.nih.gov/tools/primer-blast/>). Relative quantification of mRNA abundance was ascertained as described by Michael W. Pfaffl [55] using the mean of housekeeping genes U1 small nuclear RNA (snRNA), U6 snRNA, and B2M for normalization. Primers used are listed in Table S1.

Sequencing and bioinformatic analysis

RNA was isolated as described above, and library preparation was performed using SMARTer Stranded Total RNA Sample Prep Kit (Takara;

cat. no. 634873), which includes rRNA removal. Sequencing was performed using a NextSeq 500 High Output Kit (75 cycles).

Data preprocessing

The quality of the datasets was examined with fastqc v.0.11.9 (<https://www.bioinformatics.babraham.ac.uk/projects/fastqc/>; accessed on 22 June 2020) before and after trimming. Adapters were trimmed using Trim_Galore v.0.6.4 (https://www.bioinformatics.babraham.ac.uk/projects/trim_galore/; accessed on 22 June 2020), which used cutadapt v.2.8 [56], removing all reads shorter than 30 nt after the adapter removal (settings: -length 30). Nucleotides with a phred score below 20 were removed using fastq_quality_filter from the FASTX toolkit v.0.0.14 (https://github.com/agordon/fastx_toolkit; accessed on 22 June 2020), also removing reads that became shorter than 90% of their original length (settings: -q 20 -p 90). The remaining reads were aligned to the human genome (GRCh38) with the associated annotation from Ensembl [57] using STAR v.2.7.3a [58] with standard settings. All subsequent analyses were executed in R version 3.6.3 [59].

Differential gene expression analysis

Alignments were assigned to their feature via featureCounts from the Rsubread package v.2.2.6 [60]. The resulting count matrix was used for the differential gene expression analysis via the DESeq2 package v.1.28.1 [61]. Genes

with a $p < 0.1$ and a log2FoldChange lower than -2 or higher than 2 (4-fold increase or decrease) were considered to be differentially expressed.

GO term analysis

IDs of differentially expressed genes were converted from ensembl to entrez format via the package org.Hs.eg.db v.3.11.4 [62], and GO terms were assigned to each gene using goana from the R package limma version 3.44.3 [63]. For a better overview, the amount of GO terms was reduced by using owltools version 2020-04-06 (<https://github.com/owlcollab/owltools>; accessed on 25 June 2020) with the generic GO subset from the Gene Ontology Resource [64]. For visualization, the R package ggplot2 version 3.3.5 [65] was used. Total RNA sequencing data were deposited at NCBI GEO (GEO: GSE192656).

Western blot

Cells were harvested by scraping, and total protein was extracted using PBS containing 0.5% Triton X-100. Proteins were separated via SDS-PAGE, containing 4% polyacrylamide stacking gel and 12% polyacrylamide resolving gel, and transferred to PVDF Western Blotting Membrane (Roche Consumer Health Deutschland; cat. no. 030100400001). Specific primary antibodies binding to p-PKR (Thr446) (Abcam; cat. no. ab32036), PKR (Proteintech; cat. no. 18244-1-AP), and γ -tubulin (Sigma-Aldrich; cat. no. T6557) followed by horseradish-peroxidase-coupled secondary anti-

bodies (anti-mouse-immunoglobulin G (IgG), Sigma-Aldrich, cat. no. A9917; anti-rabbit-IgG: Sigma-Aldrich, cat. no. A0545) were used to determine the protein abundance. Visualization was achieved utilizing luminol-based chemiluminescent substrates Lumi-Light Western Blotting Substrate (Roche Consumer Health Deutschland; cat. no. 12015200001) and Lumi-Light Plus Western Blotting Substrate (Roche Consumer Health Deutschland; cat. no. 12015196001) as well as INTAS ECL Chemocam Imager (Intas Science Imaging Instruments).

ACKNOWLEDGMENTS

This research was funded by the Deutsche Forschungsgemeinschaft DFG, Research Training Group (RTG) 2355 (project number 325443116), to O.R. and A.G. and the DFG Collaborative Research Center 1021 (project number 197785619–SFB 1021) and Clinical Research Unit 309 (Project P1, 284237345-KFO309) to F.W. We would like to thank Stefan Günther (Deep Sequencing Platform, Max Planck Institute for Heart and Lung Research, Bad Nauheim) for RNA sequencing. We would also like to thank Albrecht Bindereif and all the members of our group as well as Frauke May for the constructive discussions on the project. Special thanks to Christopher Hoffmann for his support in unpredictable situations.

AUTHOR CONTRIBUTIONS

J.B. and Y.N. conducted the experiments. P.B. analyzed the sequencing data. J.B. and P.B. designed the figures. L.S., A.G., and F.W. provided essential materials and resources, conceptualization, planning of experiments, and discussion. J.B. and O.R. conceived and wrote the manuscript.

DECLARATION OF INTERESTS

The authors declare no competing interests.

REFERENCES

- [1] Chen, L.-L. (2016). The biogenesis and emerging roles of circular RNAs. *Nat Rev Mol Cell Biol* 17, 205–211. DOI: 10.1038/nrm.2015.32.
- [2] Memczak, S., Jens, M., Elefsinioti, A., Torti, F., Krueger, J., Rybak, A., Maier, L., Mackowiak, S. D., Gregersen, L. H., and Munschauer, M., et al. (2013). Circular RNAs are a large class of animal RNAs with regulatory potency. *Nature* 495, 333–338. DOI: 10.1038/nature11928.
- [3] Jeck, W. R., Sorrentino, J. A., Wang, K., Slevin, M. K., Burd, C. E., Liu, J., Marzluff, W. F., and Sharpless, N. E. (2013). Circular RNAs are abundant, conserved, and associated with ALU repeats, *RNA* 19, 141–157. DOI: 10.1261/rna.035667.112.
- [4] Starke, S., Jost, I., Rossbach, O., Schneider, T., Schreiner, S., Hung, L.-H., and Bindereif, A. (2015). Exon circularization requires canonical splice signals. *Cell Rep*, 103–111. DOI: 10.1016/j.celrep.2014.12.002.
- [5] Kristensen, L. S., Hansen, T. B., Venø, M. T., and Kjems, J. (2018). Circular RNAs in cancer: opportunities and challenges in the field. *Oncogene*, 555–565. DOI: 10.1038/onc.2017.361.

- [6] Wang, P. L., Bao, Y., Yee, M.-C., Barrett, S. P., Hogan, G. J., Olsen, M. N., Dinneny, J. R., Brown, P. O., and Salzman, J. (2014). Circular RNA is expressed across the eukaryotic tree of life. *PLoS ONE* 9, e90859. DOI: 10.1371/journal.pone.0090859.
- [7] Cocquerelle, C., Mascrez, B., Héтуin, D., and Bailleul, B. (1993). Mis-splicing yields circular RNA molecules. *FASEB J* 7, 155–160. DOI: 10.1096/fasebj.7.1.7678559.
- [8] Jost, I., Shalamova, L. A., Gerresheim, G. K., Niepmann, M., Bindereif, A., and Rossbach, O. (2018). Functional sequestration of microRNA-122 from Hepatitis C Virus by circular RNA sponges. *RNA Biol* 15, 1032–1039. DOI: 10.1080/15476286.2018.1435248.
- [9] Müller, S., Wedler, A., Breuer, J., Glaß, M., Bley, N., Lederer, M., Haase, J., Misiak, C., Fuchs, T., and Ottmann, A., et al. (2020). Synthetic circular miR-21 RNA decoys enhance tumor suppressor expression and impair tumor growth in mice. *NAR Cancer* 2.3 DOI: 10.1093/narcan/zcaa014.
- [10] Salzman, J., Gawad, C., Wang, P. L., Lacayo, N., and Brown, P. O. (2012). Circular RNAs are the predominant transcript isoform from hundreds of human genes in diverse cell types, *PLoS ONE* 7, e30733. DOI: 10.1371/journal.pone.0030733.
- [11] Salzman, J., Chen, R. E., Olsen, M. N., Wang, P. L., and Brown, P. O. (2013). Cell-type specific features of circular RNA expression. *PLoS Genet* 9, e1003777. DOI: 10.1371/journal.pgen.1003777.
- [12] Hansen, T. B., Jensen, T. I., Clausen, B. H., Bramsen, J. B., Finsen, B., Damgaard, C. K., and Kjems, J. (2013). Natural RNA circles function as efficient microRNA sponges. *Nature*, 384–388. DOI: 10.1038/nature11993.
- [13] Jeck, W. R., and Sharpless, N. E. (2014). Detecting and characterizing circular RNAs. *Nat Biotechnol* 32, 453–461. DOI: 10.1038/nbt.2890.
- [14] Guo, J. U., Agarwal, V., Guo, H., and Bartel, D. P. (2014). Expanded identification and characterization of mammalian circular RNAs. *Genome Biol* 15, 409. DOI: 10.1186/s13059-014-0409-z.
- [15] Ebbesen, K. K., Kjems, J., and Hansen, T. B. (2016). Circular RNAs: Identification, biogenesis and function. *Biochim Biophys Acta* 1859, 163–168. DOI: 10.1016/j.bbagr.2015.07.007.
- [16] Holdt, L. M., Kohlmaier, A., and Teupser, D. (2018). Molecular roles and function of circular RNAs in eukaryotic cells. *Cell Mol Life Sci* 75, 1071–1098. DOI: 10.1007/s00018-017-2688-5.

- [17] Ashwal-Fluss, R., Meyer, M., Pamudurti, N. R., Ivanov, A., Bartok, O., Hanan, M., Evantal, N., Memczak, S., Rajewsky, N., and Kadener, S. (2014). circRNA biogenesis competes with pre-mRNA splicing. *Mol Cell* 56, 55–66. DOI: 10.1016/j.molcel.2014.08.019.
- [18] Zhang, Y., Zhang, X.-O., Chen, T., Xiang, J.-F., Yin, Q.-F., Xing, Y.-H., Zhu, S., Yang, L., and Chen, L.-L. (2013). Circular intronic long noncoding RNAs. *Mol Cell* 51, 792–806. DOI: 10.1016/j.molcel.2013.08.017.
- [19] Piwecka, M., Glažar, P., Hernandez-Miranda, L. R., Memczak, S., Wolf, S. A., Rybak-Wolf, A., Filipchyk, A., Klironomos, F., Cerda Jara, C. A., and Fenske, P., et al. (2017). Loss of a mammalian circular RNA locus causes miRNA deregulation and affects brain function. *Science* 357. DOI: 10.1126/science.aam8526.
- [20] Breuer, J., and Rossbach, O. (2020). Production and Purification of Artificial Circular RNA Sponges for Application in Molecular Biology and Medicine. *Methods Protoc* 3. DOI: 10.3390/mps3020042.
- [21] Li, Y., Masaki, T., Yamane, D., McGivern, D. R., and Lemon, S. M. (2013). Competing and noncompeting activities of miR-122 and the 5' exonuclease Xrn1 in regulation of hepatitis C virus replication. *Proc Natl Acad Sci U S A* 110, 1881–1886. DOI: 10.1073/pnas.1213515110.
- [22] Henke, J. I., Goergen, D., Zheng, J., Song, Y., Schüttler, C. G., Fehr, C., Jünemann, C., and Niepmann, M. (2008). microRNA-122 stimulates translation of hepatitis C virus RNA. *EMBO J* 27, 3300–3310. DOI: 10.1038/emboj.2008.244.
- [23] Machlin, E. S., Sarnow, P., and Sagan, S. M. (2011). Masking the 5' terminal nucleotides of the hepatitis C virus genome by an unconventional microRNA-target RNA complex. *Proc Natl Acad Sci U S A* 108, 3193–3198. DOI: 10.1073/pnas.1012464108.
- [24] Nieder-Röhrmann, A., Dünnes, N., Gerresheim, G. K., Shalamova, L. A., Herchenröther, A., and Niepmann, M. (2017). Cooperative enhancement of translation by two adjacent microRNA-122/Argonaute 2 complexes binding to the 5' untranslated region of hepatitis C virus RNA. *J Gen Virol* 98, 212–224. DOI: 10.1099/jgv.0.000697.
- [25] Hildebrandt-Eriksen, E. S., Aarup, V., Persson, R., Hansen, H. F., Munk, M. E., and Ørum, H. (2012). A locked nucleic acid oligonucleotide targeting microRNA 122 is well-tolerated in cynomolgus monkeys. *Nucleic Acid Ther* 22, 152–161. DOI: 10.1089/nat.2011.0332.
- [26] Feng, Y.-H., and Tsao, C.-J. (2016). Emerging role of microRNA-21 in

- cancer. *Biomed Rep* 5, 395–402. DOI: 10.3892/br.2016.747.
- [27] Feng, Y.-H., Wu, C.-L., Tsao, C.-J., Chang, J.-G., Lu, P.-J., Yeh, K.-T., Uen, Y.-H., Lee, J.-C., and Shiau, A.-L. (2011). Deregulated expression of sprouty2 and microRNA-21 in human colon cancer: Correlation with the clinical stage of the disease. *Cancer Biol Ther* 11, 111–121. DOI: 10.4161/cbt.11.1.13965.
- [28] Fulci, V., Chiaretti, S., Goldoni, M., Azzalin, G., Carucci, N., Tavolaro, S., Castellano, L., Magrelli, A., Citarella, F., and Messina, M., et al. (2007). Quantitative technologies establish a novel microRNA profile of chronic lymphocytic leukemia. *Blood* 109, 4944–4951. DOI: 10.1182/blood-2006-12-062398.
- [29] Liu, X., Abraham, J. M., Cheng, Y., Wang, Z., Wang, Z., Zhang, G., Ashktorab, H., Smoot, D. T., Cole, R. N., and Boronina, T. N., et al. (2018). Synthetic Circular RNA Functions as a miR-21 Sponge to Suppress Gastric Carcinoma Cell Proliferation. *Mol Ther Nucleic Acids* 13, 312–321. DOI: 10.1016/j.omtn.2018.09.010.
- [30] Shankarappa, S. A., Koyakutty, M., and Nair, S. V. (2014). Efficacy versus Toxicity - The Ying and Yang in Translating Nanomedicines. *J. Nanosci. Nanotechnol.* 4, 23. DOI: 10.5772/59127.
- [31] Pindel, A., and Sadler, A. (2011). The role of protein kinase R in the interferon response. *J Interferon Cytokine Res* 31, 59–70. DOI: 10.1089/jir.2010.0099.
- [32] Morais, P., Adachi, H., and Yu, Y.-T. (2021). The Critical Contribution of Pseudouridine to mRNA COVID-19 Vaccines. *Front Cell Dev Biol* 9, 789427. DOI: 10.3389/fcell.2021.789427.
- [33] Chen, Y. G., Kim, M. V., Chen, X., Batista, P. J., Aoyama, S., Wilusz, J. E., Iwasaki, A., and Chang, H. Y. (2017). Sensing Self and Foreign Circular RNAs by Intron Identity. *Mol Cell* 67, 228–238.e5. DOI: 10.1016/j.molcel.2017.05.022.
- [34] Wesselhoeft, R. A., Kowalski, P. S., Parker-Hale, F. C., Huang, Y., Bisaria, N., and Anderson, D. G. (2019). RNA Circularization Diminishes Immunogenicity and Can Extend Translation Duration In Vivo. *Mol Cell* 74, 508–520.e4. DOI: 10.1016/j.molcel.2019.02.015.
- [35] Tabak, H. F., van der Horst, G., Smit, J., Winter, A. J., Mul, Y., and Groot Koerkamp, M. J. (1988). Discrimination between RNA circles, interlocked RNA circles and lariats using two-dimensional polyacrylamide gel electrophoresis. *Nucleic Acids Res* 16, 6597–6605. DOI: 10.1093/nar/16.14.6597.
- [36] Schlee, M., and Hartmann, G. (2016). Discriminating self from non-self in nucleic acid sensing.

- Nat Rev Immunol* 16, 566–580. DOI: 10.1038/nri.2016.78.
- [37] Cadena, C., and Hur, S. (2017). Antiviral Immunity and Circular RNA: No End in Sight. *Mol Cell* 67, 163–164. DOI: 10.1016/j.molcel.2017.07.005.
- [38] Lässig, C., and Hopfner, K.-P. (2017). Discrimination of cytosolic self and non-self RNA by RIG-I-like receptors. *J. Biol Chem* 292, 9000–9009. DOI: 10.1074/jbc.R117.788398.
- [39] Liu, C.-X., Li, X., Nan, F., Jiang, S., Gao, X., Guo, S.-K., Xue, W., Cui, Y., Dong, K., and Ding, H., et al. (2019). Structure and Degradation of Circular RNAs Regulate PKR Activation in Innate Immunity. *Cell* 177, 865–880.e21. DOI: 10.1016/j.cell.2019.03.046.
- [40] Li, X., Liu, C.-X., Xue, W., Zhang, Y., Jiang, S., Yin, Q.-F., Wei, J., Yao, R.-W., Yang, L., and Chen, L.-L. (2017). Coordinated circRNA Biogenesis and Function with NF90/NF110 in Viral Infection. *Mol Cell* 67, 214–227.e7. DOI: 10.1016/j.molcel.2017.05.023.
- [41] Lu, C., Xu, H., Ranjith-Kumar, C. T., Brooks, M. T., Hou, T. Y., Hu, F., Herr, A. B., Strong, R. K., Kao, C. C., and Li, P. (2010). The structural basis of 5' triphosphate double-stranded RNA recognition by RIG-I C-terminal domain. *Structure* 18, 1032–1043. DOI: 10.1016/j.str.2010.05.007.
- [42] Petkovic, S., and Müller, S. (2015). RNA circularization strategies in vivo and in vitro. *Nucleic Acids Res* 43, 2454–2465. DOI: 10.1093/nar/gkv045.
- [43] Litke, J. L., and Jaffrey, S. R. (2019). Highly efficient expression of circular RNA aptamers in cells using autocatalytic transcripts. *Nat Biotechnol*, 667–675. DOI: 10.1038/s41587-019-0090-6.
- [44] Wesselhoeft, R. A., Kowalski, P. S., and Anderson, D. G. (2018). Engineering circular RNA for potent and stable translation in eukaryotic cells. *Nat Commun*, 2629. DOI: 10.1038/s41467-018-05096-6.
- [45] Puttaraju, M., and Been, M. D. (1992). Group I permuted intron-exon (PIE) sequences self-splice to produce circular exons. *Nucleic Acids Res* 20, 5357–5364. DOI: 10.1093/nar/20.20.5357.
- [46] Ford, E., and Ares, M. (1994). Synthesis of circular RNA in bacteria and yeast using RNA cyclase ribozymes derived from a group I intron of phage T4. *Proc Natl Acad Sci U S A* 91, 3117–3121. DOI: 10.1073/pnas.91.8.3117.
- [47] Pfafenrot, C., Schneider, T., Müller, C., Hung, L.-H., Schreiner, S., Ziebuhr, J., and Bindereif, A. (2021). Inhibition of SARS-CoV-2 coronavirus proliferation by designer antisense-circRNAs.

- Nucleic Acids Res* 49, 12502–12516. DOI: 10.1093/nar/gkab1096.
- [48] Lavenniah, A., Luu, T. D. A., Li, Y. P., Lim, T. B., Jiang, J., Ackers-Johnson, M., and Foo, R. S.-Y. (2020). Engineered Circular RNA Sponges Act as miRNA Inhibitors to Attenuate Pressure Overload-Induced Cardiac Hypertrophy. *Mol Ther* 28, 1506–1517. DOI: 10.1016/j.ymthe.2020.04.006.
- [49] Yan, L., and Chen, Y. G. (2020). Circular RNAs in Immune Response and Viral Infection. *Trends Biochem Sci* 45, 1022–1034. DOI: 10.1016/j.tibs.2020.08.006.
- [50] Mu, X., Greenwald, E., Ahmad, S., and Hur, S. (2018). An origin of the immunogenicity of in vitro transcribed RNA. *Nucleic Acids Res* 46, 5239–5249. DOI: 10.1093/nar/gky177.
- [51] Karikó, K., Buckstein, M., Ni, H., and Weissman, D. (2005). Suppression of RNA recognition by Toll-like receptors: the impact of nucleoside modification and the evolutionary origin of RNA. *Immunity* 23, 165–175. DOI: 10.1016/j.immuni.2005.06.008.
- [52] Karikó, K., and Weissman, D. (2007). Naturally occurring nucleoside modifications suppress the immunostimulatory activity of RNA: implication for therapeutic RNA development. *Curr Opin Drug Discov Devel* 10, 523–532.
- [53] Chen, Y. G., Chen, R., Ahmad, S., Verma, R., Kasturi, S. P., Amaya, L., Broughton, J. P., Kim, J., Cadena, C., and Pulendran, B., et al. (2019). N6-Methyladenosine Modification Controls Circular RNA Immunity. *Mol Cell* 76, 96–109.e9. DOI: 10.1016/j.molcel.2019.07.016.
- [54] Zhang, F., Romano, P. R., Nagamura-Inoue, T., Tian, B., Dever, T. E., Mathews, M. B., Ozato, K., and Hinnebusch, A. G. (2001). Binding of double-stranded RNA to protein kinase PKR is required for dimerization and promotes critical autophosphorylation events in the activation loop. *J. Biol Chem* 276, 24946–24958. DOI: 10.1074/jbc.M102108200.
- [55] Pfaffl, M. W. (2001). A new mathematical model for relative quantification in real-time RT-PCR. *Nucleic Acids Res* 29, e45. DOI: 10.1093/nar/29.9.e45.
- [56] Martin, M. (2011). Cutadapt removes adapter sequences from high-throughput sequencing reads 17, 10. DOI: 10.14806/ej.17.1.200.
- [57] Howe, K. L., Achuthan, P., Allen, J., Allen, J., Alvarez-Jarreta, J., Amode, M. R., Armean, I. M., Azov, A. G., Bennett, R., and Bhai, J., et al. (2021). Ensembl 2021. *Nucleic Acids Res* 49, D884–D891. DOI: 10.1093/nar/gkaa942.
- [58] Dobin, A., Davis, C. A., Schlesinger, F., Drenkow, J.,

- Zaleski, C., Jha, S., Batut, P., Chaisson, M., and Gingeras, T. R. (2013). STAR: ultrafast universal RNA-seq aligner. *Bioinformatics* 29, 15–21. DOI: 10.1093/bioinformatics/bts635.
- [59] R Core Team (2020). R: A Language and Environment for Statistical Computing (R Foundation for Statistical Computing). <https://www.R-project.org/>.
- [60] Liao, Y., Smyth, G. K., and Shi, W. (2019). The R package Rsubread is easier, faster, cheaper and better for alignment and quantification of RNA sequencing reads. *Nucleic Acids Res* 47, e47. DOI: 10.1093/nar/gkz114.
- [61] Love, M. I., Huber, W., and Anders, S. (2014). Moderated estimation of fold change and dispersion for RNA-seq data with DESeq2. *Genome Biol* 15, 550. DOI: 10.1186/s13059-014-0550-8.
- [62] Carlson, M.. org.Hs.eg.db: Genome wide annotation for Human. R package version 3.8.2. <https://bioconductor.org/packages/release/data/annotation/html/org.Hs.eg.db.html>.
- [63] Ritchie, M. E., Phipson, B., Di Wu, Hu, Y., Law, C. W., Shi, W., and Smyth, G. K. (2015). Limma powers differential expression analyses for RNA-sequencing and microarray studies. *Nucleic Acids Res* 43, e47. DOI: 10.1093/nar/gkv007.
- [64] Gene Ontology Consortium (2021). The Gene Ontology resource: enriching a GOLD mine. *Nucleic Acids Res.* 49, D325–D334. <https://doi.org/10.1093/nar/gkaa1113>
- [64] Wickham, H. (2016). ggplot2. Elegant graphics for data analysis (Springer International Publishing).

SUPPLEMENTARY DATA**Table S1: RT-qPCR Primer used.**

Primer	Sequence (5'-3')
CXCL2_fwd	CACAGTGGCTGACATGTGATA
CXCL2_rev	AGGTCAAACCCAAGTTAGTTCA
CXCL3_fwd	GAGCCGGGGATTGCTGG
CXCL3_rev	CTCTCCCGCTTCTCGCAC
CXCL8_fwd	GGTGCAGTTTTGCCAAGGAG
CXCL8_rev	TGGGGTGGAAAGGTTTGGAG
CXCL10_fwd	AGGAACCTCCAGTCTCAGCA
CXCL10_rev	CAAAATTGGCTTGCAGGAAT
EGR1_fwd	CAGGTCAGCAGCTTCCCTTC
EGR1_rev	TCATGTCCGAAAGCCCTGTG
INFB1_fwd	TGGGAGGATTCTGCATTACC
INFB1_rev	CAGCATCTGCTGGTTGAAGA
IRAK2_fwd	GGACCCTTGTCCCTCAGTTGG
IRAK2_rev	CACCCAGGACAGCAGATGTT
MDA-5_fwd	GCATATGCGCTTTCCCAGTG
MDA-5_rev	CTTCATCAGCTCTGGCTCG
OSA1_fwd	TGGATTCTGCTGGTGAGACC
OSA1_rev	ATGGCCTTTGGCAAGAGGTAAG
PKR_fwd	TCCATGGGGAATTACATAGGC
PKR_rev	AGCGCCAATTGTTTTGCTT
RIG-I_fwd	AAATCAGAACACAGGCAGAGGAA
RIG-I_rev	GTCCCATGTCTGAAGGCGTAA
TLR3_fwd	CCTTTTGCCCTTTGGGATGC
TLR3_rev	TGAAGTTGGCGGCTGGTAAT
TLR7_fwd	CCTTGTGCGCCGTGTA AAAA
TLR7_rev	GGGCACATGCTGAAGAGAGT
TLR8_fwd	CCAAACTGCCAAGCTCCCTA
TLR8_rev	CAGCACCTTCAGATGAGGCA
TRAF1_fwd	GGTGCAGGTGTCAATGAAGC
TRAF1_rev	ACAAGCCCCCATGAGAAACA

Table S2: P-values of CXCL2, CXCL3, CXCL8, EGR1 and TRAF1 in context of the time dependent immunogenicity to ciRS-21-ds and poly(I:C) in contrast to ciRS-21-rnd and ciRS-21-bu treatment. Statistical significance was determined by Student's t-test. White background p-value < 0.05, significant; grey background p-value > 0.05, not significant.

		CXCL2	CXCL3	CXCL8	IRAK2	EGR1	TRAF1
0 h	mock						
	ciRS-21-bu	0.09	0.06	0.84	8.42E-03	0.72	0.86
	ciRS-21-rnd	3.09E-02	5.01E-02	0.59	0.16	0.32	0.46
	ciRS-21-ds	0.58	0.44	0.64	0.25	0.53	0.11
	LMW Poly(I:C)	2.46E-02	0.14	0.17	5.93E-03	0.84	0.65
	HMW Poly(I:C)	5.43E-02	0.33	0.24	0.13	0.91	0.35
0.5 h	mock						
	ciRS-21-bu	0.15	4.50E-02	0.09	0.83	1.94E-09	0.28
	ciRS-21-rnd	2.89E-02	6.62E-03	4.69E-03	0.37	1.06E-09	0.20
	ciRS-21-ds	8.23E-04	2.05E-04	3.18E-04	8.10E-03	8.82E-12	0.23
	LMW Poly(I:C)	8.11E-03	4.08E-03	1.83E-03	0.06	2.74E-11	0.19
	HMW Poly(I:C)	0.18	0.06	0.11	0.28	2.56E-10	0.49
2 h	mock						
	ciRS-21-bu	0.75	0.11	0.18	1.90E-02	0.43	0.55
	ciRS-21-rnd	0.70	0.27	4.85E-03	0.55	3.38E-04	1.45E-02
	ciRS-21-ds	5.32E-06	0.82	1.12E-05	1.25E-03	1.07E-09	2.80E-05
	LMW Poly(I:C)	3.91E-07	2.05E-04	6.45E-10	6.25E-04	1.84E-12	1.09E-06
	HMW Poly(I:C)	2.12E-07	1.13E-02	2.46E-08	2.93E-03	1.34E-13	2.94E-07
3 h	mock						
	ciRS-21-bu	0.10	0.53	0.82	8.09E-03	6.88E-03	0.79
	ciRS-21-rnd	0.28	1.24E-03	6.91E-01	0.61	3.94E-02	0.53
	ciRS-21-ds	8.46E-08	5.24E-06	1.32E-07	0.22	1.25E-12	2.44E-06
	LMW Poly(I:C)	1.17E-07	2.65E-06	1.05E-09	0.61	2.22E-14	2.45E-09
	HMW Poly(I:C)	7.29E-09	1.66E-06	4.48E-09	0.17	2.81E-13	1.50E-09
4 h	mock						
	ciRS-21-bu	0.15	1.22E-02	0.48	0.96	2.26E-02	0.54
	ciRS-21-rnd	3.63E-05	2.05E-03	1.06E-03	1.91E-02	0.06	2.43E-03
	ciRS-21-ds	3.39E-09	3.55E-05	5.29E-07	4.55E-02	1.02E-13	7.00E-09
	LMW Poly(I:C)	3.84E-10	4.37E-06	1.22E-08	0.16	1.59E-13	3.52E-09
	HMW Poly(I:C)	2.35E-11	1.30E-08	7.40E-07	0.06	2.01E-13	1.22E-09
5 h	mock						
	ciRS-21-bu	0.09	3.31E-03	0.78	2.41E-02	4.26E-02	0.39
	ciRS-21-rnd	0.08	0.06	0.75	0.25	1.43E-02	0.31
	ciRS-21-ds	1.74E-09	1.30E-07	3.96E-06	4.88E-05	1.70E-14	1.40E-08
	LMW Poly(I:C)	2.99E-12	4.02E-10	6.54E-07	5.53E-04	1.39E-14	1.43E-08
	HMW Poly(I:C)	2.60E-10	1.52E-08	7.37E-07	6.61E-06	3.70E-15	6.03E-09
12 h	mock						
	ciRS-21-bu	5.71E-04	8.62E-05	0.97	0.16	0.16	0.95
	ciRS-21-rnd	0.53	3.96E-03	0.69	0.58	0.85	0.80
	ciRS-21-ds	7.55E-08	1.58E-10	1.25E-04	3.59E-02	2.50E-12	2.66E-08
	LMW Poly(I:C)	4.74E-07	1.48E-11	9.28E-05	1.07E-03	5.64E-13	6.31E-09
	HMW Poly(I:C)	7.44E-08	1.27E-11	5.39E-06	2.11E-03	3.84E-13	3.93E-09
24 h	mock						
	ciRS-21-bu	9.79E-05	0.93	0.34	0.97	4.62E-02	0.15
	ciRS-21-rnd	6.21E-04	3.47E-04	0.87	0.93	2.83E-03	0.36
	ciRS-21-ds	9.45E-05	8.07E-10	5.34E-05	0.51	9.27E-09	1.42E-02
	LMW Poly(I:C)	8.00E-06	1.98E-10	1.76E-06	0.12	1.59E-09	4.23E-08
	HMW Poly(I:C)	9.65E-05	5.30E-09	4.47E-06	0.17	8.18E-10	8.85E-07

Table S3: P-values of CXCL10 and INFB1 in context of the time dependent immunogenicity to ciRS-21-ds and poly(I:C) in contrast to ciRS-21-rnd and ciRS-21-bu treatment. Statistical significance was determined by Student's t-test. White background pvalue < 0.05, significant; grey background p-value > 0.05, not significant.

		CXCL10	INFB1
0 h	mock		
	ciRS-21-bu	0.87	0.79
	ciRS-21-rnd	0.86	0.72
	ciRS-21-ds	0.92	0.69
	LMW Poly(I:C)	0.89	0.94
	HMW Poly(I:C)	0.86	0.59
0.5 h	mock		
	ciRS-21-bu	0.77	0.93
	ciRS-21-rnd	0.96	0.94
	ciRS-21-ds	0.82	0.55
	LMW Poly(I:C)	0.76	0.81
	HMW Poly(I:C)	0.82	0.33
2 h	mock		
	ciRS-21-bu	0.97	7.58E-04
	ciRS-21-rnd	0.86	0.89
	ciRS-21-ds	0.90	3.45E-05
	LMW Poly(I:C)	3.16E-05	5.63E-10
	HMW Poly(I:C)	3.31E-05	5.84E-10
3 h	mock		
	ciRS-21-bu	0.89	0.40
	ciRS-21-rnd	0.61	0.63
	ciRS-21-ds	0.83	3.09E-03
	LMW Poly(I:C)	1.79E-06	9.96E-14
	HMW Poly(I:C)	4.14E-06	1.05E-13
4 h	mock		
	ciRS-21-bu	0.90	0.37
	ciRS-21-rnd	0.97	0.74
	ciRS-21-ds	2.14E-02	6.62E-05
	LMW Poly(I:C)	1.17E-10	1.85E-12
	HMW Poly(I:C)	6.39E-11	3.73E-04
5 h	mock		
	ciRS-21-bu	0.79	0.81
	ciRS-21-rnd	0.96	0.95
	ciRS-21-ds	0.24	4.69E-04
	LMW Poly(I:C)	1.14E-08	1.65E-13
	HMW Poly(I:C)	2.70E-08	2.16E-05
12 h	mock		
	ciRS-21-bu	0.72	2.69E-05
	ciRS-21-rnd	1.00	0.97
	ciRS-21-ds	1.67E-02	1.98E-06
	LMW Poly(I:C)	1.18E-07	8.16E-16
	HMW Poly(I:C)	2.99E-07	9.05E-05
24 h	mock		
	ciRS-21-bu	1.00	0.19
	ciRS-21-rnd	0.99	0.61
	ciRS-21-ds	8.41E-04	2.26E-03
	LMW Poly(I:C)	1.55E-08	6.10E-08
	HMW Poly(I:C)	8.72E-08	1.32E-06

Table S4: P-values of CXCL2, CXCL3, CXCL8, EGR1 and TRAF1 in context of the dose dependent immunogenicity to ciRS-21-ds and poly(I:C) in contrast to ciRS-21-rnd and ciRS-21-bu treatment. Statistical significance was determined by Student's t-test. White background p-value < 0.05, significant; grey background p-value > 0.05, not significant.

		CXCL2	CXCL3	CXCL8	EGR1	IRAK2	TRAF1
21 ng	untreated	3.13E-03	1.37E-02	0.76	4.30E-05	1.51E-02	1.48E-03
	mock						
	ciRS-21-bu	2.74E-03	0.79	0.11	5.36E-04	2.84E-02	3.04E-04
	ciRS-21-rnd	1.38E-03	0.23	0.13	0.59	0.06	4.25E-04
	ciRS-21-ds	6.38E-06	4.32E-07	1.36E-03	2.63E-08	2.44E-02	8.66E-07
	LMW Poly(I:C)	8.24E-07	8.62E-08	1.99E-05	4.53E-10	1.62E-03	2.17E-08
7000 ng	HMW Poly(I:C)	3.49E-07	4.19E-08	3.61E-05	4.75E-11	2.12E-03	5.07E-10
105 ng	ciRS-21-bu	6.20E-03	0.98	2.26E-02	0.38	6.57E-03	2.39E-04
	ciRS-21-rnd	8.89E-04	0.10	1.39E-02	0.83	1.72E-02	6.62E-07
	ciRS-21-ds	7.02E-07	3.85E-07	1.74E-04	5.10E-10	2.03E-03	8.89E-08
	LMW Poly(I:C)	2.11E-07	3.60E-09	7.68E-05	1.82E-11	9.33E-03	9.59E-11
	HMW Poly(I:C)	1.36E-07	5.62E-08	8.22E-06	1.71E-11	0.24	1.25E-09
	250 ng	ciRS-21-bu	1.08E-03	7.41E-03	4.25E-02	8.69E-04	0.09
ciRS-21-rnd	2.86E-03	0.11	0.79	1.05E-02	0.26	4.40E-05	
ciRS-21-ds	1.52E-07	2.89E-08	1.30E-05	3.16E-11	1.04E-02	1.30E-09	
LMW Poly(I:C)	1.15E-07	2.16E-09	8.77E-05	5.65E-12	3.34E-02	5.22E-11	
HMW Poly(I:C)	7.21E-08	1.76E-08	1.96E-06	2.01E-11	9.64E-02	2.22E-09	
700 ng	ciRS-21-bu	6.08E-05	9.63E-06	0.14	1.20E-03	7.89E-03	4.49E-06
	ciRS-21-rnd	8.62E-04	2.43E-02	0.07	0.59	0.09	2.04E-03
	ciRS-21-ds	3.95E-09	4.41E-10	9.71E-08	5.27E-13	2.44E-04	4.16E-11
	LMW Poly(I:C)	1.32E-07	4.88E-09	1.70E-05	2.02E-12	0.39	8.12E-10
	HMW Poly(I:C)	6.02E-07	4.97E-08	4.46E-06	2.39E-12	0.08	6.27E-10
	3500 ng	ciRS-21-bu	2.06E-05	1.37E-05	3.99E-02	7.91E-05	7.21E-03
ciRS-21-rnd	6.43E-04	0.30	0.74	0.13	9.50E-03	4.43E-05	
ciRS-21-ds	3.11E-09	2.69E-10	4.38E-08	4.73E-13	2.04E-03	8.44E-11	
LMW Poly(I:C)	1.87E-07	4.76E-09	1.18E-05	1.41E-12	0.34	1.82E-09	
HMW Poly(I:C)	6.23E-07	4.08E-08	6.13E-05	3.39E-12	2.36E-02	1.03E-09	
7000 ng	ciRS-21-bu	2.52E-05	9.04E-06	1.10E-03	6.85E-05	6.71E-03	6.45E-07
	ciRS-21-rnd	9.57E-04	0.10	0.79	0.26	1.91E-03	3.15E-04
	ciRS-21-ds	9.46E-10	4.42E-08	8.48E-07	9.60E-13	1.40E-04	5.80E-11
	LMW Poly(I:C)	1.86E-07	1.87E-08	7.26E-05	1.10E-12	4.27E-02	6.43E-09
	HMW Poly(I:C)	1.15E-07	1.50E-08	1.77E-05	7.03E-12	0.11	1.05E-08

Table S5: P-values of CXCL10 and INFB1 in context of the dose dependent immunogenicity to ciRS-21-ds and poly(I:C) in contrast to ciRS-21-rnd and ciRS-21-bu treatment. Statistical significance was determined by Student's t-test. White background pvalue < 0.05, significant; grey background p-value > 0.05, not significant.

		CXCL10	INFB1
	untreated		
	mock	0.18	0.20
21 ng	ciRS-21-bu	0.30	7.97E-03
	ciRS-21-rnd	7.07E-03	0.24
	ciRS-21-ds	3.68E-04	0.09
	LMW Poly(I:C)	7.78E-11	1.39E-30
	HMW Poly(I:C)	1.20E-10	8.67E-32
105 ng	ciRS-21-bu	0.56	5.16E-02
	ciRS-21-rnd	0.48	6.99E-04
	ciRS-21-ds	3.56E-04	3.03E-05
	LMW Poly(I:C)	2.73E-13	2.18E-43
	HMW Poly(I:C)	3.65E-13	2.09E-45
250 ng	ciRS-21-bu	0.90	4.69E-03
	ciRS-21-rnd	0.27	0.12
	ciRS-21-ds	5.39E-06	4.24E-08
	LMW Poly(I:C)	1.57E-14	9.10E-51
	HMW Poly(I:C)	1.52E-14	7.73E-54
700 ng	ciRS-21-bu	1.85E-05	2.70E-04
	ciRS-21-rnd	8.31E-04	0.45
	ciRS-21-ds	4.43E-09	1.98E-20
	LMW Poly(I:C)	3.78E-15	8.24E-58
	HMW Poly(I:C)	1.07E-15	4.36E-63
3500 ng	ciRS-21-bu	1.12E-06	2.40E-10
	ciRS-21-rnd	1.55E-04	8.45E-03
	ciRS-21-ds	3.14E-11	3.88E-33
	LMW Poly(I:C)	1.33E-15	4.40E-62
	HMW Poly(I:C)	1.75E-15	2.86E-65
7000 ng	ciRS-21-bu	3.68E-06	6.80E-12
	ciRS-21-rnd	1.22E-04	3.61E-05
	ciRS-21-ds	3.10E-11	8.45E-32
	LMW Poly(I:C)	1.42E-15	3.67E-62
	HMW Poly(I:C)	2.02E-14	6.12E-57

Table S6: P-values of candidate mRNAs 3h after A549 treatment with 250 ng of ciRS-21- ds and poly(I:C) in contrast to ciRS-21-rnd and ciRS-21-bu. Statistical significance was determined by Student's t-test for (A) CXCL2, CXCL3, CXCL8, EGR1, IRAK2 and TRAF1, (B) CXCL10 and INFB1 as well as (C) MDA5, OAS1, PKR, RIG-I, TLR3, TLR7 and TLR8. White background p-value < 0.05, significant; grey background p-value > 0.05, not significant.

A

	CXCL2	CXCL3	CXCL8	EGR1	IRAK2	TRAF1
untreated						
mock	0.071	0.022	0.001	0.916	0.255	0.158
ciRS-21-bu	0.165	0.025	0.006	0.058	0.221	0.540
ciRS-21-rnd	0.127	0.264	0.027	0.089	0.946	0.477
ciRS-21-ds	1.76E-07	1.78E-08	9.58E-08	3.20E-10	0.63	2.90E-06
LMW Poly(I:C)	1.61E-08	1.70E-09	7.28E-09	2.98E-12	0.27	8.68E-08
HMW Poly(I:C)	2.08E-08	2.72E-10	1.30E-09	1.67E-12	0.16	8.40E-09
ssPolyU	0.211	0.701	0.025	0.028	0.042	0.007

B

	CXCL10	INFB1
untreated		
mock	0.188	0.224
ciRS-21-bu	0.291	0.092
ciRS-21-rnd	0.833	0.942
ciRS-21-ds	5.81E-05	2.62E-03
LMW Poly(I:C)	3.33E-14	1.15E-12
HMW Poly(I:C)	2.40E-14	1.35E-12
ssPolyU	0.096	0.031

C

	MDA5	OSA1	PKR	RIG-I	TLR3	TLR7	TLR8
untreated							
mock	0.07	0.86	0.64	0.60	8.54E-06	0.22	0.94
ciRS-21-bu	0.92	0.84	0.57	0.40	0.17	0.74	0.93
ciRS-21-rnd	0.92	0.27	0.89	0.99	6.14E-06	1.89E-03	4.23E-03
ciRS-21-ds	4.55E-02	7.42E-04	2.25E-02	1.20E-02	2.57E-05	6.89E-03	1.58E-03
LMW Poly(I:C)	8.32E-12	2.83E-03	0.10	7.10E-07	0.18	5.44E-05	3.93E-04
HMW Poly(I:C)	8.55E-11	9.31E-04	0.11	2.33E-06	9.73E-04	2.39E-04	1.33E-03
ssPolyU	0.86	0.59	0.52	0.53	4.02E-05	1.77E-03	1.10E-03

Appendix

Scientific Achievements

Publications

Richter A.M., Kiehl S., Köger N., Breuer J., Stiewe T., Dammann R.H. (2017). ZAR1 is a novel epigenetically inactivated tumour suppressor in lung cancer. *Clinical epigenetics*. doi: 10.1186/s13148-017-0360-4

Deutschmeyer V.*, Breuer J.*, Walesch S.K., Sokol A.M., Graumann J., Bartkuhn M., Boettger T., Rossbach O., Richter A.M. (2019). Epigenetic therapy of novel tumour suppressor ZAR1 and its cancer biomarker function. *Clinical Epigenetics*. doi: 10.1186/s13148-019-0774-2

Breuer J., Rossbach O. (2020). Production and Purification of Artificial Circular RNA Sponges for Application in Molecular Biology and Medicine. *Methods and protocols*. doi: 10.3390/mps3020042

Müller S.*, Wedler A.*, Breuer J.*, Glaß M., Bley N., Lederer M., Haase J., Misiak C., Fuchs T., Ottmann A., Schmachtel T., Shalamova L., Ewe A., Aigner A., Rossbach O., Hüttelmaier S. (2020). Synthetic circular miR-21 RNA decoys enhance tumor suppressor expression and impair tumor growth in mice. *NAR Cancer*. doi: 10.1093/narcan/zcaa014

Breuer J., Barth P., Noe J., Shalamova L., Goesmann A., Weber F. and Rossbach O. (2022). What goes around comes around: artificial circular RNAs bypass cellular antiviral responses. *Molecular Therapy Nucleic Acids*. doi: <https://doi.org/10.1016/j.omtn.2022.04.017>

*contributed equally

Poster presentations

Title: Artificial circular RNA sponges as a novel tool in molecular biology and medicine

- Grand Opening Symposium of the Berlin Institute for Medical Systems Biology
25th - 27th October 2018; Berlin, Germany
- Novel Concepts in innate immunity of the German Society for Immunology
12th – 14th June 2019; Tübingen, Germany
- RTG2355 Retreat
21st – 22nd November 2019; Rauischholzhausen, Germany
- 26th Annual Meeting of the RNA Society
25th May – 5th June 2021; online

Acknowledgements

An dieser Stelle möchte ich meinen Dank den nachstehenden Personen und Organisationen entgegen bringen, ohne deren Unterstützung die Anfertigung dieser Dissertation nicht möglich gewesen wäre:

Zunächst möchte ich Dr. Oliver Rossbach meinen Dank aussprechen, für die mir eröffnete Möglichkeit meine Arbeit als Teil seiner Arbeitsgruppe anfertigen zu dürfen, die Bereitstellung des spannenden Themas und die stetige Unterstützung. Des Weiteren möchte ich mich bei Prof. Dr. Albrecht Bindereif für das mir entgegengebrachte Vertrauen diese Arbeit in seinem Labor anfertigen zu dürfen und den fachlichen Austausch während regelmäßiger Lab Meetings bedanken.

Prof. Dr. Elena Evguenieva-Hackenberg danke ich für die Betreuung meiner Arbeit im Rahmen der TAC-Meetings, sowie für die Anfertigung des Zweitgutachtens dieser Dissertation.

Zudem danke ich der Deutschen Forschungsgemeinschaft DFG, welche sowohl die Finanzierung der vorliegenden Arbeit im Rahmen des RTG 2355, als auch die aktive Teilnahme an diversen Seminaren, Workshops und Konferenzen ermöglichte.

Vielen Dank meinen Kollegen und Mitdoktoranden. Tim, Christian, Christina, Marie, Stephen, Sophie, Yannic, Anna D. und Corinna – danke für eure fachliche Unterstützung und einen abwechslungsreichen Laboralltag. Silke danke ich für das Teilen ihrer Erfahrungen zu unzähligen Protokollen und die kurzweiligen gemeinsamen Mittagspausen. Bei Anna W. möchte ich mich herzlich bedanken, nicht nur für die gemeinsame Zeit an der Bench, sondern vor allem für ihr stets offenes Ohr und ihre Unterstützung.

Ein ganz besonderer Dank gilt Dr. Frauke May, für zahllose Gespräche, die mich immer wieder inspiriert und motiviert haben. Vielen Dank für die Zeit, die du in mich investierst.

Zuletzt danke ich meinen Eltern und Großeltern, die meinen bisherigen Lebensweg ermöglicht haben und mich immer unterstützen. Meiner Schwester Judith danke ich für ihre stetige moralische Unterstützung. Schlussendlich gilt mein Dank meinem Partner Christopher. Danke für den Ausgleich, den du mir schaffst und deinen bedingungslosen Rückhalt.